Supplement of Atmos. Chem. Phys., 21, 9955–9976, 2021
https://doi.org/10.5194/acp-21-9955-2021-supplement

Atmospheric Chemistry and Physics
Open Access

Supplement of

Secondary aerosol formation from dimethyl sulfide – improved mechanistic understanding based on smog chamber experiments and modelling

Robin Wollesen de Jonge et al.

Correspondence to: Robin Wollesen de Jonge (robin.wdejonge@nuclear.lu.se)

S1 Reaction mechanism

Table S1: Multiphase DMS mechanism. Reactions related to the MCMv3.3.1 isoprene chemistry scheme have been excluded.

#	Reaction	Rate	Ref.
1	$O \rightarrow O_3$	5.6E-34·$[N_2]$·$(T/300)^{-2.6}$ ·$[O_2]$ +6.0E-34·$[O_2]$ ·$(T/300)^{-2.6}$ ·$[O_2]$	[1]
2	$O + O_3 \rightarrow$ DUMMY	8.0E-12·exp(-2060/T)	[1]
3	$O + NO \rightarrow NO_2$	KMT01	[1]
4	$O + NO_2 \rightarrow NO$	5.5E-12·exp(188/T)	[1]
5	$O + NO_2 \rightarrow NO_3$	KMT02	[1]
6	O1D $\rightarrow$ O	3.2E-11·exp(67/T)·$[O_2]$+2.0E-11·exp(130/T)·$[N_2]$	[1]
7	$NO + O_3 \rightarrow NO_2$	1.4E-12·exp(-1310/T)	[1]
8	$NO_2 + O_3 \rightarrow NO_3$	1.4E-13·exp(-2470/T)	[1]
9	$NO + NO \rightarrow NO_2 + NO_2$	3.3E-39·exp(530/T)·$[O_2]$	[1]
10	$NO + NO_3 \rightarrow NO_2 + NO_2$	1.8E-11·exp(110/T)	[1]
11	$NO_2 + NO_3 \rightarrow NO + NO_2$	4.50E-14·exp(-1260/T)	[1]
12	$NO_2 + NO_3 \rightarrow [N_2]O5$	KMT03	[1]
13	O1D $\rightarrow$ OH + OH	2.14E-10·H_2O	[1]
14	$OH + O_3 \rightarrow HO_2$	1.70E-12·exp(-940/T)	[1]
15	$OH + H_2 \rightarrow HO_2$	7.7E-12·exp(-2100/T)	[1]
16	$OH + CO \rightarrow HO_2$	KMT05	[1]
17	$OH + H_2O_2 \rightarrow HO_2$	2.9E-12·exp(-160/T)	[1]
18	$HO_2 + O_3 \rightarrow OH$	2.03E-16·$(T/300)^{4.57}$·exp(693/T)	[1]
19	$OH + HO_2 \rightarrow$ DUMMY	4.8E-11·exp(250/T)	[1]
20	$HO_2 + HO_2 \rightarrow H_2O_2$	2.20E-13·KMT06·exp(600/T)+1.90E-33·M·KMT06· exp(980/T)	[1]
21	$OH + NO \rightarrow HONO$	KMT07	[1]
22	$OH + NO_2 \rightarrow HNO_3$	KMT08	[1]
23	$OH + NO_3 \rightarrow HO_2 + NO_2$	2.0E-11	[1]
24	$HO_2 + NO \rightarrow OH + NO_2$	3.45E-12·exp(270/T)	[1]
25	$HO_2 + NO_2 \rightarrow HO_2NO_2$	KMT09	[1]
26	$OH + HO_2NO_2 \rightarrow NO_2$	3.2E-13·exp(690/T)·1.0	[1]
27	$HO_2 + NO_3 \rightarrow OH + NO_2$	4.0E-12	[1]
28	$OH + HONO \rightarrow NO_2$	2.5E-12·exp(260/T)	[1]
29	$OH + HNO_3 \rightarrow NO_3$	KMT11	[1]
30	$O + SO_2 \rightarrow SO_3$	4.0E-32·exp(-1000/T)·M	[1]
31	$OH + SO_2 \rightarrow HSO_3$	KMT12	[1]
32	$HSO_3 \rightarrow HO_2 + SO_3$	1.3E-12·exp(-330/T)·$[O_2]$	[1]
33	$SO_3 \rightarrow H_2SO_4$	1.20E-15·H_2O	[1]
34	$O_3 \rightarrow$ O1D	J(1)	[1]
35	$O_3 \rightarrow O$	J(2)	[1]
36	$H_2O_2 \rightarrow OH + OH$	J(3)	[8] [13]
37	$NO_2 \rightarrow NO + O$	J(4)	[1]
38	$NO_3 \rightarrow NO$	J(5)	[1]
39	$NO_3 \rightarrow NO_2 + O$	J(6)	[1]
40	$HONO \rightarrow OH + NO$	J(7)	[1]
41	$HNO_3 \rightarrow OH + NO_2$	J(8)	[1]
42	$[N_2]O5 \rightarrow NO_2 + NO_3$	KMT04	[1]
43	$HO_2NO_2 \rightarrow HO_2 + NO_2$	KMT10	[1]
44	$DMS + NO_3 \rightarrow CH_3SCH_2O_2 + HNO_3$	1.9E-13·exp(520/T)	[1]
45	$DMS + OH \rightarrow CH_3SCH_2O_2$	1.12E-11·exp(-250/T)	[1]
46	$DMS + OH \rightarrow HODMSO_2$	0E0	[1]
47	$DMS + OH \rightarrow CH_3SOHCH_3$	KMT18	[2]
48	$CH_3SOHCH_3 \rightarrow DMS + OH$	(1.7E-42·O_2·exp(7810/T)/(1E0+5.5E-31·O_2·	[2]

[1] MCMv3.3.1 ; [2] Hoffmann et al. (2016) ; [3] Wu et al. (2014) ; [4] Berndt et al. (2019) ; [5] Kukui et al. (2003)
[6] Atkinson et al. (2007) ; [7] Sander et al. (2006) ; [8] Atkinson et al. (2008) ; [9] Braeuer et al. (2013) ; [10] Jacobson (2005)
[11] Demore et al. (1997) ; [12] Berndt et al. (2020) ; [13] Kahan et al. (2012) ; [14] Burkholder et al. (2015)
[E] Estimate based on equilibrium coefficients ; [C] Based on pKa value from COSMO*therm* ; [A] Assumed

#	Reaction	Rate	Ref.
		exp(7640/T)))/(8.3E-29·T·exp(5136/T))	
49	$CH_3SOHCH_3 \rightarrow HODMSO_2$	8.5E-13·[O_2]	[2]
50	$CH_3SOHCH_3 \rightarrow CH_3SOH + CH_3O_2$	5E5	[2]
51	$CH_3SOH + OH \rightarrow CH_3SO$	5E-11	[2]
52	$DMS + Cl \rightarrow CH_3SCH_2O_2 + HCl$	0.45·3.4E-10	[2]
53	$DMS + Cl \rightarrow CH_3SCH_3Cl$	0.55·3.4E-10	[2]
54	$DMS + ClO \rightarrow DMSO + Cl$	0.73·1.7E-15·exp(340/T)	[2]
55	$DMS + ClO \rightarrow CH_3SCH_2O_2 + HOCl$	0.27·1.7E-15·exp(340/T)	[2]
56	$DMS + Cl_2 \rightarrow CH_3SCH_2Cl + HCl$	3.4E-14	[2]
57	$CH_3SCH_2Cl + OH \rightarrow CH_3SOH + CH_2ClO_2$	2.5E-12	[2]
58	$CH_3SCH_3Cl + NO_2 \rightarrow DMS + ClNO_2$	2.7E-11	[2]
59	$CH_3SCH_3Cl + NO \rightarrow DMS + ClNO$	1.2E-11	[2]
60	$CH_3SCH_3Cl \rightarrow DMSO + ClO$	4E-18·[O_2]	[2]
61	$CH_3SCH_3Cl \rightarrow DMS + Cl$	9E1	[2]
62	$CH_3SOCH_3Cl \rightarrow DMSO_2 + ClO$	3E-18·[O_2]	[2]
63	$CH_3SOCH_3Cl + NO \rightarrow DMSO + ClNO$	1.2E-11	[2]
64	$CH_3SOCH_3Cl + NO_2 \rightarrow DMSO + ClNO_2$	2.1E-11	[2]
65	$CH_3SOCH_3Cl + CH_3SOCH_3Cl \rightarrow DMSO + DMSO + Cl_2$	3E-11	[2]
66	$CH_3SOCH_3Cl \rightarrow DMSO + Cl$	9E1	[2]
67	$CH_3SCH_2O_2 + HO_2 \rightarrow CH_3SCH_2OOH$	KRO_2HO_2·0.387	[1]
68	$CH_3SCH_2O_2 + NO \rightarrow CH_3SCH_2O + NO_2$	4.9E-12·exp(260/T)	[1]
69	$CH_3SCH_2O_2 + NO_3 \rightarrow CH_3SCH_2O + NO_2$	KRO_2NO_3	[1]
70	$CH_3SCH_2O_2 \rightarrow CH_3SCH_2O$	2·(K298CH_3O_2·1.0E-11)$^{0.5}$ ·RO_2·0.8	[1]
71	$CH_3SCH_2O_2 \rightarrow CH_3SCH_2OH$	2·(K298CH_3O_2·1.0E-11)$^{0.5}$ ·RO_2·0.1	[1]
72	$CH_3SCH_2O_2 \rightarrow CH_3SCHO$	2·(K298CH_3O_2·1.0E-11)$^{0.5}$ ·RO_2·0.1	[1]
73	$CH_3SCH_2O_2 \rightarrow OOCH_2SCH_2OOH$	2.2433E11·exp(-9.8016E3/T)·exp(1.0348E8/T^3)·5E0	[4]
74	$OOCH_2SCH_2OOH \rightarrow HPMTF + OH$	6.097E11·exp(-9.4892E3/T)·exp(1.102E8/T^3)	[4]
75	$OOCH_2SCH_2OOH + NO \rightarrow HOOCH_2S + NO_2 + HCHO$	4.9E-12·exp(260/T)	[1]
76	$OOCH_2SCH_2OOH + HO_2 \rightarrow HOOCH_2SCH_2OOH$	1.13E-13·exp(1300/T)	[1]
77	$HPMTF + OH \rightarrow HOOCH_2SCO$	1.4E-12·exp(0E0/T)	[3]
78	$HOOCH_2SCO \rightarrow HOOCH_2S + CO$	9.2E9·exp(-505.4/T)	[3]
79	$HOOCH_2SCO \rightarrow HCHO + OH + OCS$	1.6E7·exp(-1468.6/T)	[3]
80	$HOOCH_2S + O_3 \rightarrow HOOCH_2SO$	1.15E-12·exp(430/T)	[3]
81	$HOOCH_2S + NO_2 \rightarrow HOOCH_2SO + NO$	6.00E-11·exp(240/T)	[3]
82	$HOOCH_2SO + O_3 \rightarrow SO_2 + HCHO + OH$	4.00E-13	[3]
83	$HOOCH_2SO + NO_2 \rightarrow SO_2 + HCHO + OH + NO$	1.20E-11	[3]
84	$HODMSO_2 + NO \rightarrow DMSO_2 + HO_2 + NO_2$	KRO_2NO	[1]
85	$HODMSO_2 \rightarrow DMSO + HO_2$	8.90E+10·exp(-6040/T)	[1]
86	$CH_3SCH_2OOH + OH \rightarrow CH_3SCHO + OH$	7.03E-11	[1]
87	$CH_3SCH_2OOH \rightarrow CH_3SCH_2O + OH$	J(41)	[1]
88	$CH_3SCH_2O \rightarrow CH_3S + HCHO$	KDEC	[1]
89	$CH_3SCH_2OH + OH \rightarrow CH_3SCHO + HO_2$	2.78E-11	[1]
90	$CH_3SCHO + OH \rightarrow CH_3S + CO$	1.11E-11	[1]
91	$CH_3SCHO \rightarrow CH_3S + CO + HO_2$	J(15)	[1]
92	$DMSO_2 + OH \rightarrow DMSO_2O_2$	4.40E-14	[1]
93	$DMSO + OH \rightarrow MSIA + CH_3O_2$	6.10E-12·exp(800/T)	[1]
94	$DMSO + NO_3 \rightarrow DMSO_2 + NO_2$	2.9E-13	[2]
95	$DMSO + Cl \rightarrow CH_3SOCH_2O_2 + HCl$	1.45E-11	[2]
96	$DMSO + Cl \rightarrow CH_3SOCH_3Cl$	7.4E-11	[2]
97	$CH_3SOCH_2O_2 + NO \rightarrow CH_3SO + HCHO + NO_2$	7.5E-12	[2]
98	$CH_3SOCH_2O_2 + HO_2 \rightarrow CH_3SOCH_2OOH$	1.5E-12	[2]
99	$CH_3S + NO_2 \rightarrow CH_3SO + NO$	6.00E-11·exp(240/T)	[1]
100	$CH_3S + O_3 \rightarrow CH_3SO$	1.15E-12·exp(430/T)	[1]
101	$CH_3S \rightarrow CH_3SOO$	1.20E-16·exp(1580/T)·[O_2]	[1]

[1] MCMv3.3.1 ; [2] Hoffmann et al. (2016) ; [3] Wu et al. (2014) ; [4] Berndt et al. (2019) ; [5] Kukui et al. (2003)
[6] Atkinson et al. (2007) ; [7] Sander et al. (2006) ; [8] Atkinson et al. (2008) ; [9] Braeuer et al. (2013) ; [10] Jacobson (2005)
[11] Demore et al. (1997) ; [12] Berndt et al. (2020) ; [13] Kahan et al. (2012) ; [14] Burkholder et al. (2015)
[E] Estimate based on equilibrium coefficients ; [C] Based on pKa value from COSMO*therm* ; [A] Assumed

. . . multiphase DMS mechanism continued

#	Reaction	Rate	Ref.
102	$HCHO \rightarrow CO + HO_2 + HO_2$	J(11)	[1]
103	$HCHO \rightarrow H_2 + CO$	J(12)	[1]
104	$NO_3 + HCHO \rightarrow HNO_3 + CO + HO_2$	5.5E-16	[1]
105	$OH + HCHO \rightarrow HO_2 + CO$	5.4E-12·exp(135/T)	[1]
106	$DMSO_2O_2 + HO_2 \rightarrow DMSO_2OOH$	KRO_2HO_2·0.387	[1]
107	$DMSO_2O_2 + NO \rightarrow DMSO_2O + NO_2$	KRO_2NO	[1]
108	$DMSO_2O_2 + NO_3 \rightarrow DMSO_2O + NO_2$	KRO_2NO_3	[1]
109	$DMSO_2O_2 \rightarrow CH_3SO_2CHO$	2.00E-12·RO_2·0.2	[1]
110	$DMSO_2O_2 \rightarrow DMSO_2O$	2.00E-12·RO_2·0.6	[1]
111	$DMSO_2O_2 \rightarrow DMSO_2OH$	2.00E-12·RO_2·0.2	[1]
112	$MSIA + OH \rightarrow CH_3O_2 + SO_2$	0E0·9.00E-11	[1]
113	$MSIA + OH \rightarrow CH_3SO_2$	1E-10·exp(0E0/T)	[5]
114	$MSIA + NO_3 \rightarrow CH_3SO_2 + HNO_3$	1E-13	[2]
115	$CH_3O_2 + HO_2 \rightarrow CH_3OOH$	3.8E-13·exp(780/T)·(1-1/(1+498·exp(-1160/T)	[1]
116	$CH_3O_2 + HO_2 \rightarrow HCHO$	3.8E-13·exp(780/T)·(1/(1+498·exp(-1160/T)))	[1]
117	$CH_3O_2 + NO \rightarrow CH_3NO_3$	2.3E-12·exp(360/T)·0.001	[1]
118	$CH_3O_2 + NO \rightarrow CH_3O + NO_2$	2.3E-12·exp(360/T)·0.999	[1]
119	$CH_3O_2 + NO_2 \rightarrow CH_3O_2NO_2$	KMT13	[1]
120	$CH_3O_2 + NO_3 \rightarrow CH_3O + NO_2$	1.2E-12	[1]
121	$CH_3O_2 \rightarrow CH_3O$	2·KCH_3O_2·RO_2·7.18·exp(-885/T)	[1]
122	$CH_3O_2 \rightarrow CH_3OH$	2·KCH_3O_2·RO_2·0.5·(1-7.18·exp(-885/T))	[1]
123	$CH_3O_2 \rightarrow HCHO$	2·KCH_3O_2·RO_2·0.5·(1-7.18·exp(-885/T))	[1]
124	$CH_3SO + NO_2 \rightarrow CH_3O_2 + SO_2 + NO$	1.20E-11·0.25	[1]
125	$CH_3SO + NO_2 \rightarrow CH_3SO_2 + NO$	1.20E-11·0.75	[1]
126	$CH_3SO + O_3 \rightarrow CH_3O_2 + SO_2$	4.00E-13	[1]
127	$CH_3SO \rightarrow CH_3SOO_2$	3.12E-16·exp(1580/T)·[O_2]	[1]
128	$CH_3SOO + NO \rightarrow CH_3SO + NO_2$	1.1E-11	[1]
129	$CH_3SOO + NO_2 \rightarrow CH_3SO + NO_3$	2.2E-11	[1]
130	$CH_3SOO \rightarrow CH_3O_2 + SO_2$	5.60E+16·exp(-10870/T)	[1]
131	$CH_3SOO \rightarrow CH_3S$	3.50E+10·exp(-3560/T)	[1]
132	$CH_3SOO + HO_2 \rightarrow CH_3SOOH$	4E-12	[2]
133	$CH_3SOO \rightarrow CH_3SO_2$	1E0	[2]
134	$DMSO_2OOH + OH \rightarrow CH_3SO_2CHO + OH$	1.26E-12	[1]
135	$DMSO_2OOH + OH \rightarrow DMSO_2O_2$	3.60E-12	[1]
136	$DMSO_2OOH \rightarrow DMSO_2O + OH$	J(41)	[1]
137	$DMSO_2O \rightarrow CH_3SO_2 + HCHO$	KDEC	[1]
138	$CH_3SO_2CHO + OH \rightarrow CH_3SO_2 + CO$	1.78E-12	[1]
139	$CH_3SO_2CHO \rightarrow CH_3SO_2 + CO + HO_2$	J(15)	[1]
140	$DMSO_2OH + OH \rightarrow CH_3SO_2CHO + HO_2$	5.23E-13	[1]
141	$DMSO_2OH + OH \rightarrow DMSO_2O$	1.40E-13	[1]
142	$CH_3OOH \rightarrow CH_3O + OH$	J(41)	[1]
143	$OH + CH_3OOH \rightarrow CH_3O_2$	5.3E-12·exp(190/T)·0.6	[1]
144	$OH + CH_3OOH \rightarrow HCHO + OH$	5.3E-12·exp(190/T)·0.4	[1]
145	$CH_3NO_3 \rightarrow CH_3O + NO_2$	J(51)	[1]
146	$OH + CH_3NO_3 \rightarrow HCHO + NO_2$	4.0E-13·exp(-845/T)	[1]
147	$CH_3O \rightarrow HCHO + HO_2$	7.2E-14·exp(-1080/T)·[O_2]	[1]
148	$CH_3O_2NO_2 \rightarrow CH_3O_2 + NO_2$	KMT14	[1]
149	$CH_3OH + OH \rightarrow HO_2 + HCHO$	2.85E-12·exp(-345/T)	[1]
150	$CH_3SO_2 + O_3 \rightarrow CH_3SO_3$	3.00E-13	[1]
151	$CH_3SO_2 \rightarrow CH_3O_2 + SO_2$	5.00E+13·exp(-9673/T)	[1]
152	$CH_3SO_2 \rightarrow CH_3SO_2O_2$	1.03E-16·exp(1580/T)·[O_2]	[1]
153	$CH_3SO_2 + OH \rightarrow MSA$	5E-11	[2]
154	$CH_3SO_2 + NO_2 \rightarrow CH_3SO_3 + NO$	2.2E-11	[2]
155	$CH_3SOO_2 + HO_2 \rightarrow CH_3SO_2 + OH$	$KAPHO_2$·0.44	[1]

[1] MCMv3.3.1 ; [2] Hoffmann et al. (2016) ; [3] Wu et al. (2014) ; [4] Berndt et al. (2019) ; [5] Kukui et al. (2003)
[6] Atkinson et al. (2007) ; [7] Sander et al. (2006) ; [8] Atkinson et al. (2008) ; [9] Braeuer et al. (2013) ; [10] Jacobson (2005)
[11] Demore et al. (1997) ; [12] Berndt et al. (2020) ; [13] Kahan et al. (2012) ; [14] Burkholder et al. (2015)
[E] Estimate based on equilibrium coefficients ; [C] Based on pKa value from COSMO*therm* ; [A] Assumed

#	Reaction	Rate	Ref.
156	$CH_3SOO_2 + HO_2 \rightarrow CH_3SOOOH$	$KAPHO_2 \cdot 0.41$	[1]
157	$CH_3SOO_2 + HO_2 \rightarrow MSIA + O_3$	$KAPHO_2 \cdot 0.15$	[1]
158	$CH_3SOO_2 + NO \rightarrow CH_3SO_2 + NO_2$	1.00E-11	[1]
159	$CH_3SOO_2 + NO_2 \rightarrow CH_3SOO_2NO_2$	$1.20E\text{-}12 \cdot (T/300)^{-0.9}$	[1]
160	$CH_3SOO_2 + NO_3 \rightarrow CH_3SO_2 + NO_2$	$KRO_2NO_3 \cdot 1.74$	[1]
161	$CH_3SOO_2 \rightarrow CH_3SO$	9.10E+10·exp(-3560/T)	[1]
162	$CH_3SOO_2 \rightarrow CH_3SO_2$	$1.00E\text{-}11 \cdot RO_2 \cdot 0.7$	[1]
163	$CH_3SOO_2 \rightarrow MSIA$	$1.00E\text{-}11 \cdot RO_2 \cdot 0.3$	[1]
164	$CH_3SO_3 + HO_2 \rightarrow MSA$	5.00E-11	[1]
165	$CH_3SO_3 \rightarrow CH_3O_2 + SO_3$	5.00E+13·exp(-9946/T)	[1]
166	$CH_3SO_2O_2 + HO_2 \rightarrow CH_3SO_2OOH$	$KAPHO_2 \cdot 0.41$	[1]
167	$CH_3SO_2O_2 + HO_2 \rightarrow CH_3SO_3 + OH$	$KAPHO_2 \cdot 0.44$	[1]
168	$CH_3SO_2O_2 + HO_2 \rightarrow MSA + O_3$	$KAPHO_2 \cdot 0.15$	[1]
169	$CH_3SO_2O_2 + NO \rightarrow CH_3SO_3 + NO_2$	1.00E-11	[1]
170	$CH_3SO_2O_2 + NO_2 \rightarrow CH_3SO_4NO_2$	$1.20E\text{-}12 \cdot (T/300)^{0.9}$	[1]
171	$CH_3SO_2O_2 + NO_3 \rightarrow CH_3SO_3 + NO_2$	$KRO_2NO_3 \cdot 1.74$	[1]
172	$CH_3SO_2O_2 \rightarrow CH_3SO_2$	3.01E+10·exp(-3560/T)	[1]
173	$CH_3SO_2O_2 \rightarrow CH_3SO_3$	$1.00E\text{-}11 \cdot RO_2 \cdot 0.7$	[1]
174	$CH_3SO_2O_2 \rightarrow MSA$	$1.00E\text{-}11 \cdot RO_2 \cdot 0.3$	[1]
175	$CH_3SOOOH + OH \rightarrow CH_3SOO_2$	9.00E-11	[1]
176	$CH_3SOOOH \rightarrow CH_3SO_2 + OH$	J(41)	[1]
177	$CH_3SOO_2NO_2 + OH \rightarrow MSIA + NO_2$	1.00E-11	[1]
178	$CH_3SOO_2NO_2 \rightarrow CH_3SOO_2 + NO_2$	5.40E+16·exp(-13112/T)	[1]
179	$MSA + OH \rightarrow CH_3SO_3$	2.24E-14	[1]
180	$CH_3SO_2OOH + OH \rightarrow CH_3SO_2O_2$	3.60E-12	[1]
181	$CH_3SO_2OOH \rightarrow CH_3SO_3 + OH$	J(41)	[1]
182	$CH_3SO_4NO_2 + OH \rightarrow CH_3SO_2O_2 + HNO_3$	3.60E-13	[1]
183	$CH_3SO_4NO_2 \rightarrow CH_3SO_2O_2 + NO_2$	5.40E+16·exp(-13112/T)	[1]
184	$Cl + O_3 \rightarrow ClO$	2.8E-11·exp(-250/T)	[9] [2] [6]
185	$Cl + H_2 \rightarrow HCl + HO_2$	3.9E-11·exp(-2310/T)	[9] [2] [6]
186	$Cl + HO_2 \rightarrow HCl$	3.4E-11	[9] [2] [6]
187	$Cl + HO_2 \rightarrow ClO + OH$	6.3E-11·exp(-570/T)	[9] [2] [6]
188	$Cl + H_2O_2 \rightarrow HCl + HO_2$	1.1E-11·exp(-980/T)	[9] [2] [6]
189	$Cl_2 + OH \rightarrow HOCl + Cl$	3.6E-12·exp(-1200/T)	[9] [2] [6]
190	$ClO + O_3 \rightarrow ClO_2$	1.13E-17·exp(-3600·(1E0/T-1E0/298E0))	[9] [2]
191	$ClO + O_3 \rightarrow OClO$	1.48E-18·exp(-4000·(1E0/T-1E0/298E0))	[9] [2]
192	$ClO + OH \rightarrow HO_2 + Cl$	0.94·7.3E-12·exp(300/T)	[9] [2] [6]
193	$ClO + OH \rightarrow HCl$	0.06·7.3E-12·exp(300/T)	[9] [2] [6]
194	$ClO + HO_2 \rightarrow HOCl$	2.2E-12·exp(340/T)	[9] [2] [6]
195	$ClO + ClO \rightarrow Cl_2$	1E-12·exp(-1590/T)	[9] [2] [6]
196	$ClO + ClO \rightarrow Cl + ClO_2$	3E-11·exp(-2450/T)	[9] [2] [6]
197	$ClO + ClO \rightarrow Cl + OClO$	3.5E-13·exp(-1370/T)	[9] [2] [6]
198	$ClO + ClO \rightarrow Cl_2O_2$	KMT46, 1.52E-15	[9] [2]
199	$Cl \rightarrow ClO_2$	$KMT47 \cdot [O_2]$, $5.17E\text{-}14 \cdot [O_2]$	[9] [2]
200	$ClO_2 \rightarrow Cl$	$2.8E\text{-}10 \cdot exp(-1820/T) \cdot [N_2]$	[9] [2] [6]
201	$Cl + ClO_2 \rightarrow Cl_2$	0.95·2.42E-10	[9] [2] [7]
202	$Cl + ClO_2 \rightarrow ClO + ClO$	0.05·2.42E-10	[9] [2] [7]
203	$Cl_2O_2 \rightarrow ClO + ClO$	KMT48, 2.87E-3	[9] [2]
204	$Cl_2O_2 + O_3 \rightarrow ClO + ClO_2$	1E-19	[9] [2] [6]
205	$Cl_2O_2 + Cl \rightarrow Cl_2 + ClO_2$	7.6E-11·exp(65/T)	[9] [2] [6]
206	$OClO + OH \rightarrow HOCl$	1.4E-12·exp(600/T)	[9] [2] [6]
207	$Cl + OClO \rightarrow ClO + ClO$	3.2E-11·exp(170/T)	[9] [2] [6]
208	$ClO + OClO \rightarrow Cl_2O_3$	KMT49, 1.08E-19	[9] [2]
209	$Cl_2O_3 \rightarrow ClO + OClO$	KMT50 + J(65), 6.17E-2	[9] [2]

[1] MCMv3.3.1 ; [2] Hoffmann et al. (2016) ; [3] Wu et al. (2014) ; [4] Berndt et al. (2019) ; [5] Kukui et al. (2003)
[6] Atkinson et al. (2007) ; [7] Sander et al. (2006) ; [8] Atkinson et al. (2008) ; [9] Braeuer et al. (2013) ; [10] Jacobson (2005)
[11] Demore et al. (1997) ; [12] Berndt et al. (2020) ; [13] Kahan et al. (2012) ; [14] Burkholder et al. (2015)
[E] Estimate based on equilibrium coefficients ; [C] Based on pKa value from COSMO*therm* ; [A] Assumed

#	Reaction	Rate	Ref.
210	$HCl + OH \rightarrow Cl$	1.7E-12·exp(-230/T)	[9] [2] [6]
211	$HOCl + OH \rightarrow ClO$	5.60E-13·exp(-500·(1E0/T-1E0/298E0))	[9] [2] [7]
212	$HOCl + Cl \rightarrow HCl + ClO$	0.76·1.62E-12·exp(-130·(1E0/T-1E0/298E0))	[9] [2] [7]
213	$HOCl + Cl \rightarrow Cl_2 + OH$	0.24·1.62E-12·exp(-130·(1E0/T-1E0/298E0))	[9] [2] [7]
214	$ClO + NO \rightarrow Cl + NO_2$	6.2E-12·exp(295/T)	[9] [2] [6]
215	$OClO + NO \rightarrow ClO + NO_2$	1.16E-13·exp(350/T)	[9] [2] [6]
216	$Cl + NO_3 \rightarrow ClO + NO_2$	2.40E-11	[9] [2] [6]
217	$ClO + NO_3 \rightarrow ClO_2 + NO_2$	0.68·4.61E-13	[9] [2] [6]
218	$ClO + NO_3 \rightarrow OClO + NO_2$	0.32·4.61E-13	[9] [2] [6]
219	$Cl + NO \rightarrow ClNO$	KMT51, 1.92E-12	[9] [2]
220	$Cl + ClNO \rightarrow Cl_2 + NO$	8.11E-11·exp(100·(1E0/T-1E0/298E0))	[9] [2] [7]
221	$Cl + NO_2 \rightarrow ClNO_2$	KMT52, 5.80E-14	[9] [2]
222	$ClNO_2 + OH \rightarrow HOCl + NO_2$	3.62E-14·exp(-1250·(1E0/T-1E0/298E0))	[9] [2] [7]
223	$ClO + NO_2 \rightarrow ClNO_3$	KMT53, 1.85E-19	[9] [2]
224	$ClNO_3 \rightarrow ClO + NO_2$	1.47E-3·exp(-11438·(1E0/T-1E0/298E0)) + J(70)	[9] [2]
225	$ClNO_3 + OH \rightarrow ClO + HNO_3$	0.5·1.2E-12·exp(-330/T)	[9] [2] [6]
226	$ClNO_3 + OH \rightarrow HOCl + NO_3$	0.5·1.2E-12·exp(-330/T)	[9] [2] [6]
227	$ClNO_3 + Cl \rightarrow Cl_2 + NO_3$	6.2E-12·exp(145/T)	[9] [2] [6]
228	$Cl + CH_4 \rightarrow CH_3O_2 + HCl$	6.6E-12·exp(-1240/T)	[9] [2]
229	$Cl + CH_3OOH \rightarrow CH_3O_2 + HCl$	5.7E-11	[9] [2]
230	$Cl + CH_3O_2 \rightarrow HCHO + ClO$	0.5·1.60E-10	[9] [2] [7]
231	$Cl + CH_3O_2 \rightarrow HO_2 + HCl + HCOOH$	0.5·1.60E-10	[9] [2] [7]
232	$ClO + CH_3O_2 \rightarrow ClO_2 + HCHO + HO_2$	1.63E-12·exp(-238·(1E0/T-1E0/298E0))	[9] [2]
233	$Cl + HCHO \rightarrow HCl + CO + HO_2$	7.23E-11·exp(-34·(1E0/T-1E0/298E0))	[9] [2]
234	$ClO + HCHO \rightarrow HOCl + CO + HO_2$	8.7E-16·exp(-2100·(1E0/T-1E0/298E0))	[9] [2]
235	$Cl + CH_3CHO \rightarrow HCl + CH_3CO_3$	8E-11	[9] [2]
236	$Cl_2 \rightarrow Cl + Cl$	J(61)	[9] [2] [7]
237	$ClO \rightarrow Cl + O$	J(62)	[9] [2] [7]
238	$OClO \rightarrow ClO + O$	J(63)	[9] [2] [7]
239	$Cl_2O_2 \rightarrow Cl + ClO_2$	J(64)	[9] [2] [7]
240	$Cl_2O_3 \rightarrow ClO + OClO$	J(65)	[9] [2] [6]
241	$HOCl \rightarrow Cl + OH$	J(66)	[9] [2] [6]
242	$ClNO \rightarrow Cl + NO$	J(67)	[9] [2] [6]
243	$ClNO_2 \rightarrow Cl + NO_2$	J(68)	[9] [2] [6]
244	$ClNO_3 \rightarrow Cl + NO_3$	J(69)	[9] [2] [7]
245	$ClNO_3 \rightarrow ClO + NO_2$	J(70)	[9] [2] [7]
246	$CH_3SOCH_2OOH \rightarrow CH_3SO + HCHO + OH$	J(41)	[9] [2]
247	$CH_3SCH_2Cl \rightarrow CH_3S + CH_2ClO_2$	J(71)	[9] [2]
248	$CH_3SOOH \rightarrow CH_3SO + OH$	J(41)	[9] [2]
249	$CH_3Cl + OH \rightarrow CH_2ClO_2$	$7.33E\text{-}18 \cdot T^2 \cdot exp(-809/T)$	[9] [2]
250	$CH_3Cl + Cl \rightarrow CH_2ClO_2 + HCl$	4.85E-13·exp(-1150·(1E0/T-1E0/298E0))	[9] [2]
251	$CH_2ClO_2 + HO_2 \rightarrow CH_2ClOOH$	3.2E-13·exp(820/T)·0.3	[1]
252	$CH_2ClO_2 + HO_2 \rightarrow CHOCl$	3.2E-13·exp(820/T)·0.7	[1]
253	$CH_2ClO_2 + NO \rightarrow CH_2ClO + NO_2$	$KRO_2NO \cdot 1.5$	[9] [2]
254	$CH_2ClO_2 + NO_3 \rightarrow CH_2ClO + NO_2$	KRO_2NO_3	[9] [2]
255	$CH_2ClO_2 \rightarrow CH_2ClO$	$2 \cdot (KCH_3O_2 \cdot 1.9E\text{-}13 \cdot exp(870/T))^{0.5} \cdot RO_2 \cdot 0.6$	[1]
256	$CH_2ClO_2 \rightarrow CH_2ClOH$	$2 \cdot (KCH_3O_2 \cdot 1.9E\text{-}13 \cdot exp(870/T))^{0.5} \cdot RO_2 \cdot 0.2$	[1]
257	$CH_2ClO_2 \rightarrow CHOCl$	$2 \cdot (KCH_3O_2 \cdot 1.9E\text{-}13 \cdot exp(870/T))^{0.5} \cdot RO_2 \cdot 0.2$	[1]
258	$CH_2ClOOH + OH \rightarrow CH_2ClO_2$	1.90E-12·exp(190/T)	[1]
259	$CH_2ClOOH + OH \rightarrow CHOCl + OH$	4.14E-12	[1]
260	$CH_2ClOOH \rightarrow CH_2ClO + OH$	J(41)	[1]
261	$CHOCl + NO_3 \rightarrow CO + Cl + HNO_3$	KNO_3AL	[1]
262	$CHOCl + OH \rightarrow CO + Cl$	6.12E-12	[1]
263	$CHOCl \rightarrow HO_2 + CO + Cl$	J(11)	[1]

[1] MCMv3.3.1 ; [2] Hoffmann et al. (2016) ; [3] Wu et al. (2014) ; [4] Berndt et al. (2019) ; [5] Kukui et al. (2003)
[6] Atkinson et al. (2007) ; [7] Sander et al. (2006) ; [8] Atkinson et al. (2008) ; [9] Braeuer et al. (2013) ; [10] Jacobson (2005)
[11] Demore et al. (1997) ; [12] Berndt et al. (2020) ; [13] Kahan et al. (2012) ; [14] Burkholder et al. (2015)
[E] Estimate based on equilibrium coefficients ; [C] Based on pKa value from COSMO*therm* ; [A] Assumed

#	Reaction	Rate	Ref.
264	$CH_2ClO \rightarrow CHOCl + HO_2$	KROPRIM·[O_2]	[1]
265	$CH_2ClOH + OH \rightarrow CHOCl + HO_2$	1.08E-12	[1]
266	$DMS + Br \rightarrow CH_3SCH_2O_2 + HBr$	9E-11·exp(-2390/T)	[9] [2]
267	$DMS + Br \rightarrow CH_3SCH_3Br$	KMT54	[9] [2]
268	$DMS + BrO \rightarrow DMSO + Br$	1.5E-14·exp(1000/T)	[9] [2]
269	$CH_3SCH_3Br \rightarrow DMSO + BrO$	1E-18·[O_2]	[9] [2]
270	$CH_3SCH_3Br \rightarrow DMS + Br$	1.02E4	[9] [2]
271	$DMSO + BrO \rightarrow DMSO_2 + Br$	1E-14	[9] [2]
272	$Br + O_3 \rightarrow BrO$	1.7E-11·exp(-800/T)	[9] [2] [6]
273	$Br + HO_2 \rightarrow HBr$	7.7E-12·exp(-450/T)	[9] [2] [6]
274	$Br + H_2O_2 \rightarrow HBr + HO_2$	5E-16	[9] [2] [6]
275	$Br_2 + OH \rightarrow HOBr + Br$	2E-11·exp(240/T)	[9] [2] [6]
276	$BrO + O_3 \rightarrow Br$	0.9·2E-17	[9] [2] [6]
277	$BrO + O_3 \rightarrow OBrO$	0.1·2E-17	[9] [2] [6]
278	$BrO + OH \rightarrow Br + HO_2$	1.8E-11·exp(250/T)	[9] [2] [6]
279	$BrO + HO_2 \rightarrow HOBr$	4.5E-12·exp(500/T)	[9] [2] [6]
280	$BrO + BrO \rightarrow Br + Br$	0.85·2.7E-12	[9] [2] [6]
281	$BrO + BrO \rightarrow Br_2$	0.15·2.7E-12	[9] [2] [6]
282	$HBr + OH \rightarrow Br$	6.7E-12·exp(155/T)	[9] [2] [6]
283	$Br + NO_2 \rightarrow BrNO_2$	KMT55	[9] [2] [6]
284	$Br + NO_3 \rightarrow BrO + NO_2$	1.6E-11	[9] [2] [6]
285	$BrO + NO \rightarrow Br + NO_2$	8.7E-12·exp(260/T)	[9] [2] [6]
286	$BrO + NO_2 \rightarrow BrNO_3$	KMT56	[9] [2] [6]
287	$BrNO_3 \rightarrow BrO + NO_2$	2.75E-5·exp(-12360·(1E0/T-1E0/298E0)) + J(78)	[9] [2]
288	$BrNO_3 + Br \rightarrow Br_2 + NO_3$	4.9E-11	[9] [2]
289	$HBr + NO_3 \rightarrow Br + HNO_3$	1E-16	[9] [2] [6]
290	$Br + Cl_2O_2 \rightarrow BrCl + ClO_2$	5.9E-12·exp(-170/T)	[9] [2] [6]
291	$Br + OClO \rightarrow BrO + ClO$	2.7E-11·exp(-1300/T)	[9] [2] [6]
292	$BrO + ClO \rightarrow Br + OClO$	1.6E-12·exp(430/T)	[9] [2] [6]
293	$BrO + ClO \rightarrow Br + ClO_2$	2.9E-12·exp(220/T)	[9] [2] [6]
294	$BrO + ClO \rightarrow BrCl$	5.8E-13·exp(170/T)	[9] [2] [6]
295	$Br_2 + Cl \rightarrow BrCl + Br$	3.62E-10·exp(135·(1E0/T-1E0/298E0))	[9] [2]
296	$BrCl + Br \rightarrow Br_2 + Cl$	3.32E-15	[9] [2]
297	$Br + Cl_2 \rightarrow BrCl + Cl$	1.1E-15	[9] [2]
298	$BrCl + Cl \rightarrow Br + Cl_2$	1.45E-11	[9] [2]
299	$Br + CH_3OOH \rightarrow HBr + CH_3O_2$	1.18E-14·exp(-1610·(1E0/T-1E0/298E0))	[9] [2]
300	$BrO + CH_3O_2 \rightarrow Br + HCHO + HO_2$	0.25·6.01E-12·exp(800·(1E0/T-1E0/298E0))	[9] [2]
301	$BrO + CH_3O_2 \rightarrow HOBr + HCOOH$	0.75·6.01E-12·exp(800·(1E0/T-1E0/298E0))	[9] [2]
302	$Br + HCHO \rightarrow HBr + CO + HO_2$	1.161E-12·exp(-800·(1E0/T-1E0/298E0))	[9] [2] [7]
303	$BrO + HCHO \rightarrow HOBr + CO + HO_2$	1.5E-14	[9] [2]
304	$Br + CH_3CHO \rightarrow HBr + CH_3CO_3$	3.841E-12·exp(-460·(1E0/T-1E0/298E0))	[9] [2]
305	$Br_2 \rightarrow Br + Br$	J(72)	[9] [2] [6]
306	$BrO \rightarrow Br + O$	J(73)	[9] [2] [6]
307	$OBrO \rightarrow BrO + O$	J(74)	[9] [2] [6]
308	$HOBr \rightarrow Br + OH$	J(75)	[9] [2] [6]
309	$BrNO_2 \rightarrow Br + NO_2$	J(76)	[9] [2] [6]
310	$BrNO_3 \rightarrow Br + NO_3$	J(77)	[9] [2] [6]
311	$BrNO_3 \rightarrow BrO + NO_2$	J(78)	[9] [2] [6]
312	$BrCl \rightarrow Br + Cl$	J(79)	[9] [2] [6]
313	DMS + IO → DMSO + IODINE	3.3E-13·exp(-925/T)	[9] [2]
314	IODINE + IODINE → IODINE2	2.99E-11	[9] [2]
315	IODINE + O_3 → IO	2.1E-11·exp(-830/T)	[9] [2] [6]
316	IODINE2 + OH → IODINE+ HOI	2.1E-10	[9] [2] [6]
317	IODINE + HO_2 → HI	1.5E-11·exp(-1090/T)	[9] [2] [6]

[1] MCMv3.3.1 ; [2] Hoffmann et al. (2016) ; [3] Wu et al. (2014) ; [4] Berndt et al. (2019) ; [5] Kukui et al. (2003)
[6] Atkinson et al. (2007) ; [7] Sander et al. (2006) ; [8] Atkinson et al. (2008) ; [9] Braeuer et al. (2013) ; [10] Jacobson (2005)
[11] Demore et al. (1997) ; [12] Berndt et al. (2020) ; [13] Kahan et al. (2012) ; [14] Burkholder et al. (2015)
[E] Estimate based on equilibrium coefficients ; [C] Based on pKa value from COSMO*therm* ; [A] Assumed

#	Reaction	Rate	Ref.
318	IO + HO_2 → HOI	1.4E-11·exp(540/T)	[9] [2] [6]
319	IO + IO → I_2O_2	0.485·8.03E-11·exp(500·(1E0/T-1E0/298E0))	[9] [2] [7]
320	IO + IO → OIO + IODINE	0.38·8.03E-11·exp(500·(1E0/T-1E0/298E0))	[9] [2] [7]
321	IO + IO → IODINE2	0.025·8.03E-11·exp(500·(1E0/T-1E0/298E0))	[9] [2] [7]
322	IO + IO → IODINE + IODINE	0.11·8.03E-11·exp(500·(1E0/T-1E0/298E0))	[9] [2] [7]
323	OIO + OH → HIO_3	0.5·2E-10	[9] [2]
324	OIO + OH → HOI	0.5·2E-10	[9] [2]
325	OIO + OIO → I_2O_2	5E-11	[9] [2]
326	I_2O_2 → IO + IO	2E1	[9] [2]
327	HI + OH → IODINE	1.6E-11·exp(440/T)	[9] [2] [6]
328	IODINE + NO → INO	KMT57	[9] [2] [6]
329	IODINE + NO_2 → INO_2	KMT58	[9] [2] [6]
330	IODINE + NO_3 → IO + NO_2	4.5E-10	[9] [2]
331	IODINE2 + NO_3 → IODINE + INO_3	1.5E-12	[9] [2] [6]
332	IO + NO → IODINE + NO_2	7.15E-12·exp(300/T)	[9] [2] [6]
333	IO + NO_2 → INO_3	KMT59	[9] [2] [6]
334	OIO + NO → IO + NO_2	1.1E-12·exp(542/T)	[9] [2] [6]
335	HI + NO_3 → IODINE + HNO_3	1.3E-12·exp(-1830/T)	[9] [2] [6]
336	INO + INO → IODINE2 + NO + NO	8.5E-11·exp(-2620/T)	[9] [2] [6]
337	INO_2 + INO_2 → IODINE2 + NO_2 + NO_2	4.7E-13·exp(-1670/T)	[9] [2] [6]
338	INO_2 → IODINE + NO_2	9.8E-20·M + J(88)	[9] [2]
339	INO_3 → IO + NO_2	4.5E-5·exp(-12060/T)·M + J(90)	[9] [2] [6]
340	IODINE2 + Cl → IODINE + ICl	2.1E-10	[9] [2]
341	IODINE2 + Br → IODINE + IBr	1.2E-10	[9] [2]
342	IODINE + BrO → IO + Br	1.2E-11	[9] [2]
343	IO + ClO → OClO + IODINE	0.55·4.7E-12·exp(280/T)	[9] [2] [6]
344	IO + ClO → Cl + IODINE	0.25·4.7E-12·exp(280/T)	[9] [2] [6]
345	IO + ClO → ICl	0.2·4.7E-12·exp(280/T)	[9] [2] [6]
346	IO + BrO → OIO + Br	0.8·1.5E-11·exp(510/T)	[9] [2] [6]
347	IO + BrO → IODINE + Br	0.2·1.5E-11·exp(510/T)	[9] [2] [6]
348	C3H7I + OH → $CH_3CIO_2CH_3$	1.6E-12	[9] [2]
349	$CH_3CIO_2CH_3$ + CH_3O_2 → CH_3CIOCH_3 + HCHO + HO_2	2.4E-14	[9] [2]
350	$CH_3CIO_2CH_3$ + $CH_3CIO_2CH_3$ → CH_3CIOCH_3 + CH_3CIOCH_3	5.57E-16·exp(-2200·(1E0/T-1E0/298E0))	[9] [2]
351	$CH_3CIO_2CH_3$ + NO → CH_3CIOCH_3 + NO_2	9.04E-12·exp(360·(1E0/T-1E0/298E0))	[9] [2]
352	CH_3CIOCH_3 → CH_3COCH_3 + IODINE	1E1	[9] [2]
353	C2H5I + OH → CH_3CHIO_2	0.13·3.69E-13·exp(-800·(1E0/T-1E0/298E0))	[9] [2]
354	C2H5I + OH → $CH_2ICH_2O_2$	0.87·3.69E-13·exp(-800·(1E0/T-1E0/298E0))	[9] [2]
355	$CH_2ICH_2O_2$ + CH_3O_2 → CH_2ICH_2OH + HCHO	0.2·2E-12	[9] [2]
356	$CH_2ICH_2O_2$ + CH_3O_2 → CH_2ICHO + CH_3OH	0.2·2E-12	[9] [2]
357	$CH_2ICH_2O_2$ + CH_3O_2 → CH_2ICH_2O + HCHO + HO_2	0.6·2E-12	[9] [2]
358	$CH_2ICH_2O_2$ + $CH_2ICH_2O_2$ → CH_2ICH_2OH + CH_2ICHO	0.43·3.98E-12·exp(1240·(1E0/T-1E0/298E0))	[9] [2]
359	$CH_2ICH_2O_2$ + $CH_2ICH_2O_2$ → CH_2ICH_2O + CH_2ICH_2O	0.57·3.98E-12·exp(1240·(1E0/T-1E0/298E0))	[9] [2]
360	$CH_2ICH_2O_2$ + NO → CH_2ICH_2O + NO_2	9.7E-12	[9] [2]
361	CH_2ICH_2OH + OH → CH_2ICHO + HO_2	4.6E-12	[9] [2]
362	CH_2ICH_2O → CH_2ICHO + HO_2	9.48E-15·exp(-550·(1E0/T-1E0/298E0))·[O_2]	[9] [2]
363	CH_2ICHO + OH → CH_2ICO_3	3.1E-12	[9] [2]
364	CH_2ICO_3 + HO_2 → CH_2ICO_3H	0.71·1.41E-11·exp(1040·(1E0/T-1E0/298E0))	[9] [2]
365	CH_2ICO_3 + HO_2 → CH_2ICOOH	0.29·1.41E-11·exp(1040·(1E0/T-1E0/298E0))	[9] [2]
366	CH_2ICO_3 + CH_3O_2 → CH_2ICOOH + HCHO	0.3·1E-11	[9] [2]
367	CH_2ICO_3 + CH_3O_2 → CH_2IO_2 + HCHO + HO_2	0.7·1E-11	[9] [2]
368	CH_2ICO_3 + NO → CH_2IO_2 + NO_2	2E-11·exp(270·(1E0/T-1E0/298E0))	[9] [2]
369	CH_2ICO_3 + NO_2 → $CH_2ICOOONO_2$	KMT62	[9] [2]
370	$CH_2ICOOONO_2$ → CH_2ICO_3 + NO_2	KMT63	[9] [2]
371	$CH_2ICOOONO_2$ + OH → $O_2CHICOOONO_2$	6.26E-13	[9] [2]

[1] MCMv3.3.1 ; [2] Hoffmann et al. (2016) ; [3] Wu et al. (2014) ; [4] Berndt et al. (2019) ; [5] Kukui et al. (2003)
[6] Atkinson et al. (2007) ; [7] Sander et al. (2006) ; [8] Atkinson et al. (2008) ; [9] Braeuer et al. (2013) ; [10] Jacobson (2005)
[11] Demore et al. (1997) ; [12] Berndt et al. (2020) ; [13] Kahan et al. (2012) ; [14] Burkholder et al. (2015)
[E] Estimate based on equilibrium coefficients ; [C] Based on pKa value from COSMO*therm* ; [A] Assumed

#	Reaction	Rate	Ref.
372	$O_2CHICOOONO_2 + NO \rightarrow CHOI + CO + NO_2 + NO_2$	1.36E-11·exp(360·(1E0/T-1E0/298E0))	[9] [2]
373	$CH_2ICO_3H + OH \rightarrow CH_2ICO_3$	4.29E-12	[9] [2]
374	$CH_2ICOOH + OH \rightarrow CH_2IO_2$	3.59E-12·exp(190·(1E0/T-1E0/298E0))	[9] [2]
375	$CH_3CHIO_2 + CH_3O_2 \rightarrow CH_3CHO + IODINE + HCHO + HO_2$	0.6·8.8E-13	[9] [2]
376	$CH_3CHIO_2 + CH_3O_2 \rightarrow CH_3CHIOH + HCHO$	0.2·8.8E-13	[9] [2]
377	$CH_3CHIO_2 + CH_3O_2 \rightarrow CH_3CIO + CH_3OH$	0.2·8.8E-13	[9] [2]
378	$CH_3CHIO_2 + NO \rightarrow CH_3CHO + IODINE + NO_2$	1.87E-11·exp(360·(1E0/T-1E0/298E0))	[9] [2]
379	$CH_3CHIOH + OH \rightarrow CH_3CIO + HO_2$	2.77E-12	[9] [2]
380	$CH_3CIO + OH \rightarrow CIOCH_2O_2$	3.88E-14	[9] [2]
381	$CIOCH_2O_2 + CH_3O_2 \rightarrow IODINE + CO + HCHO + HCHO +$	2E-12	[9] [2]
382	$CIOCH_2O_2 + NO \rightarrow IODINE + CO + HCHO + NO_2$	1.36E-11·exp(360·(1E0/T-1E0/298E0))	[9] [2]
383	$CH_2I_2 + OH \rightarrow CHI_2O_2$	2.75E-14·exp(-929·(1E0/T-1E0/298E0))	[9] [2]
384	$CH_2I_2 + Cl \rightarrow CHI_2O_2 + HCl$	4.7E-13·exp(-1135·(1E0/T-1E0/298E0))	[9] [2]
385	$CHI_2O_2 + HO_2 \rightarrow CHOI + HOI$	0.3·5.87E-12·exp(700·(1E0/T-1E0/298E0))	[9] [2]
386	$CHI_2O_2 + HO_2 \rightarrow COI_2$	0.7·5.87E-12·exp(700·(1E0/T-1E0/298E0))	[9] [2]
387	$CHI_2O_2 + CH_3O_2 \rightarrow CHI_2OH + HCHO$	0.2·2E-12	[9] [2]
388	$CHI_2O_2 + CH_3O_2 \rightarrow COI_2 + CH_3OH$	0.2·2E-12	[9] [2]
389	$CHI_2O_2 + CH_3O_2 \rightarrow CHOI + IODINE + HO_2 + HCHO$	0.6·2E-12	[9] [2]
390	$CHI_2O_2 + CHI_2O_2 \rightarrow CHOI + CHOI + IODINE + IODINE$	7E-12	[9] [2]
391	$CHI_2O_2 + NO \rightarrow CHOI + IODINE + NO_2$	1.7E-11	[9] [2]
392	$CHI_2OH + OH \rightarrow COI_2 + HO_2$	9.34E-13	[9] [2]
393	$COI_2 + OH \rightarrow COI + HOI$	5E-15	[9] [2]
394	$CH_3I + OH \rightarrow CH_2IO_2$	4.3E-12·exp(-1120/T)	[9] [2] [8]
395	$CH_3I + Cl \rightarrow CH_2IO_2 + HCl$	1.01E-12·exp(-1000·(1E0/T-1E0/298E0))	[9] [2] [7]
396	$CH_2IO_2 + HO_2 \rightarrow CH_2IO_2H$	0.85·6.7E-12	[9] [2] [8]
397	$CH_2IO_2 + HO_2 \rightarrow CHOI$	0.15·6.7E-12	[9] [2] [8]
398	$CH_2IO_2 + CH_3O_2 \rightarrow CH_2IOH + HCHO$	0.2·2E-12	[9] [2]
399	$CH_2IO_2 + CH_3O_2 \rightarrow CHOI + CH_3OH$	0.2·2E-12	[9] [2]
400	$CH_2IO_2 + CH_3O_2 \rightarrow CH_2IO + HO_2 + HCHO$	0.6·2E-12	[9] [2]
401	$CH_2IO_2 + CH_2IO_2 \rightarrow CH_2IO + CH_2IO$	1.05E-12	[9] [2]
402	$CH_2IO_2 + NO \rightarrow CH_2IO + NO_2$	1.1E-11	[9] [2]
403	$CH_2IO_2H + OH \rightarrow CH_2IO_2$	3.59E-12·exp(190·(1E0/T-1E0/298E0))	[9] [2]
404	$CH_2IO_2H + OH \rightarrow CHOI + OH$	5.79E-12	[9] [2]
405	$CH_2IOH + OH \rightarrow CHOI + HO_2$	1.06E-12	[9] [2]
406	$CH_2IO \rightarrow CHOI + HO_2$	9.48E-15·exp(-550·(1E0/T-1E0/298E0))·[O_2]	[9] [2]
407	$CHOI + OH \rightarrow IODINE + CO$	1.16E-12	[9] [2]
408	$CHOI + Cl \rightarrow COI + HCl$	7.48E-12·exp(-710·(1E0/T-1E0/298E0))	[9] [2] [8]
409	$COI \rightarrow CO + IODINE$	4.1E-10·exp(-2960/T)·[N_2]	[9] [2] [8]
410	$CO + IODINE \rightarrow COI$	1.3E-33·$(T/300)^{-3.8}$ ·[N_2]	[9] [2] [8]
411	$IODINE2 \rightarrow IODINE + IODINE$	J(80)	[9] [2] [6]
412	$IO \rightarrow IODINE + O$	J(81)	[9] [2] [6]
413	$OIO \rightarrow IODINE$	J(82)	[9] [2]
414	$OIO \rightarrow IO + O$	J(83)	[9] [2]
415	$I_2O_2 \rightarrow IODINE + IODINE$	J(84)	[9] [2]
416	$HI \rightarrow IODINE + HO_2$	J(85)	[9] [2] [6]
417	$HOI \rightarrow IODINE + OH$	J(86)	[9] [2] [6]
418	$INO \rightarrow IODINE + NO$	J(87)	[9] [2] [7]
419	$INO_2 \rightarrow IODINE + NO_2$	J(88)	[9] [2] [7]
420	$INO_3 \rightarrow IODINE + NO_3$	J(89)	[9] [2] [7]
421	$INO_3 \rightarrow IO + NO_2$	J(90)	[9] [2] [7]
422	$ICl \rightarrow IODINE + Cl$	J(91)	[9] [2] [6]
423	$IBr \rightarrow IODINE + Br$	J(92)	[9] [2] [6]
424	$C3H7I \rightarrow IODINE + IC3H7O_2$	J(97)	[9] [2]
425	$C2H5I \rightarrow IODINE + C2H5O_2$	J(98)	[9] [2]

[1] MCMv3.3.1 ; [2] Hoffmann et al. (2016) ; [3] Wu et al. (2014) ; [4] Berndt et al. (2019) ; [5] Kukui et al. (2003)
[6] Atkinson et al. (2007) ; [7] Sander et al. (2006) ; [8] Atkinson et al. (2008) ; [9] Braeuer et al. (2013) ; [10] Jacobson (2005)
[11] Demore et al. (1997) ; [12] Berndt et al. (2020) ; [13] Kahan et al. (2012) ; [14] Burkholder et al. (2015)
[E] Estimate based on equilibrium coefficients ; [C] Based on pKa value from COSMO*therm* ; [A] Assumed

#	Reaction	Rate	Ref.
426	$CH_2ICHO \rightarrow CH_2IO_2 + CO + HO_2$	J(11)	[9] [2] [9] [2]
427	$CH_2ICO_3H \rightarrow CH_2IO_2 + OH$	J(41)	[9] [2] [9] [2]
428	$CH_2I_2 \rightarrow IODINE + CH_2IO_2$	J(99)	[9] [2]
429	$CH_3I \rightarrow IODINE + CH_3O_2$	J(96)	[14]
430	$CH_2IO_2H \rightarrow CH_2IO + OH$	J(41)	[9] [2]
431	$CHOI \rightarrow IODINE + CO + HO_2$	J(11)	[9] [2] [9] [2]
432	$CH_2ICl \rightarrow IODINE + CH_2ClO_2$	J(100)	[9] [2] [8]
433	$CH_2IBr \rightarrow IODINE + CH_2BRO_2$	J(101)	[9] [2] [8]
434	$CHBr_3 + OH \rightarrow CBr_3O_2$	1.8E-13·exp(-600·(1E0/T-1E0/298E0))	[9] [2] [7]
435	$CHBr_3 + Cl \rightarrow CBr_3O_2 + HCl$	2.8E-13·exp(850·(1E0/T-1E0/298E0))	[9] [2] [7]
436	$CBr_3O_2 + HO_2 \rightarrow COBr_2 + HOBr$	4.7E-13·exp(710/T)	[9] [2] [8]
437	$CBr_3O_2 + CH_3O_2 \rightarrow CBr_3OH + HCHO$	0.3·6.6E-12	[9] [2]
438	$CBr_3O_2 + CH_3O_2 \rightarrow CBr_3O + HCHO + HO_2$	0.7·6.6E-12	[9] [2]
439	$CBr_3O_2 + CBr_3O_2 \rightarrow CBr_3O + CBr_3O$;	3.3E-13·exp(740/T)	[9] [2] [8]
440	$CBr_3O_2 + NO \rightarrow COBr_2 + Br + NO_2$	1.81E-11·exp(270·(1E0/T-1E0/298E0))	[9] [2] [7]
441	$CBr_3O_2 + NO_2 \rightarrow CBr_3OONO_2$	KMT60	[9] [2] [8]
442	$CBr_3OONO_2 \rightarrow CBr_3O_2 + NO_2$	KMT61	[9] [2] [8]
443	$CBr_3OH + OH \rightarrow CBr_3O$	3.6E-14	[9] [2]
444	$CBr_3O \rightarrow COBr_2 + Br$	4E13·exp(-4600/T)	[9] [2] [8]
445	$DIBRET + Cl \rightarrow DIBRETO_2 + HCl$	4.3E-13·exp(-800·(1E0/T-1E0/298E0))	[9] [2] [7]
446	$CH_3BR + Cl \rightarrow CH_2BRO_2 + HCl$	4.42E-13·exp(-1030·(1E0/T-1E0/298E0))	[9] [2]
447	$COBr_2 + OH \rightarrow COBr + HOBr$	5E-15	[9] [2] [8]
448	$COBr \rightarrow CO + Br$	4.1E-10·exp(-2960/T)·$[N_2]$	[9] [2] [8]
449	$CO + Br \rightarrow COBr$	1.3E-33·$(T/300)^{-3.8}$ ·$[N_2]$	[9] [2] [8]
450	$CHBr_3 \rightarrow Br + DIBRETO_2$	J(93)	[14]
451	$DIBRET \rightarrow Br + CH_2BrO_2$	J(94)	[14]
452	$COBr_2 \rightarrow Br + Br + CO$	J(95)	[14]
453	$CH_2Br_2 + OH \rightarrow CHBr_2O_2$	1.5E-12·exp(-775/T)	[9] [2] [8]
454	$CHBr_2O_2 + HO_2 \rightarrow CHOBr + HOBr$	0.3·5.87E-12·exp(700·(1E0/T-1E0/298E0))	[9] [2] [8]
455	$CHBr_2O_2 + HO_2 \rightarrow COBr_2 + HOBr$	0.7·5.87E-12·exp(700·(1E0/T-1E0/298E0))	[9] [2] [8]
456	$CHBr_2O_2 + CH_3O_2 \rightarrow CHBr_2OH + HCHO$	0.2·2E-12	[9] [2]
457	$CHBr_2O_2 + CH_3O_2 \rightarrow COBr_2 + CH_3OH$	0.2·2E-12	[9] [2]
458	$CHBr_2O_2 + CH_3O_2 \rightarrow CHOBr + Br + HCHO + HO_2$	0.6·2E-12	[9] [2]
459	$CHBr_2O_2 + CHBr_2O_2 \rightarrow CHOBr + CHOBr + Br + Br$	7.0E-12	[9] [2] [8]
460	$CHBr_2O_2 + NO \rightarrow CHOBr + Br + NO_2$	1.7E-11	[9] [2] [8]
461	$CHBr_2OH + OH \rightarrow COBr_2 + HO_2$	9.34E-13	[9] [2]
462	$CH_3SOH + O_3 \rightarrow CH_3O_2 + HO_2 + SO_2$	2E-12	[12]
463	$Cl(aq) + Cl(aq) \rightarrow Cl_2(aq)$	8.75E7/(cw·Na)	[9] [2]
464	$Cl_2^- + Cl(aq) \rightarrow Cl_2(aq) + Cl^-$	2.1E9/(cw·Na)	[9] [2]
465	$Cl_2^- + Cl_2^- \rightarrow Cl_2(aq) + Cl^- + Cl^-$	1.8E9/(cw·Na)	[9] [2]
466	$Cl^- + O_3(aq) \rightarrow ClO^-$	3E-3/(cw·Na)	[9] [2]
467	$Cl(aq) + H_2O_2(aq) \rightarrow Cl^- + HO_2(aq)$	2E9/(cw·Na)	[9] [2]
468	$Cl_2^- + H_2O_2(aq) \rightarrow Cl^- + Cl^- + HO_2(aq)$	5E4·exp(-3340.0·(1E0/T-1E0/298E0))/(cw·Na)	[9] [2]
469	$Cl_2^- \rightarrow Cl^- + ClOH^-$	23.4·m(H_2O) + $[OH^-]$·4.5E7	[9] [2]
470	$Cl_2^- + HO_2(aq) \rightarrow Cl^- + Cl^-$	1.3E10/(cw·Na)	[9] [2]
471	$Cl_2^- + O_2^- \rightarrow Cl^- + Cl^-$	6E9/(cw·Na)	[9] [2]
472	$Cl_2^- + OH(aq) \rightarrow HOCl(aq) + Cl^-$	1E9/(cw·Na)	[9] [2]
473	$Cl_2^- \rightarrow Cl^- + Cl^- + OH(aq)$	$[OH^-]$·4E6	[9] [2]
474	$Cl_3^- + HO_2(aq) \rightarrow Cl_2^- + Cl^-$	1E9/(cw·Na)	[9] [2]
475	$Cl_3^- + O_2^- \rightarrow Cl_2^- + Cl^-$	3.8E9/(cw·Na)	[9] [2]
476	$Cl_2(aq) + HO_2(aq) \rightarrow Cl_2^-$	1E9/(cw·Na)	[9] [2]
477	$Cl_2(aq) + O_2^- \rightarrow Cl_2^-$	1E9/(cw·Na)	[9] [2]
478	$HOCl(aq) + H_2O_2(aq) \rightarrow Cl^-$	1.1E4/(cw·Na)	[9] [2]
479	$ClO^- + H_2O_2(aq) \rightarrow Cl^-$	1.7E5/(cw·Na)	[9] [2]

[1] MCMv3.3.1 ; [2] Hoffmann et al. (2016) ; [3] Wu et al. (2014) ; [4] Berndt et al. (2019) ; [5] Kukui et al. (2003)
[6] Atkinson et al. (2007) ; [7] Sander et al. (2006) ; [8] Atkinson et al. (2008) ; [9] Braeuer et al. (2013) ; [10] Jacobson (2005)
[11] Demore et al. (1997) ; [12] Berndt et al. (2020) ; [13] Kahan et al. (2012) ; [14] Burkholder et al. (2015)
[E] Estimate based on equilibrium coefficients ; [C] Based on pKa value from COSMO*therm* ; [A] Assumed

#	Reaction	Rate	Ref.
480	HOCl(aq) + HO_2(aq) → Cl(aq)	7.5E6/(cw·Na)	[9] [2]
481	HOCl(aq) + O_2^- → Cl(aq)	7.5E6/(cw·Na)	[9] [2]
482	ClO^- + O_2^- → Cl(aq)	2E8/(cw·Na)	[9] [2]
483	HOCl(aq) + OH(aq) → ClO(aq)	2E9/(cw·Na)	[9] [2]
484	ClO^- + OH(aq) → ClO(aq)	8.8E9/(cw·Na)	[9] [2]
485	Cl_2^- + HSO_3^- → Cl^- + Cl^- + SO_3^-	1.7E8·exp(-400.0·(1E0/T-1E0/298E0))/(cw·Na)	[9] [2]
486	Cl_2^- + SO_3^{2-} → Cl^- + Cl^- + SO_3^-	6.2E7/(cw·Na)	[9] [2]
487	HOCl(aq) + SO_3^{2-} → Cl^- + HSO_4^-	7.6E8/(cw·Na)	[9] [2]
488	HOCl(aq) + HSO_3^- → Cl^- + HSO_4^-	7.6E8/(cw·Na)	[9] [2]
489	Cl^- + $HSO5^-$ → HOCl(aq) + SO_4^{2-}	1.8E-3·exp(-7352.0·(1E0/T-1E0/298E0))/(cw·Na)	[9] [2]
490	Cl_2^- + NO_2^- → Cl^- + Cl^- + NO_2(aq)	6E7/(cw·Na)	[9] [2]
491	Cl(aq) + Cl^- → Cl_2^-	8.5E9/(cw·Na)	[9] [2]
492	Cl_2^- → Cl(aq) + Cl^-	6E4	[9] [2]
493	Cl_2(aq) + Cl^- → Cl_3^-	2E4/(cw·Na)	[9] [2]
494	Cl_3^- → Cl_2(aq) + Cl^-	1.1E5	[9] [2]
495	Cl_2(aq) → Cl^- + HOCl(aq)	m(H_2O)·0.4·exp(-8000.0·(1E0/T-1E0/298E0))	[9] [2]
496	Cl^- + HOCl(aq) → Cl_2(aq)	[H^+]·2.1E4·exp(-3500.0·(1E0/T-1E0/298E0))/(cw·Na)	[9] [2]
497	HCl(aq) → Cl^-	5E11·exp(6890.0·(1E0/T-1E0/298E0))	[9] [2]
498	Cl^- → HCl(aq)	[H^+]·2.9E5	[9] [2]
499	HOCl(aq) → ClO^-	1.5E3	[9] [2]
500	ClO^- → HOCl(aq)	[H^+]·5E10	[9] [2]
501	Cl^- + OH(aq) → $ClOH^-$	4.3E9/(cw·Na)	[9] [2]
502	$ClOH^-$ → Cl^- + OH(aq)	6.1E9	[9] [2]
503	Cl(aq) → $ClOH^-$	[OH^-]·1.8E10 +m(H_2O)·4.1E3	[9] [2]
504	$ClOH^-$ → Cl(aq)	23E0 + [H^+]·2.1E10	[9] [2]
505	$ClOH^-$ + Cl^- → Cl_2^-	1E4/(cw·Na)	[9] [2]
506	Cl^- + SO_4^- → Cl(aq) + SO_4^{2-}	2.52E8/(cw·Na)	[9] [2]
507	Cl(aq) + SO_4^{2-} → Cl^- + SO_4^-	2.1E8/(cw·Na)	[9] [2]
508	Cl^- + NO_3(aq) → Cl(aq) + NO_3^-	3.4E8·exp(-4300.0·(1E0/T-1E0/298E0))/(cw·Na)	[9] [2]
509	Cl(aq) + NO_3^- → Cl^- + NO_3(aq)	1E8/(cw·Na)	[9] [2]
510	Br(aq) + Br(aq) → Br_2(aq)	1E9/(cw·Na)	[9] [2]
511	Br_2^- + Br_2^- → Br_2(aq) + Br^- + Br^-	1.7E9/(cw·Na)	[9] [2]
512	Br^- + O_3(aq) → BrO^-	210.0·exp(-4450.0·(1E0/T-1E0/298E0))/(cw·Na)	[9] [2]
513	Br(aq) + HO_2(aq) → Br^-	1.6E8/(cw·Na)	[9] [2]
514	Br(aq) + H_2O_2(aq) → Br^- + HO_2(aq)	4E9/(cw·Na)	[9] [2]
515	Br_2(aq) + HO_2(aq) → Br_2^-	1.1E8/(cw·Na)	[9] [2]
516	Br_2(aq) + O_2^- → Br_2^-	5.6E9/(cw·Na)	[9] [2]
517	Br_2(aq) + H_2O_2(aq) → Br^- + Br^-	1.3E3/(cw·Na)	[9] [2]
518	Br_2^- + OH(aq) → Br^- + HOBr(aq)	1E9/(cw·Na)	[9] [2]
519	Br_2^- → Br^- + Br^- + OH(aq)	[OH^-]·1.1E4	[9] [2]
520	Br_2^- + HO_2(aq) → Br^- + Br^-	4.4E9/(cw·Na)	[9] [2]
521	Br_2^- + HO_2(aq) → Br_2(aq) + H_2O_2(aq)	4.4E9/(cw·Na)	[9] [2]
522	Br_2^- + O_2^- → Br^- + Br^-	1.7E8/(cw·Na)	[9] [2]
523	Br_2^- + H_2O_2(aq) → Br^- + Br^- + HO_2(aq)	1E5/(cw·Na)	[9] [2]
524	Br_3^- + HO_2(aq) → Br_2^- + Br^-	1E7/(cw·Na)	[9] [2]
525	Br_3^- + O_2^- → Br_2^- + Br^-	3.8E9/(cw·Na)	[9] [2]
526	BrO(aq) + BrO(aq) → BrO_2^- + BrO^-	2.8E9/(cw·Na)	[9] [2]
527	BrO_2^- + BrO(aq) → BrO_2(aq) + BrO^-	4E8/(cw·Na)	[9] [2]
528	Br_2^- + BrO_2^- → Br^- + Br^- + BrO_2(aq)	8E7/(cw·Na)	[9] [2]
529	BrO_2^- + OH(aq) → BrO_2(aq)	1.8E9/(cw·Na)	[9] [2]
530	HOBr(aq) + OH(aq) → BrO(aq)	2E9/(cw·Na)	[9] [2]
531	BrO^- + OH(aq) → BrO(aq)	4.5E9/(cw·Na)	[9] [2]
532	HOBr(aq) + HO_2(aq) → Br(aq)	1E9/(cw·Na)	[9] [2]
533	HOBr(aq) + O_2^- → Br(aq)	3.5E9/(cw·Na)	[9] [2]

[1] MCMv3.3.1 ; [2] Hoffmann et al. (2016) ; [3] Wu et al. (2014) ; [4] Berndt et al. (2019) ; [5] Kukui et al. (2003)
[6] Atkinson et al. (2007) ; [7] Sander et al. (2006) ; [8] Atkinson et al. (2008) ; [9] Braeuer et al. (2013) ; [10] Jacobson (2005)
[11] Demore et al. (1997) ; [12] Berndt et al. (2020) ; [13] Kahan et al. (2012) ; [14] Burkholder et al. (2015)
[E] Estimate based on equilibrium coefficients ; [C] Based on pKa value from COSMO*therm* ; [A] Assumed

. . . multiphase DMS mechanism continued

#	Reaction	Rate	Ref.
534	$BrO^- + O_2^- \rightarrow Br(aq)$	2E8/(cw·Na)	[9] [2]
535	$HOBr(aq) + H_2O_2(aq) \rightarrow Br^-$	3.5E6/(cw·Na)	[9] [2]
536	$BrO^- + H_2O_2(aq) \rightarrow Br^-$	2E5/(cw·Na)	[9] [2]
537	$Br_2^- + HSO_3^- \rightarrow Br^- + Br^- + SO_3^-$	5E7·exp(-780.0·(1E0/T-1E0/298E0))/(cw·Na)	[9] [2]
538	$Br_2^- + SO_3^{2-} \rightarrow Br^- + Br^- + SO_3^-$	3.3E7·exp(-650.0·(1E0/T-1E0/298E0))/(cw·Na)	[9] [2]
539	$Br^- + SO_4^- \rightarrow Br(aq) + SO_4^{2-}$	2.1E9/(cw·Na)	[9] [2]
540	$HOBr(aq) + SO_3^{2-} \rightarrow Br^- + HSO_4^-$	5E9/(cw·Na)	[9] [2]
541	$HOBr(aq) + HSO_3^- \rightarrow Br^- + HSO_4^-$	5E9/(cw·Na)	[9] [2]
542	$Br^- + HSO5^- \rightarrow HOBr(aq) + SO_4^{2-}$	1E0·exp(-5338.0·(1E0/T-1E0/298E0))/(cw·Na)	[9] [2]
543	$Br^- + NO_3(aq) \rightarrow Br(aq) + NO_3^-$	3.8E9/(cw·Na)	[9] [2]
544	$Br_2^- + NO_2^- \rightarrow Br^- + Br^- + NO_2(aq)$	1.2E7·exp(-1720.0·(1E0/T-1E0/298E0))/(cw·Na)	[9] [2]
545	$Br^- + BrNO_2(aq) \rightarrow Br_2(aq) + NO_2^-$	2.55E4/(cw·Na)	[9] [2]
546	$Br_2^- + Cl_2^- \rightarrow Br_2(aq) + Cl^- + Cl^-$	4E9/(cw·Na)	[9] [2]
547	$Br^- + HOCl(aq) \rightarrow BrCl(aq)$	1.3E6/(cw·Na)	[9] [2]
548	$Br^- + ClO^- \rightarrow BrCl(aq)$	3.65E10/(cw·Na)	[9] [2]
549	$Br^- + ClNO_2(aq) \rightarrow BrCl(aq) + NO_2^-$	5E6/(cw·Na)	[9] [2]
550	$BrNO_2(aq) + Cl^- \rightarrow BrCl(aq) + NO_2^-$	1E1/(cw·Na)	[9] [2]
551	$Br(aq) + Br^- \rightarrow Br_2^-$	1.2E10/(cw·Na)	[9] [2]
552	$Br_2^- \rightarrow Br(aq) + Br^-$	1.9E4	[9] [2]
553	$Br_2(aq) + Br^- \rightarrow Br_3^-$	9.6E8/(cw·Na)	[9] [2]
554	$Br_3^- \rightarrow Br_2(aq) + Br^-$	5.5E7	[9] [2]
555	$Br_2(aq) \rightarrow Br^- + HOBr(aq)$	m(H_2O)·1.7·exp(-7500.0·(1E0/T-1E0/298E0))	[9] [2]
556	$Br^- + HOBr(aq) \rightarrow Br_2(aq)$	[H^+]·1.6E10/((cw·Na))	[9] [2]
557	$HBr(aq) \rightarrow Br^-$	5E11	[9] [2]
558	$Br^- \rightarrow HBr(aq)$	[H^+]·5E2	[9] [2]
559	$HOBr(aq) \rightarrow BrO^-$	1E2	[9] [2]
560	$BrO^- \rightarrow HOBr(aq)$	[H^+]·5E10	[9] [2]
561	$Br^- + OH(aq) \rightarrow BrOH^-$	1.1E10/(cw·Na)	[9] [2]
562	$BrOH^- \rightarrow Br^- + OH(aq)$	3.3E7	[9] [2]
563	$Br(aq) \rightarrow BrOH^-$	[OH^-]·1.3E10 + m(H_2O)·2.45E-2	[9] [2]
564	$BrOH^- \rightarrow Br(aq)$	4.2E6 + [H^+]·4.4E10	[9] [2]
565	$BrOH^- + Br^- \rightarrow Br_2^-$	1.9E8/(cw·Na)	[9] [2]
566	$Br_2^- \rightarrow BrOH^- + Br^-$	[OH^-]·2.7E6	[9] [2]
567	$HOBr(aq) + HOBr(aq) \rightarrow Br^- + HBrO_2(aq)$	2E-5/(cw·Na)	[9] [2]
568	$Br^- + HBrO_2(aq) \rightarrow HOBr(aq) + HOBr(aq)$	[H^+]·3E6/((cw·Na))	[9] [2]
569	$HBrO_2(aq) \rightarrow BrO_2^-$	6.3E5	[9] [2]
570	$BrO_2^- \rightarrow HBrO_2(aq)$	[H^+]·5E10	[9] [2]
571	$HOBr(aq) + HBrO_2(aq) \rightarrow Br^- + BrO_3^-$	3.2E0/(cw·Na)	[9] [2]
572	$Br^- + BrO_3^- \rightarrow HOBr(aq) + HBrO_2(aq)$	([H^+]^{2E0})·2.0E0/((cw·Na))	[9] [2]
573	$HBrO_2(aq) + HBrO_2(aq) \rightarrow HOBr(aq) + BrO_3^-$	3E3/(cw·Na)	[9] [2]
574	$HOBr(aq) + BrO_3^- \rightarrow HBrO_2(aq) + HBrO_2(aq)$	[H^+]·1E-8/((cw·Na))	[9] [2]
575	$Br_2O_4(aq) \rightarrow BrO_3^- + HBrO_2(aq)$	m(H_2O)·2.2E3	[9] [2]
576	$BrO_3^- + HBrO_2(aq) \rightarrow Br_2O_4(aq)$	[H^+]·42.0E0/((cw·Na))	[9] [2]
577	$Br_2O_4(aq) \rightarrow BrO_2(aq) + BrO_2(aq)$	7.4E4	[9] [2]
578	$BrO_2(aq) + BrO_2(aq) \rightarrow Br_2O_4(aq)$	1.4E9/(cw·Na)	[9] [2]
579	$BrCl(aq) \rightarrow HOBr(aq) + Cl^-$	1E5	[9] [2]
580	$HOBr(aq) + Cl^- \rightarrow BrCl(aq)$	[H^+]·5.6E9/((cw·Na))	[9] [2]
581	$BrCl^- \rightarrow Br^- + Cl(aq)$	1.9E3	[9] [2]
582	$Br^- + Cl(aq) \rightarrow BrCl^-$	1.2E10/(cw·Na)	[9] [2]
583	$BrCl^- \rightarrow Br(aq) + Cl^-$	6.1E4	[9] [2]
584	$Br(aq) + Cl^- \rightarrow BrCl^-$	1E8/(cw·Na)	[9] [2]
585	$BrCl^- + Br^- \rightarrow Br_2^- + Cl^-$	8E9/(cw·Na)	[9] [2]
586	$Br_2^- + Cl^- \rightarrow BrCl^- + Br^-$	4.3E6/(cw·Na)	[9] [2]
587	$BrCl^- + Cl^- \rightarrow Cl_2^- + Br^-$	1.1E2/(cw·Na)	[9] [2]

[1] MCMv3.3.1 ; [2] Hoffmann et al. (2016) ; [3] Wu et al. (2014) ; [4] Berndt et al. (2019) ; [5] Kukui et al. (2003)
[6] Atkinson et al. (2007) ; [7] Sander et al. (2006) ; [8] Atkinson et al. (2008) ; [9] Braeuer et al. (2013) ; [10] Jacobson (2005)
[11] Demore et al. (1997) ; [12] Berndt et al. (2020) ; [13] Kahan et al. (2012) ; [14] Burkholder et al. (2015)
[E] Estimate based on equilibrium coefficients ; [C] Based on pKa value from COSMO*therm* ; [A] Assumed

#	Reaction	Rate	Ref.
588	$Cl_2^- + Br^- \rightarrow BrCl^- + Cl^-$	4E9/(cw·Na)	[9] [2]
589	$Br_2Cl^- \rightarrow BrCl(aq) + Br^-$	4.3E5	[9] [2]
590	$BrCl(aq) + Br^- \rightarrow Br_2Cl^-$	7.7E9/(cw·Na)	[9] [2]
591	$Br_2Cl^- \rightarrow Br_2(aq) + Cl^-$	3.8E4	[9] [2]
592	$Br_2(aq) + Cl^- \rightarrow Br_2Cl^-$	5E4/(cw·Na)	[9] [2]
593	$BrCl_2^- \rightarrow BrCl(aq) + Cl^-$	1.7E5	[9] [2]
594	$BrCl(aq) + Cl^- \rightarrow BrCl_2^-$	1E6/(cw·Na)	[9] [2]
595	$BrCl_2^- \rightarrow Br^- + Cl_2(aq)$	9E3	[9] [2]
596	$Br^- + Cl_2(aq) \rightarrow BrCl_2^-$	6E9/(cw·Na)	[9] [2]
597	$Br^- + ClOH^- \rightarrow BrCl^-$	1E9/(cw·Na)	[9] [2]
598	$BrCl^- \rightarrow Br^- + ClOH^-$	$[OH^-]$·3E6	[9] [2]
599	$BrOH^- + Cl^- \rightarrow BrCl^-$	1.9E8/(cw·Na)	[9] [2]
600	$BrCl^- \rightarrow BrOH^- + Cl^-$	$[OH^-]$·2E7	[9] [2]
601	IODINE(aq) + IODINE(aq) → IODINE2(aq)	1.1E10/(cw·Na)	[9] [2]
602	IODINE(aq) + I_2^- → $I3^-$	6.5E9/(cw·Na)	[9] [2]
603	$I_2^- + I_2^- \rightarrow I3^- + I^-$	2.5E9/(cw·Na)	[9] [2]
604	$I^- + O_3(aq) \rightarrow HOI(aq)$	2.17E9·exp(-8790.0·(1E0/T-1E0/298E0))/(cw·Na)	[9] [2]
605	IODINE2(aq) + $HO_2(aq)$ → I_2^-	6E9/(cw·Na)	[9] [2]
606	IODINE2(aq) + O_2^- → I_2^-	6E9/(cw·Na)	[9] [2]
607	$I3^- + HO_2(aq) \rightarrow I_2^- + I^-$	2.5E8/(cw·Na)	[9] [2]
608	$I3^- + O_2^- \rightarrow I_2^- + I^-$	2.5E8/(cw·Na)	[9] [2]
609	$HIO_2(aq) + H_2O_2(aq) \rightarrow IO_3^-$	6E1/(cw·Na)	[9] [2]
610	$IO_2^- + H_2O_2(aq) \rightarrow IO_3^-$	6E1/(cw·Na)	[9] [2]
611	$IO(aq) + IO(aq) \rightarrow HOI(aq) + HIO_2(aq)$	1.5E9/(cw·Na)	[9] [2]
612	IODINE2(aq) + HSO_3^- → $I^- + I^- + HSO_4^-$	1E6/(cw·Na)	[9] [2]
613	$HOI(aq) + SO_3{}^{2-} \rightarrow I^- + HSO_4^-$	5E9/(cw·Na)	[9] [2]
614	$HOI(aq) + HSO_3^- \rightarrow I^- + HSO_4^-$	5E9/(cw·Na)	[9] [2]
615	$I^- + ICl(aq)$ → IODINE2(aq) + Cl^-	1.1E9/(cw·Na)	[9] [2]
616	$I^- + HOCl(aq) \rightarrow ICl(aq)$	3.5E11/(cw·Na)	[9] [2]
617	$I^- + HOBr(aq) \rightarrow IBr(aq)$	5E9/(cw·Na)	[9] [2]
618	$HOI(aq) + Cl_2(aq) \rightarrow HIO_2(aq) + Cl^- + Cl^-$	1E6/(cw·Na)	[9] [2]
619	$HOI(aq) + HOCl(aq) \rightarrow HIO_2(aq) + Cl^-$	5E5/(cw·Na)	[9] [2]
620	$HOI(aq) + HOBr(aq) \rightarrow HIO_2(aq) + Br^-$	1E6/(cw·Na)	[9] [2]
621	$HIO_2(aq) + HOCl(aq) \rightarrow IO_3^- + Cl^-$	1.5E3/(cw·Na)	[9] [2]
622	$IO_2^- + HOCl(aq) \rightarrow IO_3^- + Cl^-$	1.5E3/(cw·Na)	[9] [2]
623	$HIO_2(aq) + HOBr(aq) \rightarrow IO_3^- + Br^-$	1E6/(cw·Na)	[9] [2]
624	$IO_2^- + HOBr(aq) \rightarrow IO_3^- + Br^-$	1E6/(cw·Na)	[9] [2]
625	IODINE(aq) + I^- → I_2^-	9.1E9/(cw·Na)	[9] [2]
626	I_2^- → IODINE(aq) + I^-	6.7E4	[9] [2]
627	IODINE2(aq) + I^- → $I3^-$	6.2E9/(cw·Na)	[9] [2]
628	$I3^-$ → IODINE2(aq) + I^-	8.7E6	[9] [2]
629	$HI(aq) \rightarrow I^-$	5E11	[9] [2]
630	$I^- \rightarrow HI(aq)$	$[H^+]$·156E0	[9] [2]
631	$HOI(aq) \rightarrow IO^-$	1.58E0	[9] [2]
632	$IO^- \rightarrow HOI(aq)$	$[H^+]$·5E10	[9] [2]
633	$HOI(aq) + I^-$ → IODINE2(aq)	$[H^+]$·4.4E12/((cw·Na))	[9] [2]
634	IODINE2(aq) → $HOI(aq) + I^-$	3E0	[9] [2]
635	$HOI(aq) + HOI(aq) \rightarrow HIO_2(aq) + I^-$	25E0/(cw·Na)	[9] [2]
636	$HIO_2(aq) + I^- \rightarrow HOI(aq) + HOI(aq)$	$[H^+]$·2E10/((cw·Na))	[9] [2]
637	$HOI(aq) + HOI(aq) \rightarrow IO_2^- + I^-$	25E0/(cw·Na)	[9] [2]
638	$IO_2^- + I^- \rightarrow HOI(aq) + HOI(aq)$	$([H^+]^{2E0})$·2E10/((cw·Na))	[9] [2]
639	$HIO_2(aq) \rightarrow IO_2^-$	1.26E9	[9] [2]
640	$IO_2^- \rightarrow HIO_2(aq)$	$[H^+]$·5E10	[9] [2]
641	$HIO_3(aq) \rightarrow IO_3^-$	8.5E9	[9] [2]

[1] MCMv3.3.1 ; [2] Hoffmann et al. (2016) ; [3] Wu et al. (2014) ; [4] Berndt et al. (2019) ; [5] Kukui et al. (2003)
[6] Atkinson et al. (2007) ; [7] Sander et al. (2006) ; [8] Atkinson et al. (2008) ; [9] Braeuer et al. (2013) ; [10] Jacobson (2005)
[11] Demore et al. (1997) ; [12] Berndt et al. (2020) ; [13] Kahan et al. (2012) ; [14] Burkholder et al. (2015)
[E] Estimate based on equilibrium coefficients ; [C] Based on pKa value from COSMO*therm* ; [A] Assumed

…multiphase DMS mechanism continued

#	Reaction	Rate	Ref.
642	$IO_3^- \rightarrow HIO_3(aq)$	$[H^+]\cdot 5E10$	[9] [2]
643	$HIO_2(aq) + HOI(aq) \rightarrow IO_3^- + I^-$	2.4E2/(cw·Na)	[9] [2]
644	$IO_3^- + Iion \rightarrow HIO_2(aq) + HOI(aq)$	$([H^+]^{2E0})\cdot 1.2E3/((cw\cdot Na))$	[9] [2]
645	$IO_2^- + HOI(aq) \rightarrow IO_3^- + I^-$	2.4E2/(cw·Na)	[9] [2]
646	$IO_3^- + I^- \rightarrow IO_2^- + HOI(aq)$	$[H^+]\cdot 1.2E3/((cw\cdot Na))$	[9] [2]
647	$IO_2^- + IODINE2(aq) \rightarrow IO_3^- + I^- + I^-$	5.5E-5/(cw·Na)	[9] [2]
648	$IO_3^- + I^- + I^- \rightarrow IO_2^- + IODINE2(aq)$	$([H^+]^{2E0})\cdot 4.2E8/((cw\cdot Na)^{2E0})$	[9] [2]
649	$IBr(aq) + I^- \rightarrow IODINE2(aq) + Br^-$	2E9/(cw·Na)	[9] [2]
650	$IODINE2(aq) + Br^- \rightarrow IBr(aq) + I^-$	4.74E3/(cw·Na)	[9] [2]
651	$HOI(aq) + Cl^- \rightarrow ICl(aq)$	$[H^+]\cdot 2.9E10/((cw\cdot Na))$	[9] [2]
652	$ICl(aq) \rightarrow HOI(aq) + Cl^-$	2.4E6	[9] [2]
653	$HOI(aq) + Br^- \rightarrow IBr(aq)$	$[H^+]\cdot 4.1E12/((cw\cdot Na))$	[9] [2]
654	$IBr(aq) \rightarrow HOI(aq) + Br^-$	8E5	[9] [2]
655	$ICl(aq) + Cl^- \rightarrow ICl_2^-$	4.24E9/(cw·Na)	[9] [2]
656	$ICl_2^- \rightarrow ICl(aq) + Cl^-$	5.5E7	[9] [2]
657	$IBr(aq) + Br^- \rightarrow IBr_2^-$	4.93E6/(cw·Na)	[9] [2]
658	$IBr_2^- \rightarrow IBr(aq) + Br^-$	1.7E5	[9] [2]
659	$ICl(aq) + Br^- \rightarrow IClBr^-$	7.7E9/(cw·Na)	[9] [2]
660	$IClBr^- \rightarrow ICl(aq) + Br^-$	4.3E5	[9] [2]
661	$IBr(aq) + Cl^- \rightarrow IClBr^-$	5E4/(cw·Na)	[9] [2]
662	$IClBr^- \rightarrow IBr(aq) + Cl^-$	3.8E4	[9] [2]
663	$DMS(aq) + O_3(aq) \rightarrow DMSO(aq)$	8.61E8·exp(-2600·(1E0/T-1E0/298E0))/(cw·Na)	[2]
664	$DMS(aq) + OH(aq) \rightarrow DMSO(aq) + HO_2(aq)$	1.9E10/(cw·Na)	[2]
665	$DMS(aq) + Cl_2^- \rightarrow CH_3SCH_3Cl(aq) + Cl^-$	3E9/(cw·Na)	[2]
666	$DMS(aq) + Br_2^- \rightarrow CH_3SCH_3Br(aq) + Br^-$	3.2E9/(cw·Na)	[2]
667	$DMS(aq) + H_2O_2(aq) \rightarrow DMSO(aq)$	3.4E-2/(cw·Na)	[2]
668	$CH_3SCH_3Cl(aq) + O_2(aq) \rightarrow DMSO(aq) + ClO(aq)$	2.41E3/(cw·Na)	[9] [2]
669	$CH_3SCH_3Br(aq) + O_2(aq) \rightarrow DMSO(aq) + BrO(aq)$	6.02E2/(cw·Na)	[2]
670	$DMSO(aq) + O_3(aq) \rightarrow DMSO_2(aq)$	3E0/(cw·Na)	[2]
671	$DMSO(aq) + OH(aq) \rightarrow MSIA(aq)$	6.65E9·exp(-1270·(1E0/T-1E0/298E0))/(cw·Na)	[2]
672	$DMSO(aq) + SO_4^- \rightarrow DMSO^- + SO_4^{\ 2-}$	2.97E9·exp(-1440·(1E0/T-1E0/298E0))/(cw·Na)	[2]
673	$DMSO(aq) + Cl(aq) \rightarrow CH_3SOCH_3Cl(aq)$	6.3E9/(cw·Na)	[2]
674	$DMSO(aq) + Cl_2^- \rightarrow CH_3SOCH_3Cl(aq) + Cl^-$	1.6E7/(cw·Na)	[2]
675	$DMSO(aq) + H_2O_2(aq) \rightarrow DMSO_2(aq)$	2.75E-6/(cw·Na)	[2]
676	$DMSO^- + Br^- \rightarrow CH_3SOCH_3Br(aq)$	5E9/(cw·Na)	[2]
677	$CH_3SOCH_3Br(aq) + Br^- \rightarrow DMSO(aq) + Br_2^-$	2.6E8/(cw·Na)	[2]
678	$CH_3SOCH_3Cl(aq) \rightarrow MSIA(aq) + HCl(aq)$	$m(H_2O)\cdot 1E7$	[2]
679	$CH_3SOCH_3OH(aq) \rightarrow MSIA(aq)$	1E7	[2]
680	$DMSO_2(aq) + OH(aq) \rightarrow CH_3SO_2CH_2(aq)$	1.77E7·exp(-1690·(1E0/T-1E0/298E0))/(cw·Na)	[2]
681	$DMSO_2(aq) + SO_4^- \rightarrow CH_3SO_2CH_2(aq) + SO_4^{2-}$	3.95E6·exp(-1360·(1E0/T-1E0/298E0))/(cw·Na)	[2]
682	$DMSO_2(aq) + Cl(aq) \rightarrow CH_3SO_2CH_2(aq) + HCl(aq)$	8.2E5/(cw·Na)	[2]
683	$DMSO_2(aq) + Cl_2^- \rightarrow CH_3SO_2CH_2(aq) + HCl(aq) + Cl^-$	8.24E3/(cw·Na)	[2]
684	$DMSO_2(aq) + O_2(aq) \rightarrow CH_3SO_2CH_2O_2(aq)$	2E9/(cw·Na)	[2]
685	$MSIA(aq) + O_3(aq) \rightarrow CH_3SO_3H(aq)$	3.5E7/(cw·Na)	[2]
686	$MSIA(aq) + OH(aq) \rightarrow CH_3SO_3H_2(aq)$	6E9/(cw·Na)	[2]
687	$CH_3SO_2^- + OH(aq) \rightarrow CH_3SO_2(aq)$	0.9·1.2E10/(cw·Na)	[2]
688	$CH_3SO_2^- + OH(aq) \rightarrow HSO_3^-$	0.1·1.2E10/(cw·Na)	[2]
689	$CH_3SO_2^- + SO_4^- \rightarrow CH_3SO_2(aq) + SO_4^{2-}$	1E9/(cw·Na)	[2]
690	$CH_3SO_2^- + Cl_2^- \rightarrow CH_3SO_2(aq) + Cl^- + Cl^-$	8E8/(cw·Na)	[2]
691	$CH_3SO_2^- + H_2O_2(aq) \rightarrow CH_3SO_3^-$	1.2E-2/(cw·Na)	[2]
692	$CH_3SO_2^- + O_3(aq) \rightarrow CH_3SO_3^-$	2E6/(cw·Na)	[2]
693	$CH_3SO_3H_2(aq) + O_2(aq) \rightarrow CH_3SO_3H(aq) + HO_2(aq)$	1.2E9/(cw·Na)	[2]
694	$CH_3SO_3H(aq) + OH(aq) \rightarrow CH_2SO_3H(aq)$	1.5E7/(cw·Na)	[2]
695	$CH_3SO_3^- + OH(aq) \rightarrow CH_2SO_3^-$	1.29E7·exp(-2630·(1E0/T-1E0/298E0))/(cw·Na)	[2]

[1] MCMv3.3.1 ; [2] Hoffmann et al. (2016) ; [3] Wu et al. (2014) ; [4] Berndt et al. (2019) ; [5] Kukui et al. (2003)
[6] Atkinson et al. (2007) ; [7] Sander et al. (2006) ; [8] Atkinson et al. (2008) ; [9] Braeuer et al. (2013) ; [10] Jacobson (2005)
[11] Demore et al. (1997) ; [12] Berndt et al. (2020) ; [13] Kahan et al. (2012) ; [14] Burkholder et al. (2015)
[E] Estimate based on equilibrium coefficients ; [C] Based on pKa value from COSMO*therm* ; [A] Assumed

#	Reaction	Rate	Ref.
696	$CH_3SO_3^- + SO_4^- \rightarrow CH_3SO_3(aq) + SO_4^{2-}$	1.13E4·exp(-2490·(1E0/T-1E0/298E0))/(cw·Na)	[2]
697	$CH_3SO_3^- + Cl(aq) \rightarrow CH_3SO_3(aq) + Cl^-$	4.9E5/(cw·Na)	[2]
698	$CH_3SO_3^- + Cl_2^- \rightarrow CH_3SO_3(aq) + Cl^- + Cl^-$	3.89E3/(cw·Na)	[2]
699	$CH_3SO_2(aq) + OH(aq) \rightarrow CH_3SO_3H(aq)$	1E10/(cw·Na)	[2]
700	$CH_3SO_2(aq) + O_3(aq) \rightarrow CH_3SO_3(aq)$	1.5E9/(cw·Na)	[2]
701	$CH_3SO_2(aq) + SO_3^{2-} \rightarrow CH_3SO_2^- + SO_4^{2-}$	1.7E9/(cw·Na)	[2]
702	$CH_3SO_2(aq) \rightarrow SO_2(aq)$	8.3E4	[2]
703	$CH_3SO_2(aq) + O_2(aq) \rightarrow CH_3SO_2O_2(aq)$	1.2E9/(cw·Na)	[2]
704	$CH_3SO_2(aq) + CH_3SO_2(aq) \rightarrow$ MSIA(aq) + $CH_3SO_3H(aq)$	8E8/(cw·Na)	[2]
705	$CH_3SO_2O_2(aq) + CH_3SO_2^- \rightarrow CH_3SO_3^- + CH_3SO_3(aq)$	6.2E8/(cw·Na)	[2]
706	$CH_3SO_3(aq) + CH_3SO_2^- \rightarrow CH_3SO_3^- + CH_3SO_2(aq)$	1E8/(cw·Na)	[2]
707	$CH_3SO_3(aq) \rightarrow SO_3(aq)$	8.3E4	[2]
708	$CH_3SO_3(aq) + HO_2(aq) \rightarrow CH_3SO_3H(aq)$	8.3E5/(cw·Na)	[2]
709	$CH_2SO_3H(aq) + O_2(aq) \rightarrow O_2CH_2SO_3H(aq)$	2E9/(cw·Na)	[2]
710	$CH_2SO_3^- + O_2(aq) \rightarrow O_2CH_2SO_3^-$	2E9/(cw·Na)	[2]
711	$O_2CH_2SO_3^- \rightarrow$ HCHO(aq) + SO_3^-	[H$^+$]·7E3	[2]
712	MSIA(aq) $\rightarrow CH_3SO_2^-$	1.2E8	[C]
713	$CH_3SO_2^- \rightarrow$ MSIA(aq)	[H$^+$]·5E10	[C]
714	$CH_3SO_3H(aq) \rightarrow CH_3SO_3^-$	4.25E13	[C]
715	$CH_3SO_3^- \rightarrow CH_3SO_3H(aq)$	[H$^+$]·5E10	[C]
716	$H_2SO_4(aq) \rightarrow HSO_4^-$	2.4E19	[2]
717	$HSO_4^- \rightarrow H_2SO_4(aq)$	[H$^+$]1E10	[2]
718	$HNO_3(aq) \rightarrow NO_3^-$	1E10·12E0·exp(29.17·(298./T-1E0) +16.83·(1E0+log(298./T)-298./T))	[2]
719	$NO_3^- \rightarrow HNO_3(aq)$	[H$^+$]1E10	[2]
720	$O_2CH_2SO_3H(aq) \rightarrow O_2CH_2SO_3^-$	3.65E12	[2]
721	$O_2CH_2SO_3^- \rightarrow O_2CH_2SO_3H(aq)$	[H$^+$]·5E10	[2]
722	Cl^- + DMSO$^-$ $\rightarrow CH_3SOCH_3Cl(aq)$	1E10/(cw·Na)	[2]
723	$CH_3SOCH_3Cl(aq) \rightarrow Cl^-$ + DMSO$^-$	3.03E7	[2]
724	DMSO$^-$ $\rightarrow CH_3SOCH_3OH(aq)$	m(H_2O)·1.25E5	[2]
725	$CH_3SOCH_3OH(aq) \rightarrow$ DMSO$^-$	[H$^+$]·5E10	[2]
726	HPMTF(aq) + OH(aq) $\rightarrow HOOCH_2SCO(aq)$	1E10/(cw·Na)	[E*]
727	$SO_2(aq) \rightarrow HSO_3^-$	1E12	[E][2]
728	$HSO_3^- \rightarrow SO_2(aq)$	[H$^+$]·(1E12/(1.71E-2·exp(7.04E0·(298E0/T-1E0))))	[E][2]
729	$HSO_3^- \rightarrow SO_3^{2-}$	1E12	[E][2]
730	$SO_3^{2-} \rightarrow HSO_3^-$	[H$^+$]·(1E12/(5.99E-8·exp(3.74E0·(298E0/T-1E0))))	[E][2]
731	$HSO_4^- \rightarrow SO_4^{2-}$	1E12	[E][2]
732	$SO_4^{2-} \rightarrow HSO_4^-$	[H$^+$]·(1E12/(1.02E-2·(exp(8.85E0·(298E0/T-1E0)) +25.14·(1E0-298E0/T+log(298E0/T)))))	[E][2]
733	$HO_2(aq) \rightarrow O_2^-$	1E12	[E][10]
734	$O_2^- \rightarrow HO_2(aq)$	[H$^+$]·(1E12/3.5E-5)	[E] [10]
735	$H_2O_2(aq) \rightarrow HO_2^-$	1E12	[E][10]
736	$HO_2^- \rightarrow H_2O_2(aq)$	[H$^+$]·(1E12/(2.21E-12·exp(-12.52E0·(298E0/T-1E0))))	[E][10]
737	$H_2O_2(aq) + HSO_3^- \rightarrow HSO_4^-$	([H$^+$]·(7.45E7·exp(-15.96E0·(298E0/T-1E0)))	[2]
738	$HSO_3^- + HO_2(aq) \rightarrow HSO_4^- + OH(aq)$	4.35E5/(cw·Na)	[2]
739	$SO_3^{2-} + HO_2(aq) \rightarrow SO_4^{2-} + OH(aq)$	5.65E5/(cw·Na)	[2]
740	$HSO_3^- + O_2^- \rightarrow HSO_4^- + OH(aq)$	4.35E4/(cw·Na)	[2]
741	$SO_3^{2-} + O_2^- \rightarrow SO_4^{2-} + OH(aq)$	5.65E4/(cw·Na)	[2]
742	$HSO_3^- + OH(aq) \rightarrow SO5^-$	4.2E9·exp(-5.03E0·(298E0/T-1E0))/(cw·Na)	[2]
743	$SO_3^{2-} + OH(aq) \rightarrow SO5^-$	4.6E9·exp(-5.03E0·(298E0/T-1E0))/(cw·Na)	[2]
744	$SO_2(aq) + O_3(aq) \rightarrow HSO_4^-$	2.4E4/(cw·Na)	[2]
745	$HSO_3^- + O_3(aq) \rightarrow HSO_4^-$	3.7E5·exp(-18.56E0·(298E0/T-1E0))/(cw·Na)	[2]
746	$SO_3^{2-} + O_3(aq) \rightarrow SO_4^{2-}$	1.5E9·exp(-17.72E0·(298E0/T-1E0))/(cw·Na)	[2]

[1] MCMv3.3.1 ; [2] Hoffmann et al. (2016) ; [3] Wu et al. (2014) ; [4] Berndt et al. (2019) ; [5] Kukui et al. (2003)
[6] Atkinson et al. (2007) ; [7] Sander et al. (2006) ; [8] Atkinson et al. (2008) ; [9] Braeuer et al. (2013) ; [10] Jacobson (2005)
[11] Demore et al. (1997) ; [12] Berndt et al. (2020) ; [13] Kahan et al. (2012) ; [14] Burkholder et al. (2015)
[E] Estimate based on equilibrium coefficients ; [C] Based on pKa value from COSMO*therm* ; [A] Assumed

#	Reaction	Rate	Ref.
747	$HSO_3{}^- + SO5^- \rightarrow HSO5^- + SO5^-$	3E5·exp(-10.4E0·(298E0/T-1E0))/(cw·Na)	[2]
748	$SO_3^{2-} + SO5^- \rightarrow HSO5^- + SO5^-$	1.3E7·exp(-6.71E0·(298E0/T-1E0))/(cw·Na)	[2]
749	$HSO_3{}^- + SO_4{}^- \rightarrow HSO_4{}^- + SO5^-$	1.3E9·exp(-5.03E0·(298E0/T-1E0))/(cw·Na)	[2]
750	$SO_3^{2-} + SO_4{}^- \rightarrow SO_4^{2-} + SO5^-$	5.3E8·exp(-5.03E0·(298E0/T-1E0))/(cw·Na)	[2]
751	$HSO_3{}^- + HSO5^- \rightarrow HSO_4{}^- + HSO_4{}^-$	7.1E6·exp(-10.47E0·(298E0/T-1E0))/(cw·Na)	[2]
752	$H_2O_2(aq) + OH(aq) \rightarrow HO_2(aq)$	2.7E7·exp(-5.7E0·(298E0/T-1E0))/(cw·Na)	[2]
753	$H_2O_2(aq) + SO_4{}^- \rightarrow HO_2(aq) + SO_4^{2-}$	1.2E3·exp(-6.71E0·(298E0/T-1E0))/(cw·Na)	[2]
754	$OH(aq) + HO_2(aq) \rightarrow DUMMY$	7E9·exp(-5.03E0·(298E0/T-1E0))/(cw·Na)	[2]
755	$OH(aq) + O_2{}^- \rightarrow DUMMY$	1E10·exp(-5.03E0·(298E0/T-1E0))/(cw·Na)	[2]
756	$OH(aq) + HSO5^- \rightarrow SO5^-$	1.7E7·exp(-6.38E0·(298E0/T-1E0))/(cw·Na)	[2]
757	$O_2{}^- + O_3(aq) \rightarrow OH(aq)$	1.5E9·exp(-5.03E0·(298E0/T-1E0))/(cw·Na)	[2]
758	$HO_2(aq) + HO_2(aq) \rightarrow H_2O_2(aq)$	8.6E5·exp(-7.94E0·(298E0/T-1E0))/(cw·Na)	[2]
759	$HO_2(aq) + O_2{}^- \rightarrow H_2O_2(aq)$	1E8·exp(-5.03E0·(298E0/T-1E0))/(cw·Na)	[2]
760	$HO_2(aq) + SO_4{}^- \rightarrow SO_4^{2-}$	5E9·exp(-5.03E0·(298E0/T-1E0))/(cw·Na)	[2]
761	$O_2{}^- + SO_4{}^- \rightarrow SO_4^{2-}$	5E9·exp(-5.03E0·(298E0/T-1E0))/(cw·Na)	[2]
762	$O_2{}^- + SO5^- \rightarrow HSO5^-$	1E8·exp(-5.03E0·(298E0/T-1E0))/(cw·Na)	[2]
763	$SO5^- + SO5^- \rightarrow SO_4{}^- + SO_4{}^-$	6E8·exp(-5.03E0·(298E0/T-1E0))/(cw·Na)	[2]
764	$NH_3(aq) \rightarrow NH_4{}^-$	$[H^+]$·1E10	[E]
765	$NH_4{}^- \rightarrow NH_3(aq)$	1E10/(1.7882E9·exp(21.0200·(298E0/T-1E0)))	[E]
766	$SO_3(aq) \rightarrow HSO_4^-$	1E10	[A]

[1] MCMv3.3.1 ; [2] Hoffmann et al. (2016) ; [3] Wu et al. (2014) ; [4] Berndt et al. (2019) ; [5] Kukui et al. (2003)
[6] Atkinson et al. (2007) ; [7] Sander et al. (2006) ; [8] Atkinson et al. (2008) ; [9] Braeuer et al. (2013) ; [10] Jacobson (2005)
[11] Demore et al. (1997) ; [12] Berndt et al. (2020) ; [13] Kahan et al. (2012) ; [14] Burkholder et al. (2015)
[E] Estimate based on equilibrium coefficients ; [C] Based on pKa value from COSMO*therm* ; [A] Assumed

S1.1 Chamber wall effects

Table S2: Temperature dependant Henry's law solubility and wall mass accommodation coefficients . COSMO*therm* calculation were estimated at 298K and coupled with temperature dependence from other sources.

Type	H^{cp}	α_w	Ref.
Cl_2	9.15E-2·exp(2490E0·(1E0/T-1E0/298E0))	-	[1]
Cl	0.2E0	-	[1]
ClO	660E0·exp(5862E0·(1E0/T-1E0/298E0))	-	[1]
ClO_2	1E0·exp(-3300E0·(1E0/T-1E0/298E0))	-	[1]
HCl	1.1E0·exp(2020E0·(1E0/T-1E0/298E0))	-	[1]
HOCl	660E0·exp(5862E0·(1E0/T-1E0/298E0))	-	[1]
ClNO	5E-2	-	[1]
$ClNO_2$	4.6E-2	-	[1]
$ClNO_3$	2.1E5·exp(8700E0·(1E0/T-1E0/298E0))	-	[1]
Br_2	0.76E0·exp(4100E0·(1E0/T-1E0/298E0))	-	[1]
Br	1.2E0	-	[1]
BrO	93E0·exp(5862E0·(1E0/T-1E0/298E0))	-	[1]
$BrNO_2$	0.3	-	[1]
$BrNO_3$	2.1E5·exp(8700E0·(1E0/T-1E0/298E0))	-	[1]
BrCl	0.94E0·exp(5600E0·(1E0/T-1E0/298E0))	-	[1]
I_2	3E0·exp(4431E0·(1E0/T-1E0/298E0))	-	[1]
I	8E-2	-	[1]
IO	450E0·exp(5862E0·(1E0/T-1E0/298E0))	-	[1]
OIO	2.1E5·exp(8700E0·(1E0/T-1E0/298E0))	-	[1]
I_2O_2	2.1E5·exp(8700E0·(1E0/T-1E0/298E0))	-	[1]
HI	2.5E0·exp(9800E0·(1E0/T-1E0/298E0))	-	[1]

[1] Braeuer et al. (2013) ; [2] Jacobson (2005) ; [3] Hoffmann et al. (2016)
[4] Kulmala and Laaksonen (1990) ; [C] COSMO*therm* with temperature dependence from Hoffmann et al. (2016); [A] Assumed

. . . Solubility continued

Type	H^{cp}	α_w	Ref.
HOI	450E0·exp(5862E0·(1E0/T-1E0/298E0))	-	[1]
HIO_3	2.1E5·exp(8700E0·(1E0/T-1E0/298E0))	-	[1]
INO_2	2.1E5·exp(8700E0·(1E0/T-1E0/298E0))	-	[1]
INO_3	2.1E5·exp(8700E0·(1E0/T-1E0/298E0))	-	[1]
ICl	110E0·exp(5600E0·(1E0/T-1E0/298E0))	-	[1]
IBr	24E0·exp(5600E0·(1E0/T-1E0/298E0))	-	[1]
O_3	1.13E-2·exp(7.72·(298E0/T-1E0))	1E-7	[2]
OH	2.5E1·exp(22.21·(298E0/T-1E0))	1E-5	[2]
H_2O_2	9.1E2·101.325·exp(6600·(1E0/T-1E0/298E0))	1E0	[2]
DMS	0.56E0·exp(4480E0·(1E0/T-1E0/298E0))	1E-7	[3]
DMSO	2.43E5·exp(2580E0·(1E0/T-1E0/298E0))	1E-5	[3]
$DMSO_2$	1.18E6·exp(5390E0·(1E0/T-1E0/298E0))	1E-5	[3]
MSIA	1.69E6·exp(1760E0·(1E0/T-1E0/298E0))	1E-5	[C]
HPMTF	1.33E4	1E-5	[C]
SO_2	1.22E0*EXP(10.55*(298E0/TEMP-1E0))	1E-7	[2]
HO_2	2E3*EXP(22.28*(298E0/TEMP-1E0))	1E-5	[2]
NO_3	2.1E5*EXP(29.19*(298E0/TEMP-1E0))	1E-5	[2]
HCHO	3.46E0*EXP(8.19*(298E0/TEMP-1E0))	1E-5	[2]
NO_2	1E-2*EXP(8.38*(298E0/TEMP-1E0))	1D.7	[2]
O_2	1.3E-3	1E-5	[2]
SO_3	1E5	1E-5	[A]
NH_3	57.6*EXP(13.79*(298./TEMP-1E0) -5.39*(1E0+log(298./TEMP)-298./TEMP))	1E0	[2]
HNO_3	2.1E5·exp(8700.0·(1E0/T-1E0/298.15))	1E0	[2]
H_2SO_4	1E0/(98E-3·exp(-11.695E0+10156E0·(1E0/360.15E0-1E0/T +0.38E0/545E0·(1E0+log(360.15/T)-360.15/T))))	1E0	[4]
MSA	1.13E8·exp(1760E0·(1E0/T-1E0/298E0))	1E0	[C]

[1] Braeuer et al. (2013) ; [2] Jacobson (2005) ; [3] Hoffmann et al. (2016)
[4] Kulmala and Laaksonen (1990) ; [C] COSMO*therm* with temperature dependence from Hoffmann et al. (2016); [A] Assumed

S2 Model setup and additional results

A preliminary version of the ADCHAM model was used to present model results on the dry experiments DMS2-4 in Rosati et al. (2021). Figures S27, S28 and S29 thus includes experimental data from Rosati et al. (2021) and similar but not identical model results. A Key difference between the two model setups includes an increase in the LWC from 3.5·10^{-7} g m^{-3} utilised by Rosati et al. (2021) to 3 mg m^{-3}. In Rosati et al. (2021) the model was constrained based on the non-corrected AMS particle mass. The change in LWC reflects the change in PM from the SMPS corrected AMS measurements used in this study. The large increase in LWC was partly compensated by decreasing the coefficient of eddy diffusion from 0.1 s^{-1} (used by Rosati et al. (2021)) to 0.02 s^{-1}. Furthermore, the friction velocity (u^*) and electric field strength (E_{field}) governing the wall loss of non-charged and charged particles, respectively, had to be modified in order to reproduce the SMPS corrected AMS PM. Values were decreased resulting in a smaller particle wall loss from u^* = 0.02 m s^{-1} and E_{field} = 10, 10 and 5 V cm^{-1} for experiment DMS 2-4 in Rosati et al. (2021), to u^* = 0.013 m s^{-1} and E_{field} = 2.5, 0.2 and 4.0 V cm^{-1}.

Ammonia concentrations in the AURA chamber were modelled explicitly in the new improved model setup by assuming an initial pool of dissolved ammonium-sulfate on the chamber walls, evaporating as NH_3 based on the LWC, acidity of the water film and temperature. Consequently, the influx of ammonia to the gas-phase varied in between experiments performed on different dates. This was not the case in Rosati et al. (2021), in which we used a fixed flux of ammonia into the chamber from the chamber wall.

S2.1 Chamber compaction and dilution due to instrument sampling

We simulated the gradual dilution of the smog chamber because of the instrument sampling and air entrainment from outside the chamber. The Teflon bag in AURA is mounted in a fixed metal frame. Based on the observations of the smog chamber we estimate that the chamber volume can be compressed from initially 5 m^3 to a minimum volume of 3 m^3 because of the instrument sampling. In the model we simulate the chamber volume compaction and gradually increasing air entrainment using a simplified parameterization which describe the fraction of the sampled air that result in a decreasing chamber volume:

$$f_{\text{compaction}} = (V(t) - V_{\text{min}})/(V_0 - V_{\text{min}}) \quad (1)$$

($V(t)$), (V_{min}) and (V_0) denote the chamber volume at time (t), the estimated minimum chamber volume (3 m^3) in AURA and the initial chamber volume (5 m^3) respectively. The remaining fraction of the sampled air ($1 - f_{\text{compaction}}$) was assumed to be particle free air mixed into the chamber from outside, which resulted in a gradual dilution of the species concentrations in the chamber.

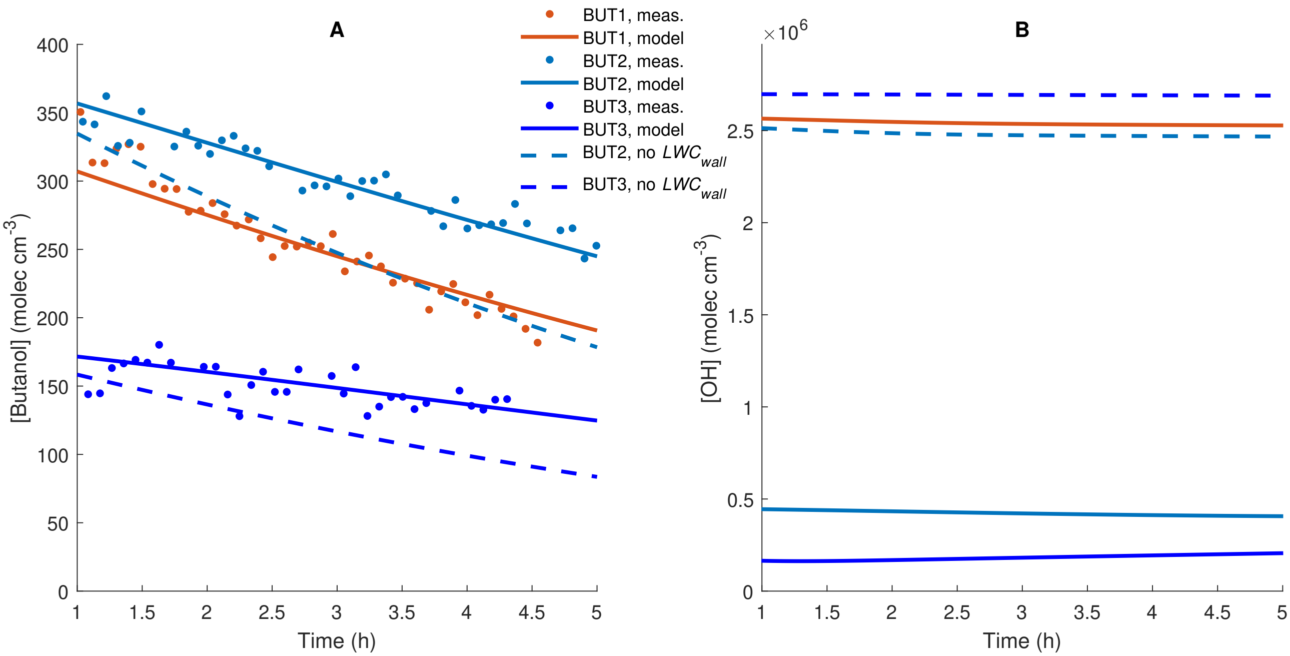

Figure S1. Model results and observations from three butanol experiments (BUT1-3). Panel **A**: Modelled and observed butanol concentrations. Panel **B**: Modelled OH concentration. BUT1: 293 K, RH ~ 5 %; BUT2: 293 K, RH 50-60 %; BUT3: 273 K, RH 70-80 %. The dashed lines show the model results from simulations without a liquid water film on the chamber walls. Experiment BUT-1 is described in detail in Rosati et al. (2021) and experimental data for this experiment is adopted from Rosati et al. (2021).

S2.2 Estimated wall liquid water content based on Butanol experiments

Fig. S1 shows the modelled and observed butanol decay and modelled OH concentrations during three different butanol experiments. In order to capture the observed butanol decay during humid experiments BUT2 and BUT3 we had to introduce a liquid water film corresponding to an effective liquid water content (LWC) of $\sim$30 g/m^3 and $\sim$500 g/m^3 on the chamber walls respectively. The LWC on the walls allow the highly water soluble H_2O_2, which serve as the main OH source, to be taken up efficiently on the chamber walls. The observed and modelled butanol loss rates are governed both by the chamber dilution and the OH oxidation. In the humid experiments (BUT2-3) the dilution is larger than in the dry experiment (BUT1) because of an inflow of 2 L/min of humidified air. In the dry experiment (BUT1) their is some indication that the butanol decay is slightly faster in the observations than in the model. This could possibly be a result of underestimated OH recycling in the MCMv3.3.1 butanol chemistry. When the model is run without any butanol the modelled OH concentration become $\sim$10 % larger. However, it may also be due to slightly underestimated chamber dilution in the model.

S2.3 COSMO*therm* calculations

We followed recommendations by Kurtén et al. (2018) in selecting conformers containing no intramolecular H-bonds as input for the COSMO*therm* calculations. This method has shown to give more accurate saturation vapour pressure estimates of multifunctional compounds that are able to form intramolecular H-bonds (Kurtén et al., 2018). The input files were computed at the BP/def2-TZVPD-FINE//BP/def-TZVP level of theory using the COSMO*conf* and TURBOMOLE programs (COSMO*conf*, 2013; TURBOMOLE, 2010).

Henry's law coefficients were calculated using COSMO*therm*-estimated saturation vapour pressure of the pure compound i (p_{sat}) and activity coefficient of compound i at infinite dilution in water (γ_i^w, with respect to pure compound reference state):

$$H_i^{cp} = \frac{1}{M_w \times p_{\mathrm{sat},i} \times \gamma_i^w} \tag{2}$$

This approach assumes low aqueous solubility for the compounds ($x_{\mathrm{sol},i}^w = 1/\gamma_i^w$), which means that the molar mass of the solution can be approximated using the molar mass of the solvent water (M_w). Table S3 shows the COSMO*therm*-estimated saturation vapour pressures and aqueous activity coefficients, as well as Henry's law coefficients calculated using the COSMO*therm* estimates.

Table S3. COSMO*therm*-estimated saturation vapour pressures, pKa and aqueous activity coefficients at 298.15 K, and Henry's law coefficients calculated from the two COSMO*therm* estimates.

	p_{sat} [atm]	γ^w	H^{cp} [mol atm^{-1} kg^{-1}]	pKa
HPMTF-hydrate	2.49×10^{-7}	2.80×10^{-1}	7.96×10^{8}	10.46
HPMTF	2.37×10^{-4}	1.76×10^{1}	1.33×10^{4}	10.30
DMSO	1.73×10^{-3}	1.32×10^{-1}	2.43×10^{5}	22.36
DMSO2	1.91×10^{-5}	2.46	1.18×10^{6}	20.38
MSA	4.16×10^{-7}	1.18	1.13×10^{8}	-2.93
MSIA	1.51×10^{-5}	2.18	1.69×10^{6}	2.62

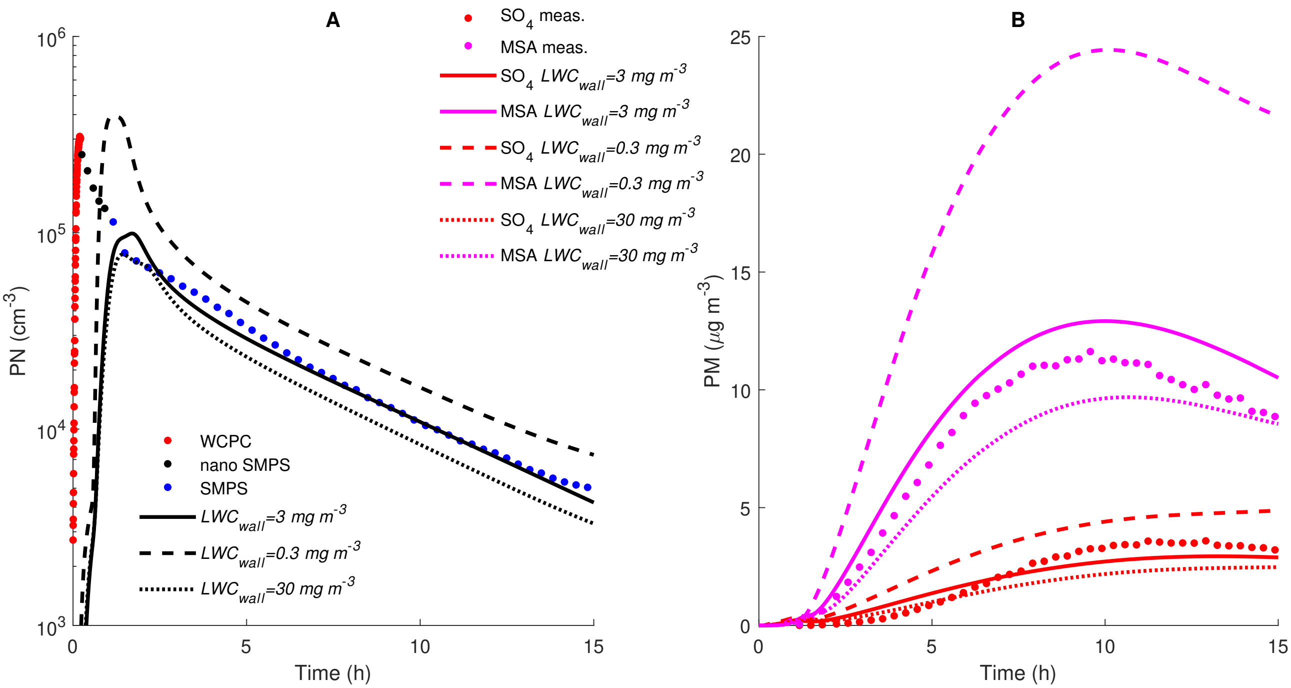

Figure S2. Modelled and measured particle number concentration (panel **A**) and particle MSA and SO_4 mass concentrations (panel **B**) for the dry chamber experiment DMS2. The model results are from different sensitivity runs with different LWC on the chamber walls.

S2.4 Sensitivity runs with variable wall liquid water content

To constrain the effect of different liquid water content on the chamber walls (LWC_{wall}), for the secondary aerosol formation from DMS, we performed several model sensitivity tests. Fig S2-S4 summarises the results from one dry experiment (DMS2) and the two humid experiments DMS6 and DMS7.

When the LWC_{wall} is lowered with one order of magnitude compared to the default model setup ($LWC_{wall} = 3\ \mathrm{mgm^{-3}}$), for the dry experiment, the ammonia gas-phase concentration increases. This results in higher new particle formation (NPF) and total particle number concentration. The lower LWC_{wall} also prevent the uptake and oxidation of MSIA on the chamber walls, and thereby increases the formation of MSA and SA in the gas-phase and the secondary SA and MSA particle mass (PM) formation (Fig. S2B). The opposite effect is seen when the LWC_{wall} is increased compared to the default model setup.

For the humid experiments the LWC_{wall} serve as an efficient sink for the $H_2O_2(g)$ which results in substantially lower $HO_2(g)$ concentrations compared to the dry experiments. This promote the SA formation via thermal decomposition of CH_3SO_3 in front of the MSA production via $CH_3SO_3 + HO_2$. Thus, lowering the LWC_{wall} with one order of magnitude compared to the default model setup for experiment DMS6 result in lower SA and decreasing NPF (Fig. S3A), despite that the $NH_3(g)$ concentration increases. This also results in overestimated MSA PM formation and delayed SO_4 PM formation (Fig. S3B). When the LWC_{wall} instead is increased with one order of magnitude compared to the default setup, the model underestimates the MSA PM and overestimates the SO_4 PM in the end of the model simulation (Fig. S3B). Increasing LWC_{wall} has minor impact on the particle number concentrations. This time it is the $NH_3(g)$ concentration which become the limiting factor for the NPF. Fig. S3 shows the model results from a simulation with $LWC_{wall} = 30\ \mathrm{gm^{-3}}$, i.e. the same LWC_{wall} as was estimated from the humid butanol experiment BUT2. With this LWC_{wall} value the modelled particle number concentration and SO_4 PM are in close agreement with the observations, however the model underestimate the maximum PM MSA with 20-30 %.

The increasing particle mass formation in the end of the simulations in experiment DMS6 is governed by the increasing $NH_3(g)$ concentration (Fig S5), which result in a second weaker NPF event. The modelled PM mass increase is mainly a result of that the non-charged newly formed particles are less efficiently lost to the walls than the aged charged particles, and that the NPF increases the particle condensation sink. This tendency of increasing PM in the end of the experiment is not seen in the observations, which may indicate that the model overestimate the $NH_3(g)$ evaporation from the chamber walls in the end of this experiment.

For the humid and cold experiment DMS7 the modelled SO_4 PM is relatively insensitive to different LWC_{wall} values (Fig. S4). However, the model strongly overestimates the MSA PM if we use the same LWC_{wall} as for the default DMS6 model setup, i.e. LWC_{wall} =15 $\mathrm{gm^{-3}}$. The closest agreement between the modelled and measured MSA is found when the $LWC_{wall} = 500\ \mathrm{gm^{-3}}$, i.e. similar LWC_{wall} as was estimated from the humid and cold butanol experiment BUT3 (Fig. S1).

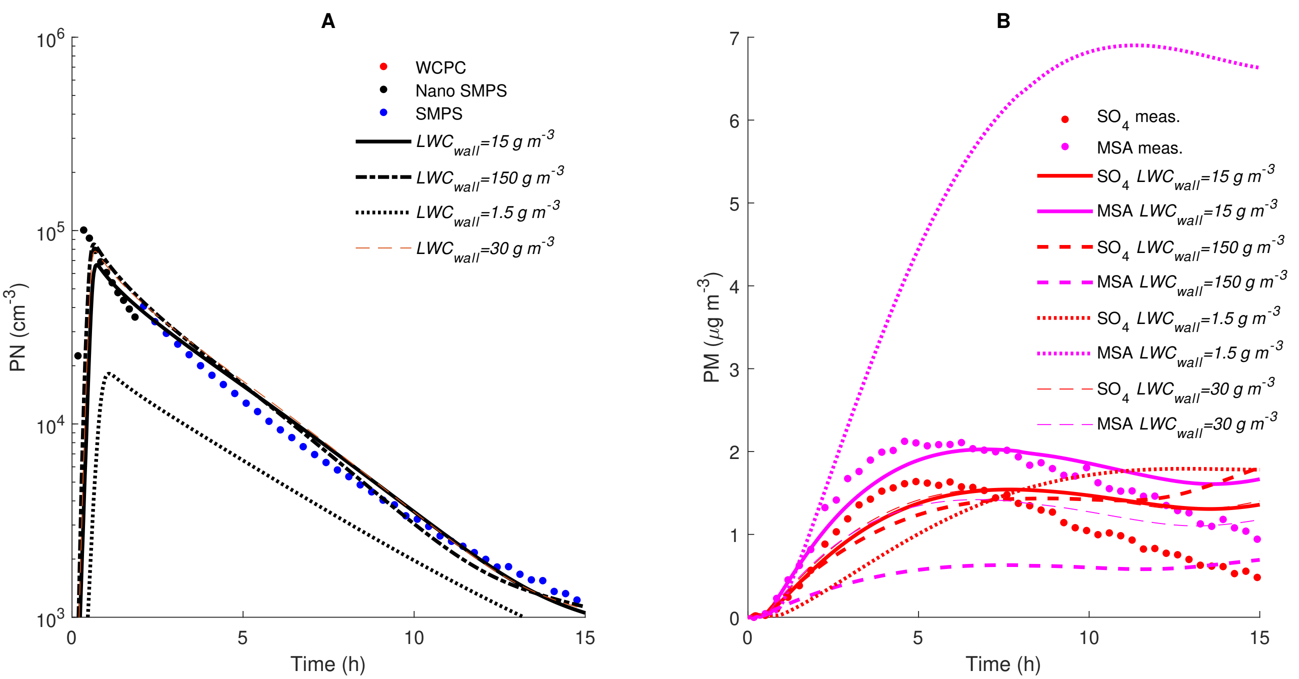

Figure S3. Modelled and measured particle number concentration (panel **A**) and particle MSA and SO_4 mass concentrations (panel **B**) for the humid chamber experiment DMS6. The model results are from different sensitivity runs with different LWC on the chamber walls.

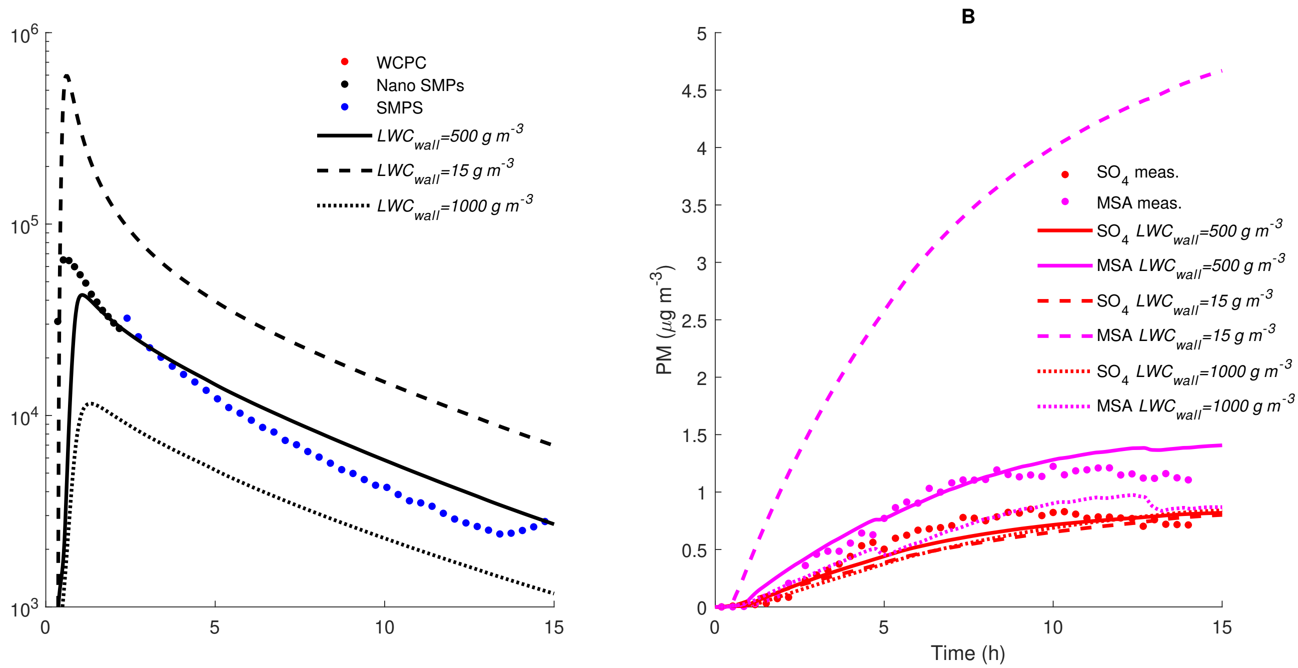

Figure S4. Modelled and measured particle number concentration (panel **A**) and particle MSA and SO_4 mass concentrations (panel **B**) for the humid and cold chamber experiment DMS7. The model results are from different sensitivity runs with different LWC on the chamber walls.

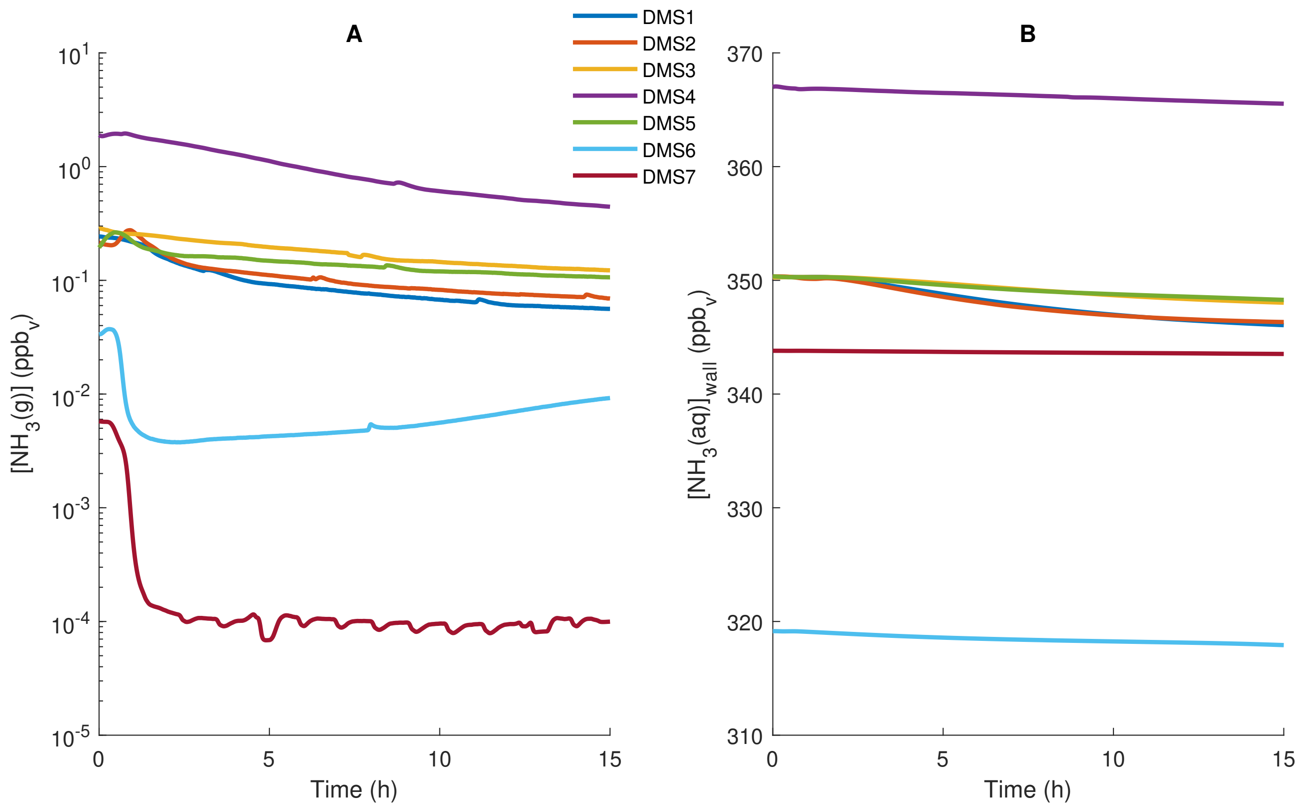

Figure S5. Modelled NH_3 concentration in the gas-phase (panel **A**) and on the chamber walls (panel **B**) for all base case model simulations of experiments DMS1-7.

S2.5 Modelled NH_3 concentrations

Figure S5 shows the modelled NH_3 concentration in the gas-phase (Fig. S5A) and on the walls (Fig. S5B) for all simulated DMS experiments. The $NH_3(g)$ concentration is governed by the loss of $NH_3(g)$ to the aerosol particle phase, the acidity of the wall liquid water and the leakage of $NH_3(g)$ into the chamber. In all dry experiments DMS1-5 the aerosol particle condensation sink (dissolution) term is greater than the evaporation of $NH_3(g)$ from the chamber walls which result in gradually decreasing NH_3 concentration both in the gas-phase and on the chamber walls. In the humid experiments DMS6 and DMS7 the condensation sink term is larger than the evaporation rate of NH_3 from the walls during the onset of the NPF in the chamber, which result in rapidly decreasing $NH_3(g)$. The very low $NH_3(g)$ concentration in DMS7 compared to the other experiments is a result of the thick liquid water film on the walls and the low temperature. The ripples in the modelled $NH_3(g)$ concentrations, mainly observed in DMS7, is caused by small temperature fluctuations of ± 1 K. The slowly increasing $NH_3(g)$ concentration in DMS6 during the second half of the model simulation is a result of decreasing secondary aerosol formation and ceasing uptake of $NH_3(g)$ to the particle phase.

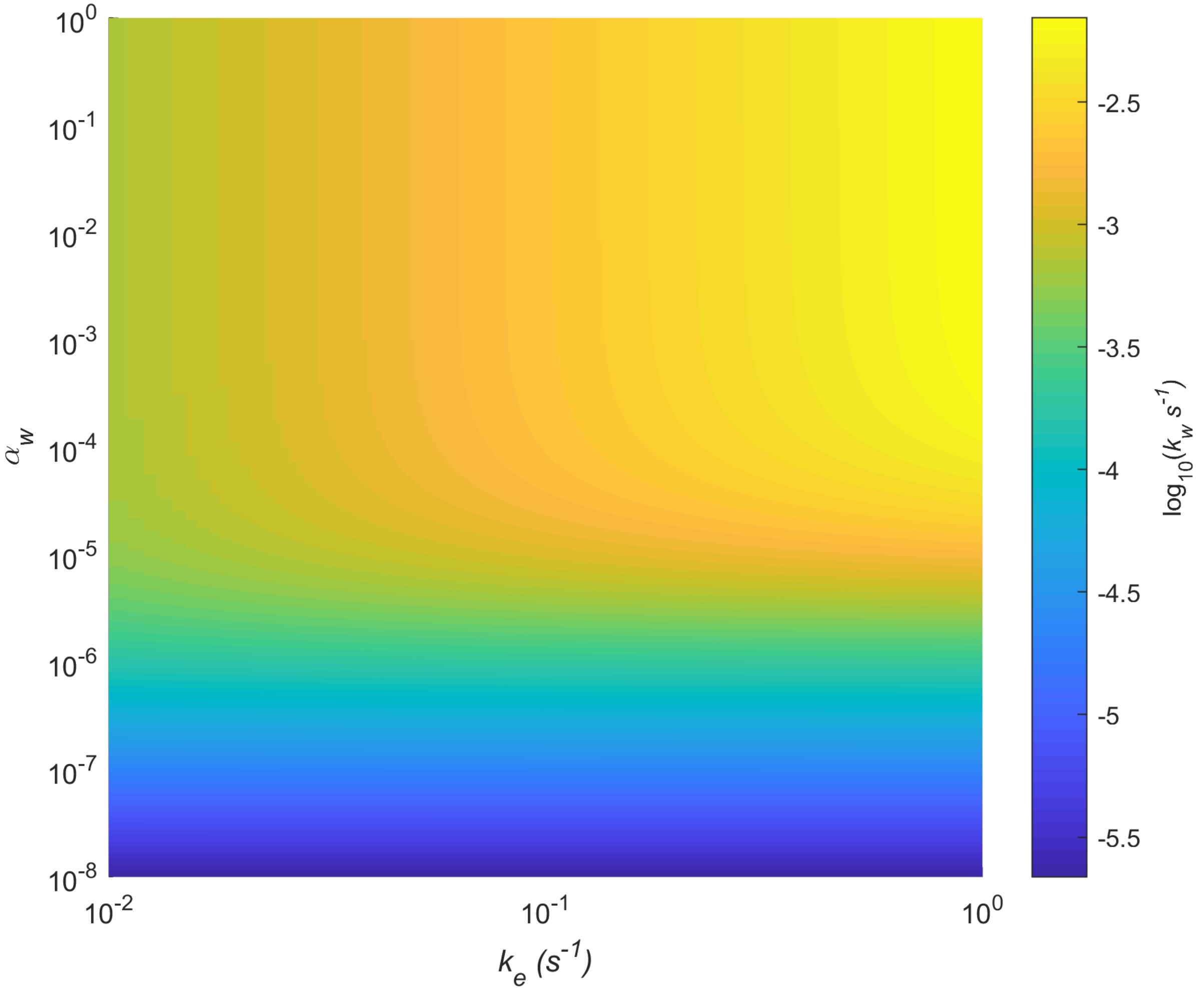

Figure S6. First order gas wall losses in a 5 m^3 smog chamber with a surface areas to volume ratio corresponding to a completely inflated AURA smog chamber. The wall loss rates were calculated with theory proposed by McMurry and Grosjean (1985) for a molecule with a diffusion coefficient (D) = 10^{-5} $m^2 s^{-1}$ and wall mass accommodation coefficients in the range 10^{-8} to 1.0

S2.6 Wall loss rates of gases

Figure S6 shows how the first order gas wall loss rates (k_w) varies as a function of the coefficient of eddy diffusion (k_e) and the wall mass accommodation α_w. The wall loss rates were derived with the theory proposed by McMurry and Grosjean (1985) (Eq. 1). For the AURA model simulations performed in this work we used a relatively low (k_e) of 0.02 s^{-1} motivated by a previous AURA smog chamber study which estimated first order wall losses of highly oxygenated organic molecules (HOM) (Quéléver et al., 2019).

S2.6.1 Sensitivity runs with variable O_3 wall uptake

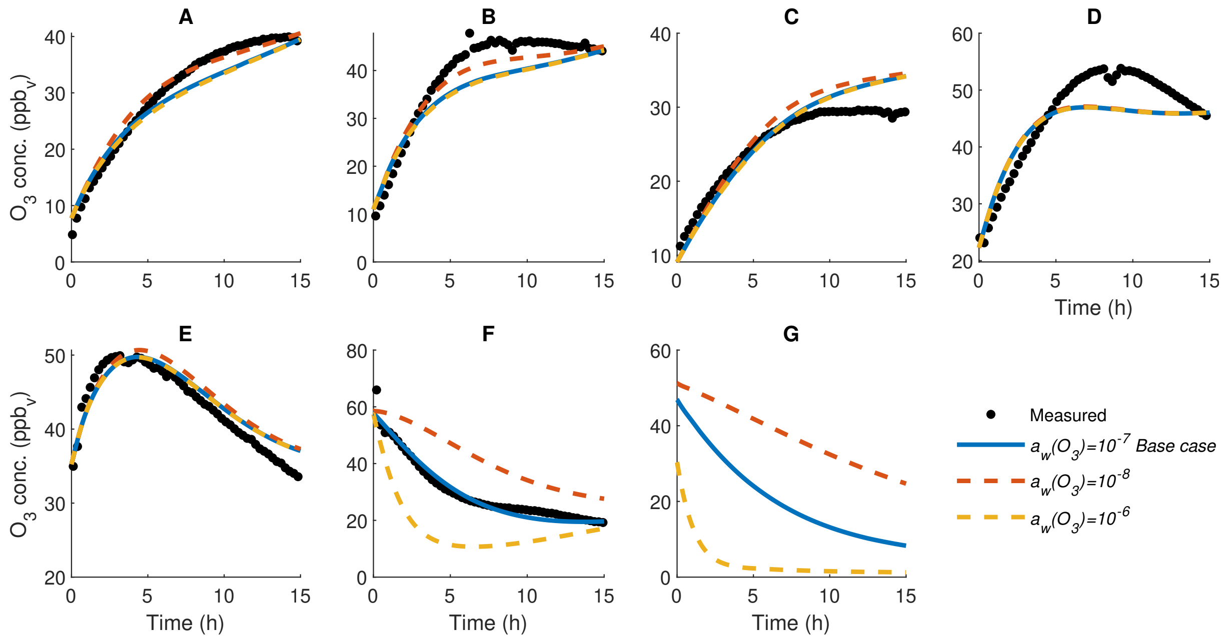

Figure S7. Measured and modelled O_3 concentration for different O_3 α_w. Panel **A**-**G** shows results from experiments DMS1-7.

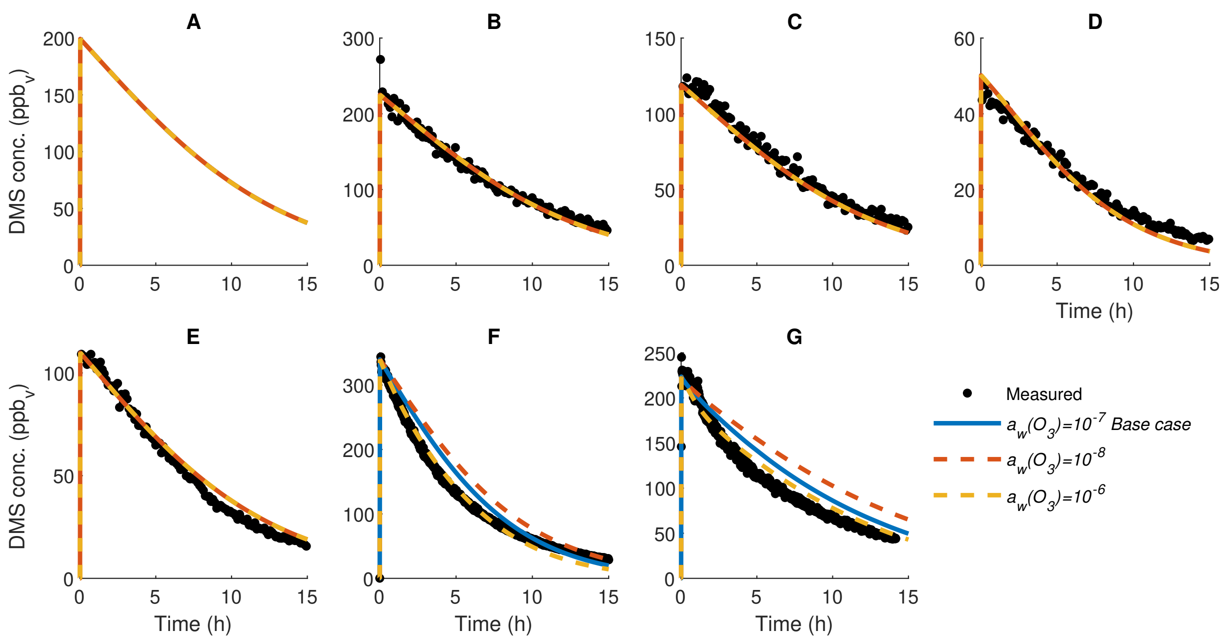

Figure S8. Measured and modelled DMS concentration for different O_3 α_w. Panel **A**-**G** shows results from experiments DMS1-7.

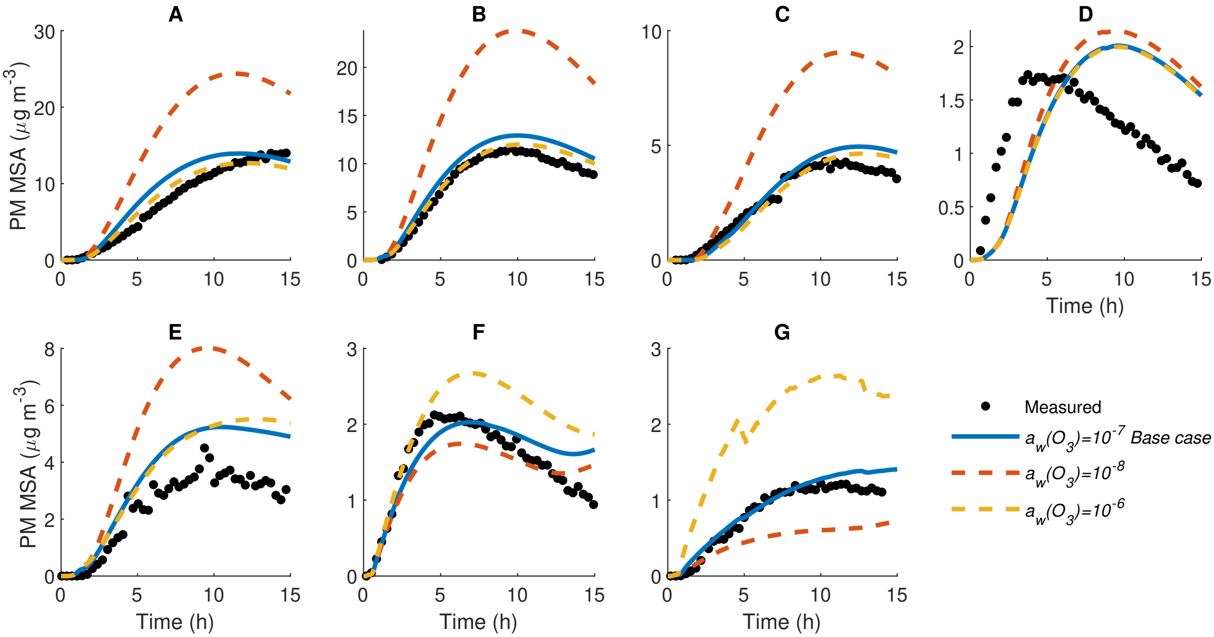

Figure S9. Measured and modelled MSA PM for different O_3 α_w. Panel **A**-**G** shows results from experiments DMS1-7.

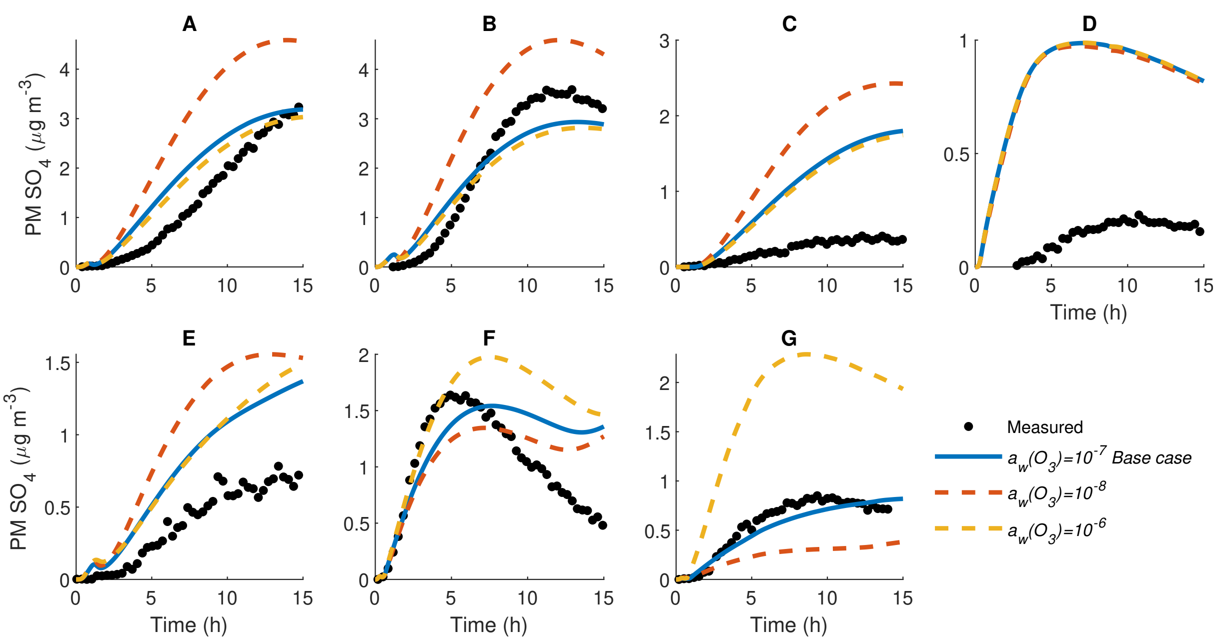

Figure S10. Measured and modelled SO_4 PM for different O_3 α_w. Panel **A**-**G** shows results from experiments DMS1-7.

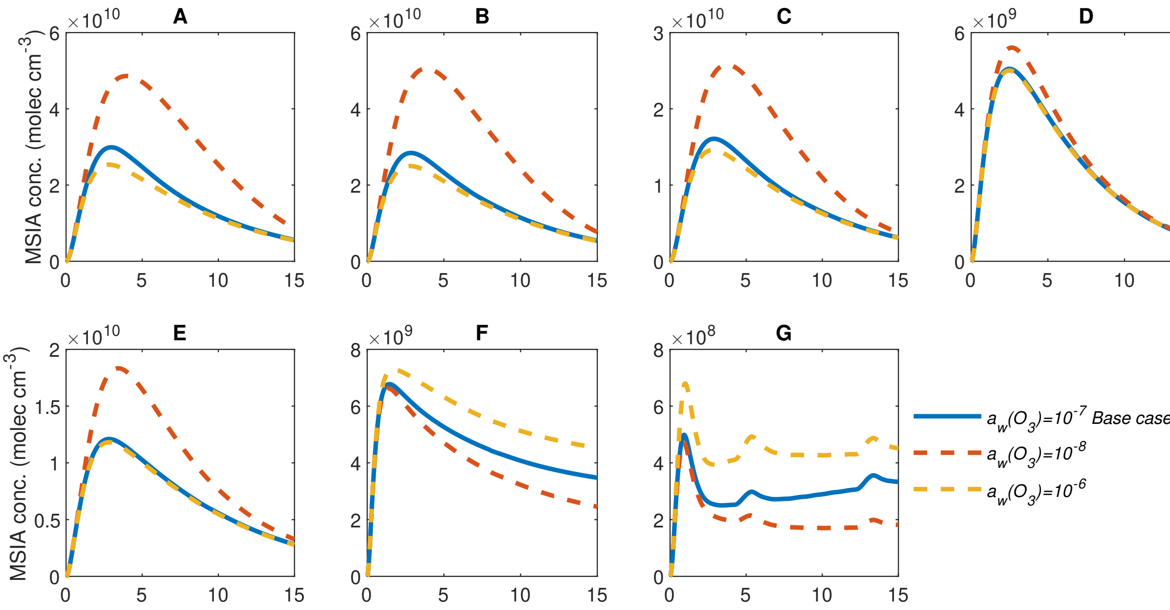

Figure S11. Modelled MSIA concentration for different O_3 α_w. Panel **A**-**G** shows results from experiments DMS1-7.

S2.6.2 Sensitivity runs with variable SO_2 wall uptake

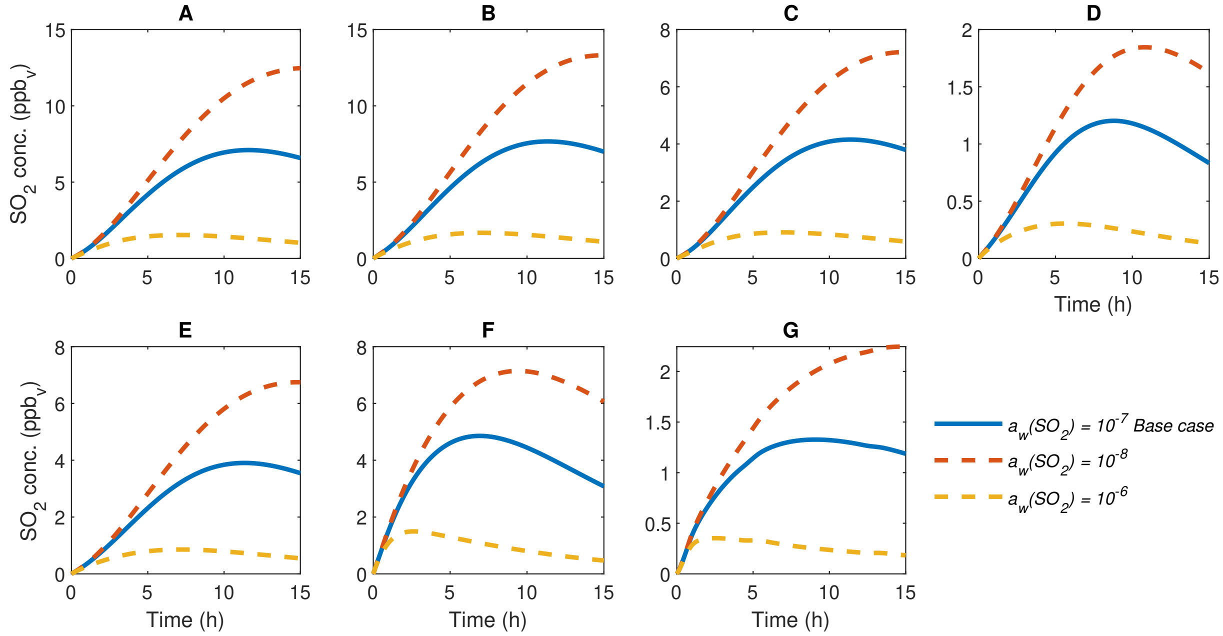

Figure S12. Modelled SO_2 concentration for different SO_2 α_w. Panel **A-G** shows results from experiments DMS1-7.

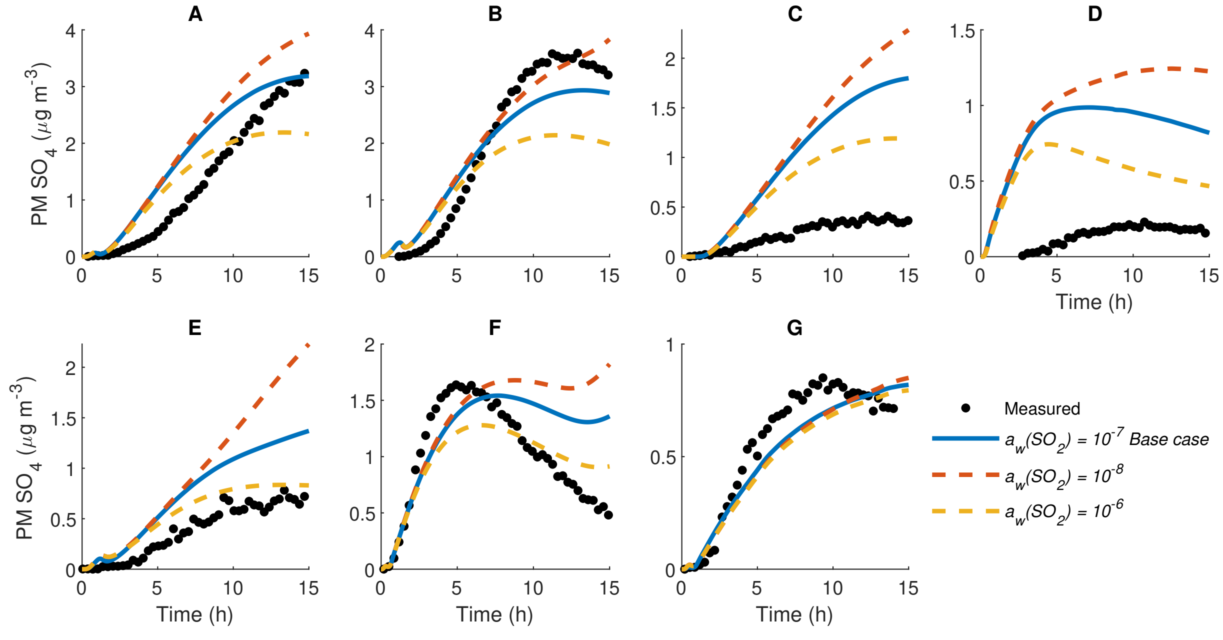

Figure S13. Measured and modelled SO_4 PM for different SO_2 α_w. Panel **A-G** shows results from experiments DMS1-7.

S2.6.3 Sensitivity runs with variable DMS wall uptake

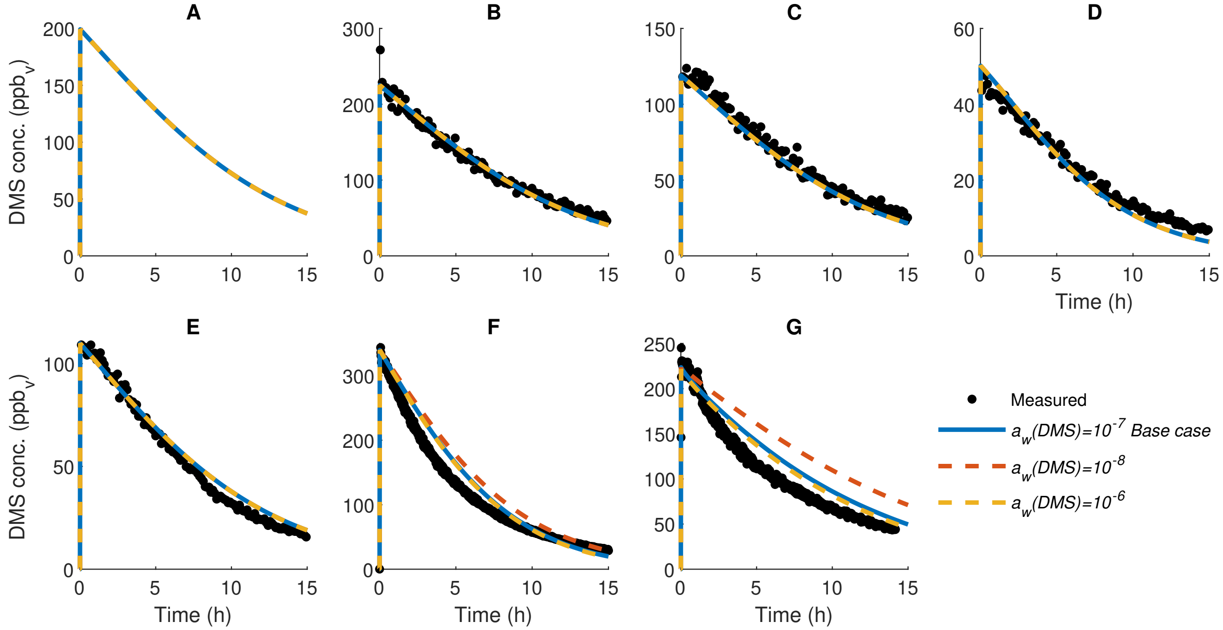

Figure S14. Measured and modelled DMS concentration for different DMS α_w. Panel **A**-**G** shows results from experiments DMS1-7.

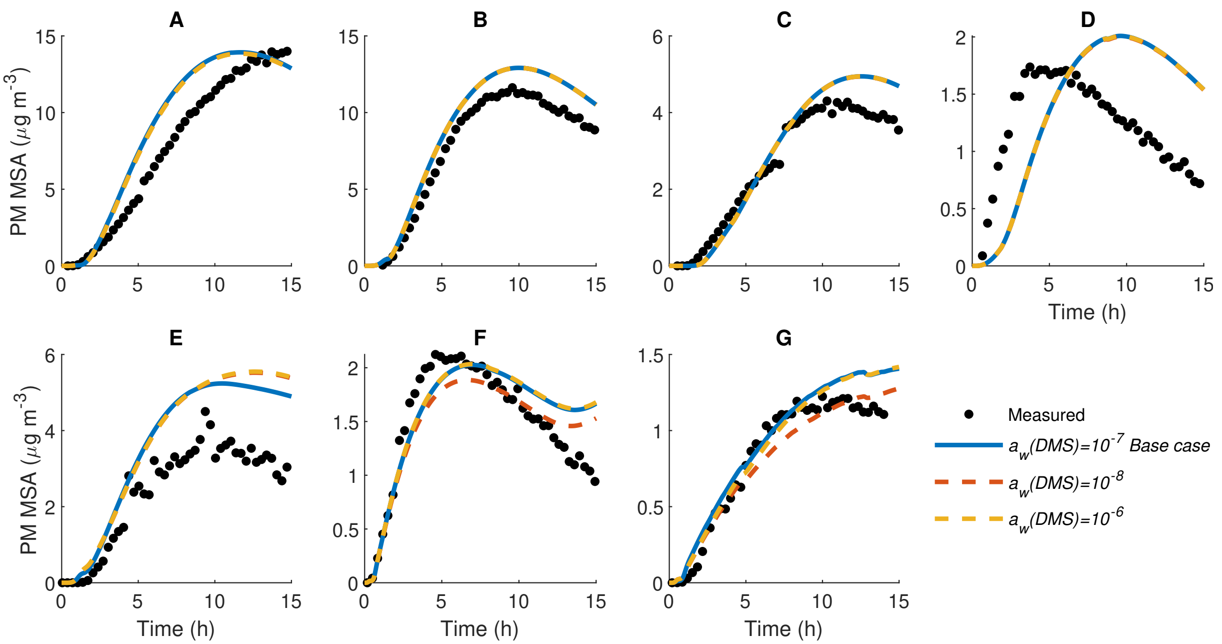

Figure S15. Measured and modelled MSA PM for different DMS α_w. Panel **A**-**G** shows results from experiments DMS1-7.

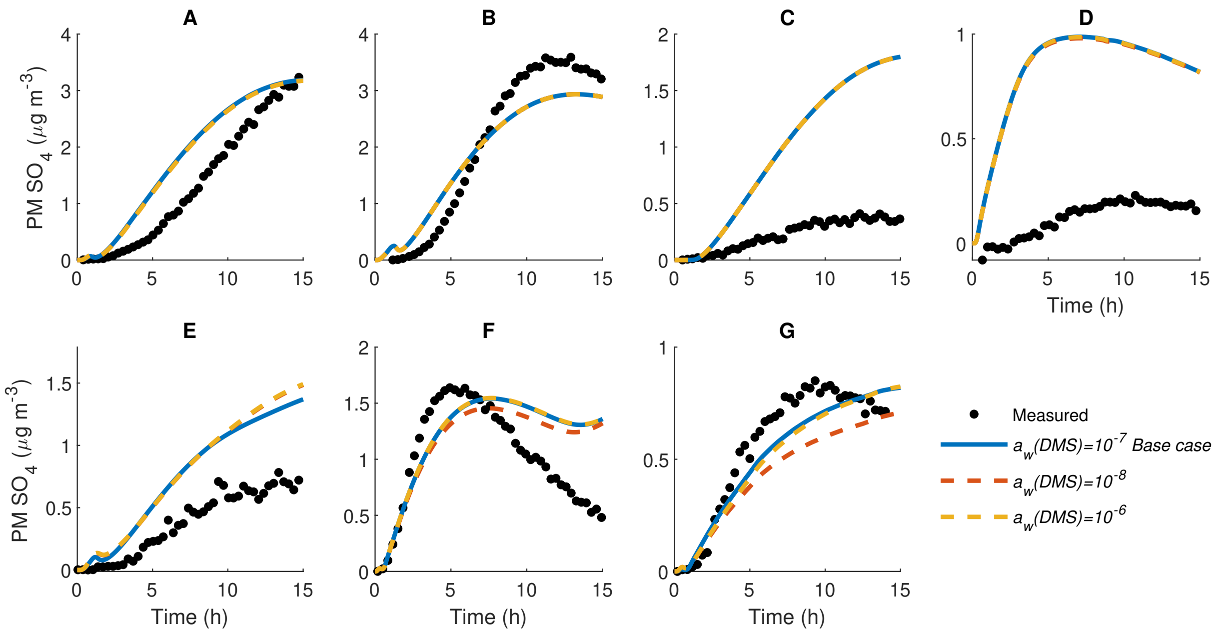

Figure S16. Measured and modelled SO_4 PM for different $DMS\ \alpha_w$. Panel **A**-**G** shows results from experiments DMS1-7.

S2.6.4 Sensitivity runs with variable DMSO, $DMSO_2$, MSIA and HPMTF wall uptake

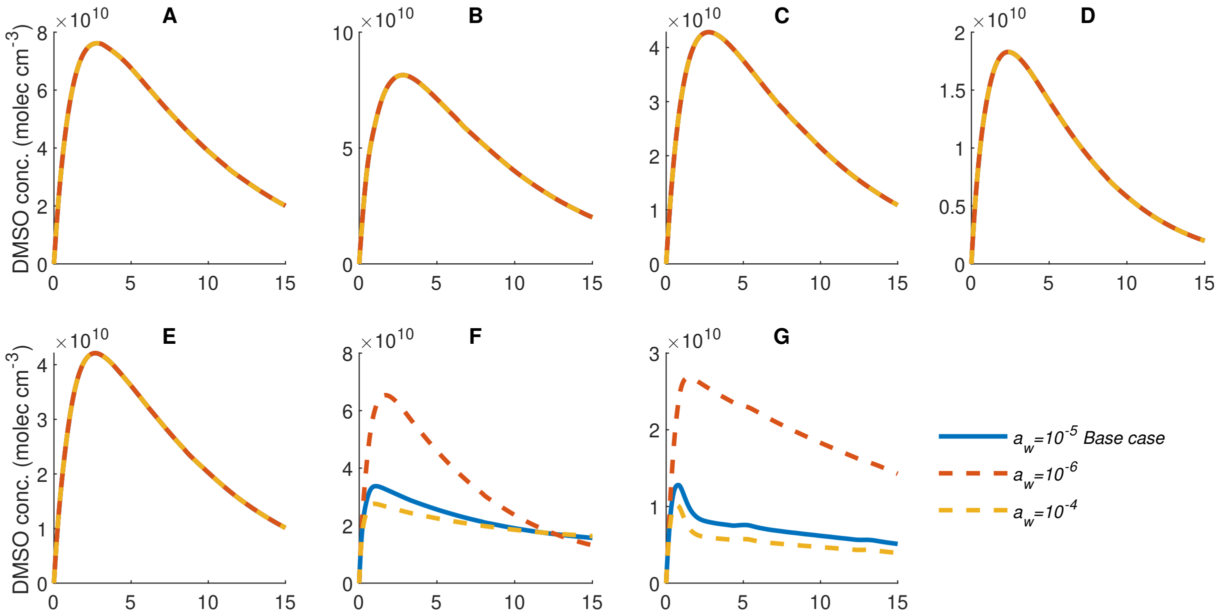

Figure S17. Modelled DMSO concentration for different α_w for the intermediate DMS oxidation products DMSO, $DMSO_2$, MSIA and HPMTF. Panel **A**-**G** shows results from experiments DMS1-7.

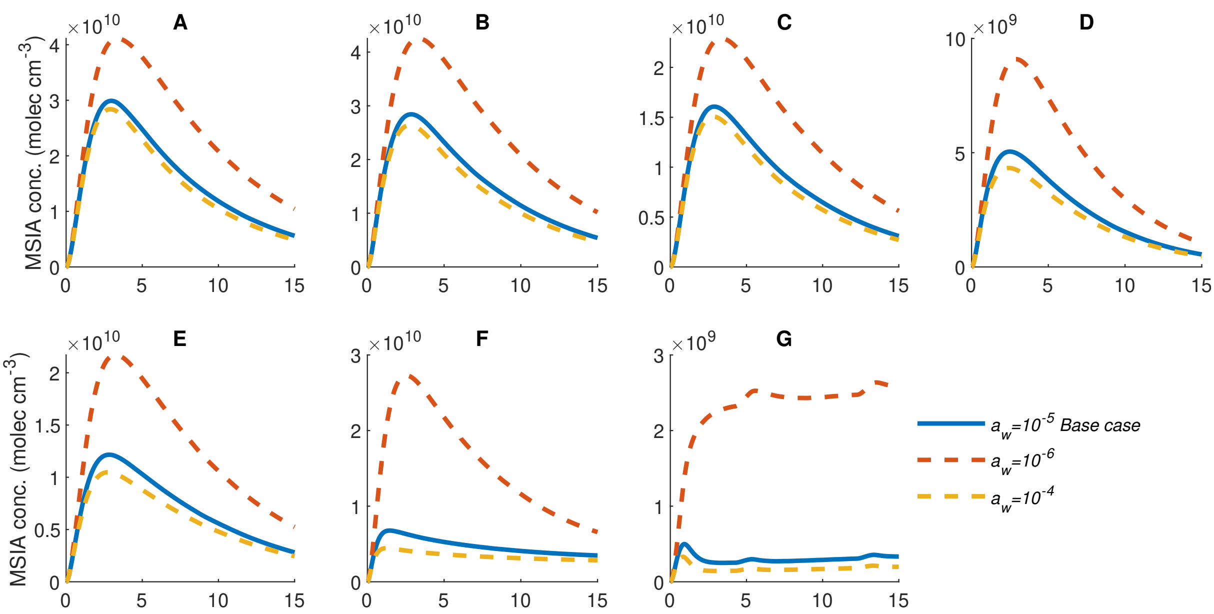

Figure S18. Modelled MSIA concentration for different α_w for the intermediate DMS oxidation products DMSO, $DMSO_2$, MSIA and HPMTF. Panel **A**-**G** shows results from experiments DMS1-7.

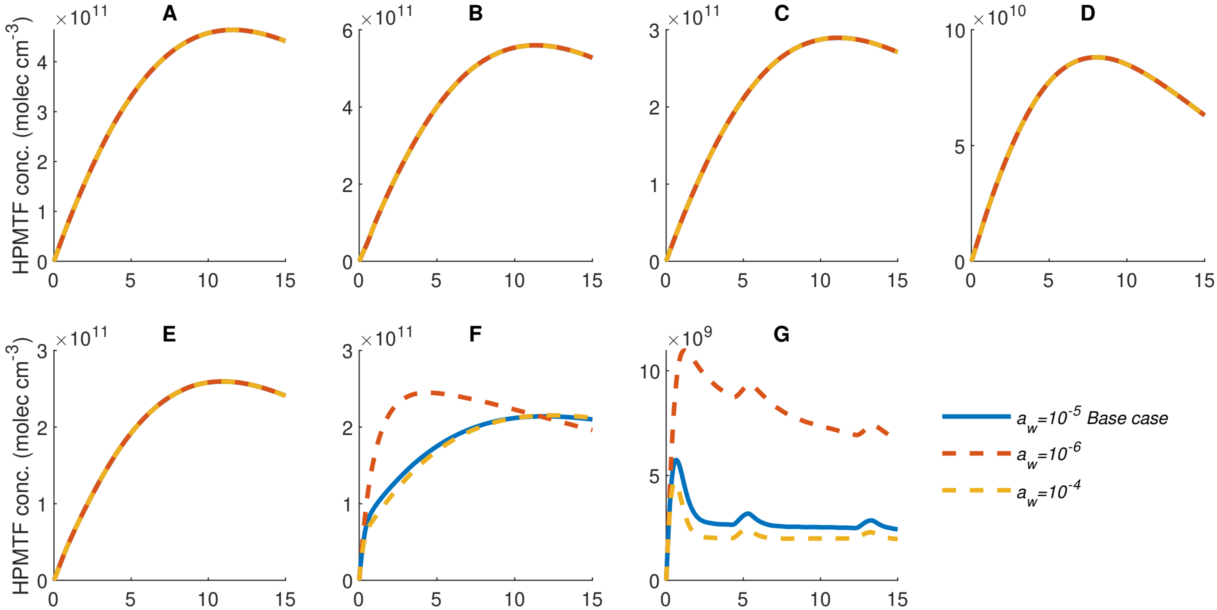

Figure S19. Modelled HPMTF concentration for different α_w for the intermediate DMS oxidation products DMSO, $DMSO_2$, MSIA and HPMTF. Panel **A**-**G** shows results from experiments DMS1-7.

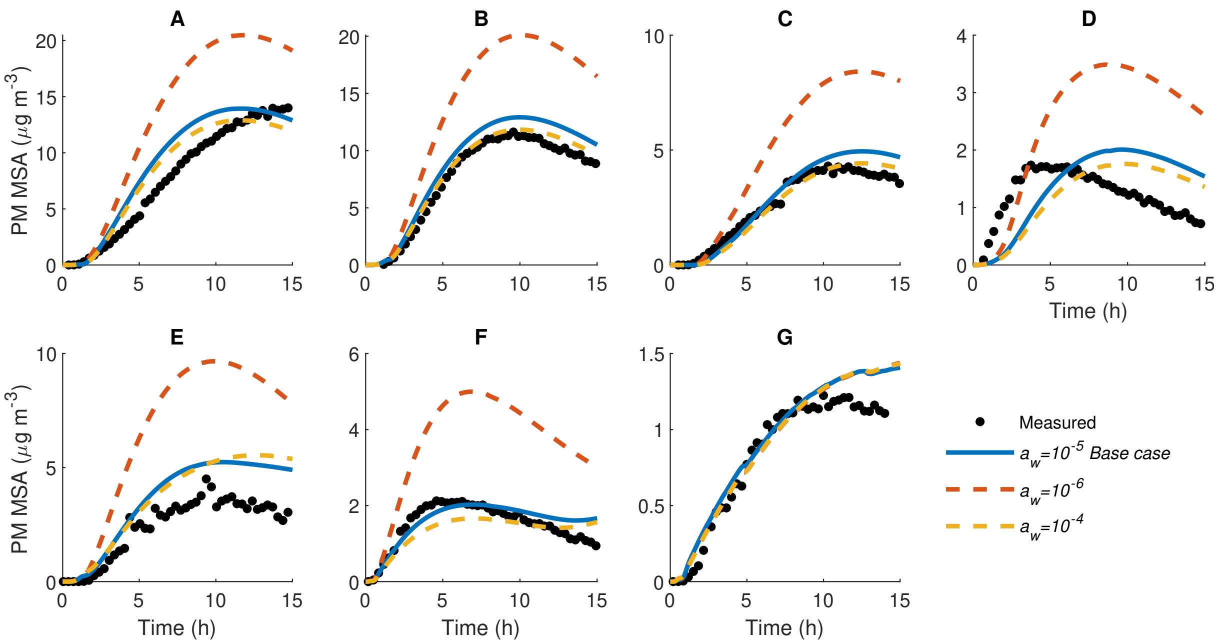

Figure S20. Measured and modelled MSA PM for different α_w for the intermediate DMS oxidation products DMSO, $DMSO_2$, MSIA and HPMTF. Panel **A**-**G** shows results from experiments DMS1-7.

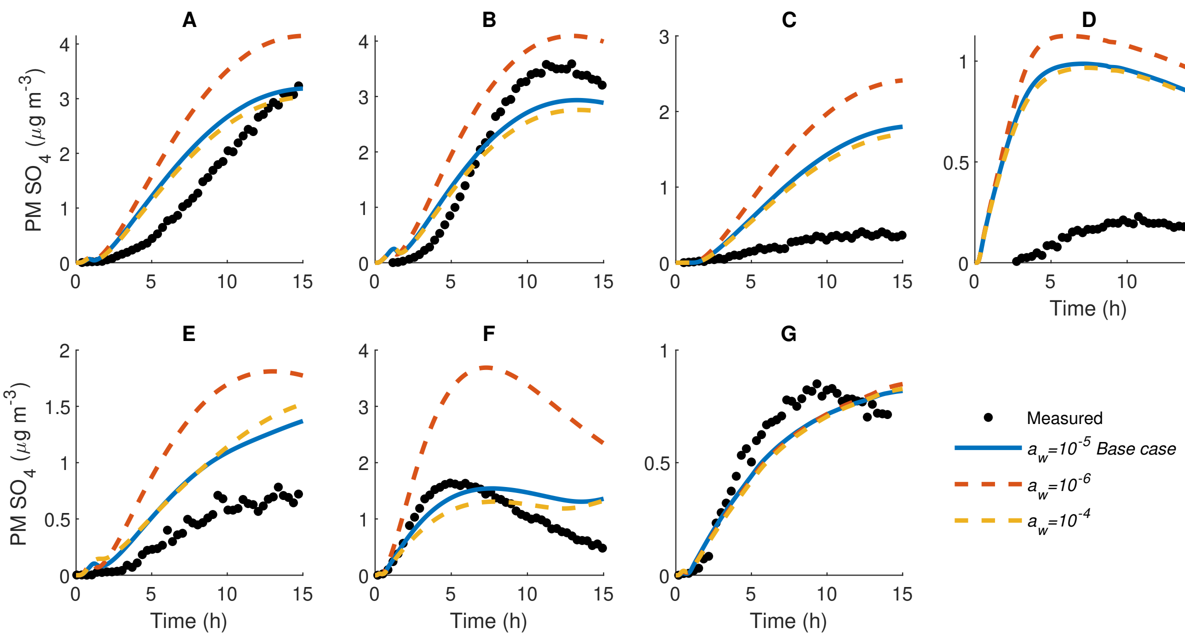

Figure S21. Measured and modelled SO_4 PM for different α_w for the intermediate DMS oxidation products DMSO, $DMSO_2$, MSIA and HPMTF. Panel **A**-**G** shows results from experiments DMS1-7.

S2.7 Gas partitioning between the gas-phase and liquid film on the chamber walls

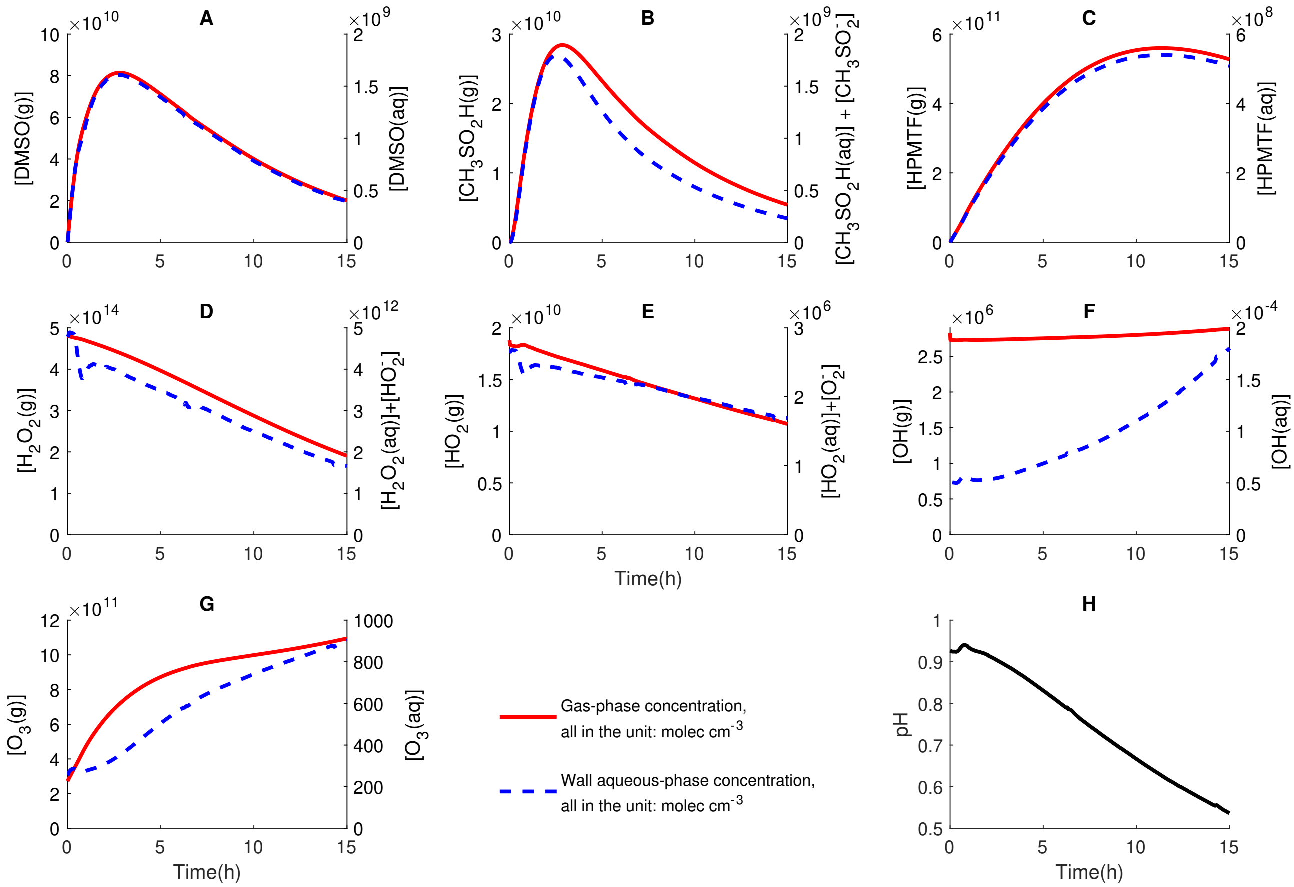

Figure S22. Modelled concentrations of the DMS oxidation products DMSO, MSIA (CH_3SO_2H) and HPMTF (panel **A**-**C**), and oxidation agents H_2O_2, HO_2, OH and O_3 (panel **D**-**G**) in the gas-phase (left y-axis) and in the chamber wall liquid water film (LWC_{wall}) (right y-axis) for the dry experiment DMS2. Panel **H** shows the modelled pH (acidity) in the liquid water film. All concentrations are given in molecules/(cm^3air).

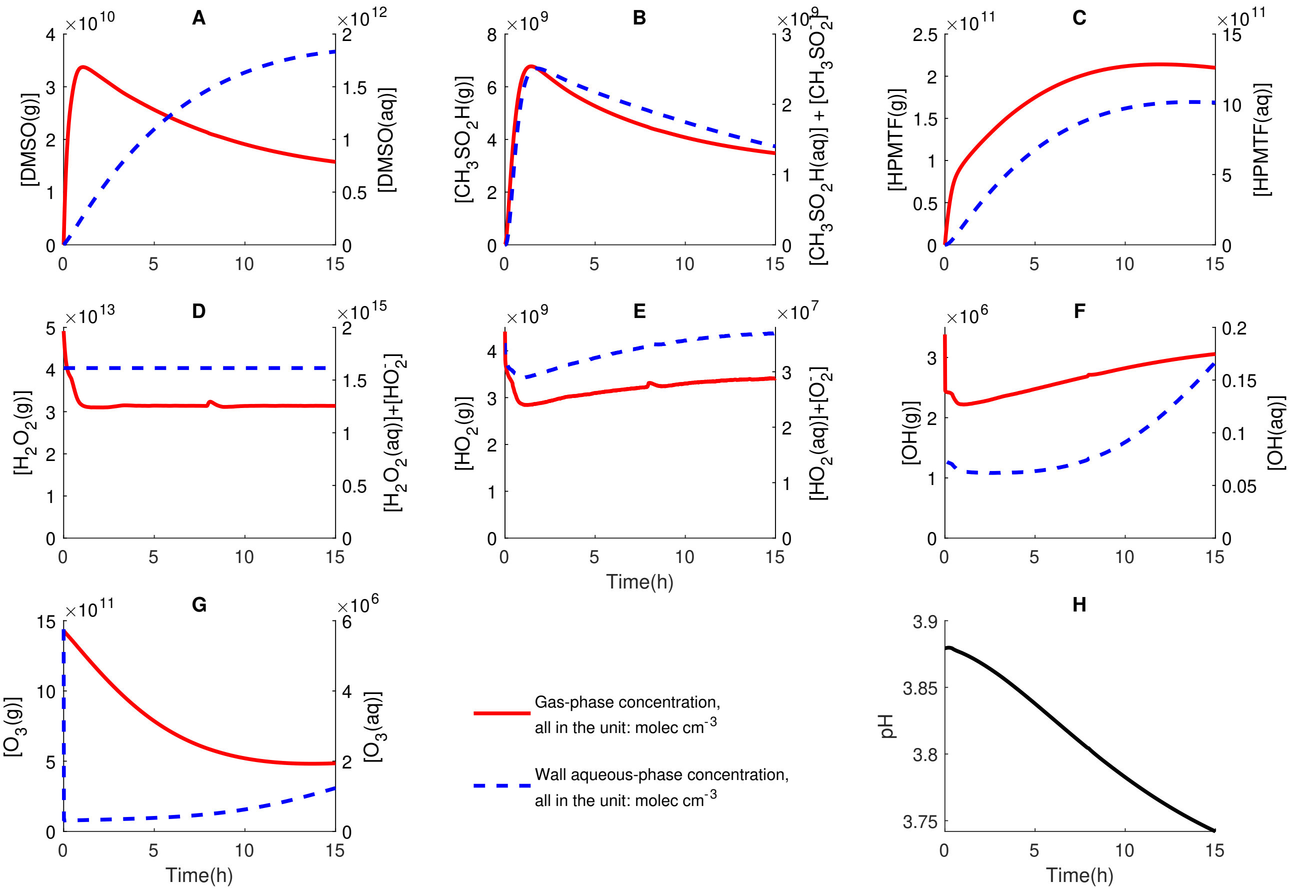

Figure S23. Modelled concentrations of the DMS oxidation products DMSO, MSIA (CH_3SO_2H) and HPMTF (panel **A**-**C**), and oxidation agents H_2O_2, HO_2, OH and O_3 (panel **D**-**G**) in the gas-phase (left y-axis) and in the chamber wall liquid water film (LWC_{wall}) (right y-axis) for the humid experiment DMS6. Panel **H** shows the modelled pH (acidity) in the liquid water film. All concentrations are given in $\mathrm{molecules}/(\mathrm{cm}^3\mathrm{air})$.

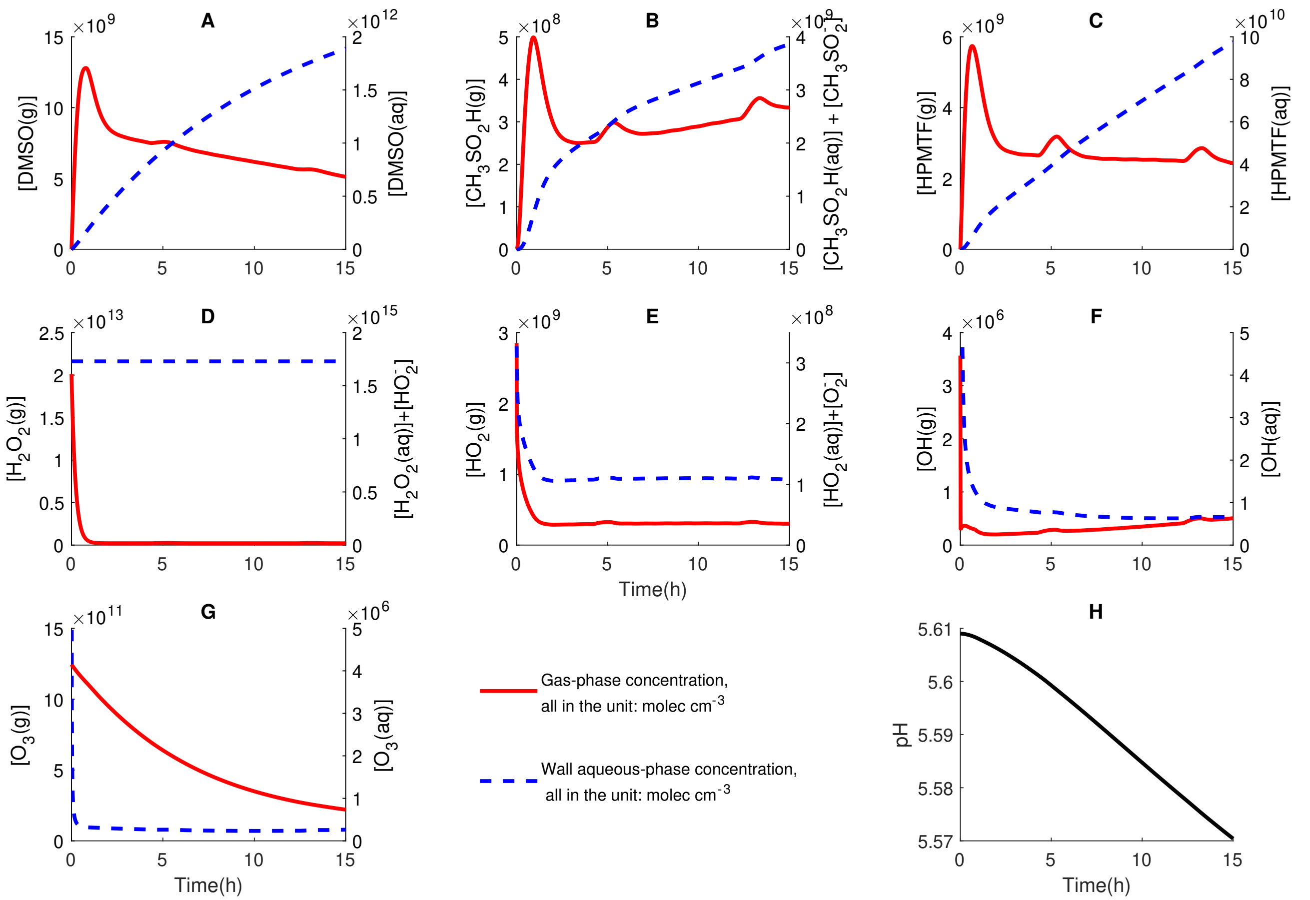

Figure S24. Modelled concentrations of the DMS oxidation products DMSO, MSIA (CH_3SO_2H) and HPMTF (panel **A**-**C**), and oxidation agents H_2O_2, HO_2, OH and O_3 (panel **D**-**G**) in the gas-phase (left y-axis) and in the chamber wall liquid water film (LWC_{wall}) (right y-axis) for the humid and cold experiment DMS7. Panel **H** shows the modelled pH (acidity) in the liquid water film. All concentrations are given in $\mathrm{molecules/(cm^3 air)}$.

S2.8 Wall loss for particles

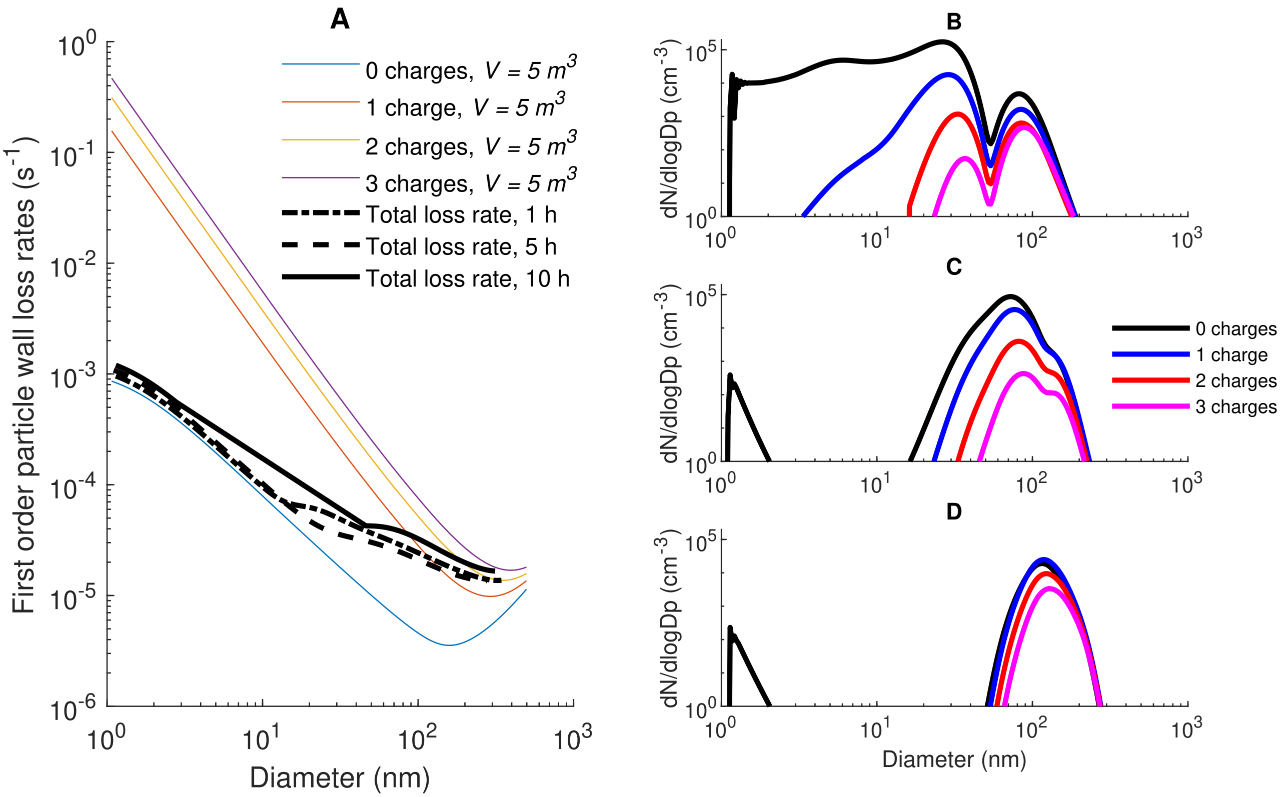

Figure S25. Example of modelled particle wall loss rates (panel **A**) and particle charge distributions after 2, 5 and 10 hours (panel **B**, **C** and **D**) for exp. DMS2. The modelled effective total particle wall loss rates take into account the fraction of particles with different number of elemental charges in each size bin. The high effective wall loss rate at the smallest particle size is a result of the relatively large fraction of charged molecules clusters that form new particles in the model. However, these particles are rapidly lost to the chamber walls and almost all nucleation mode aerosol particles above this size are non-charged.

S3 Results

S3.1 Chamber experiments

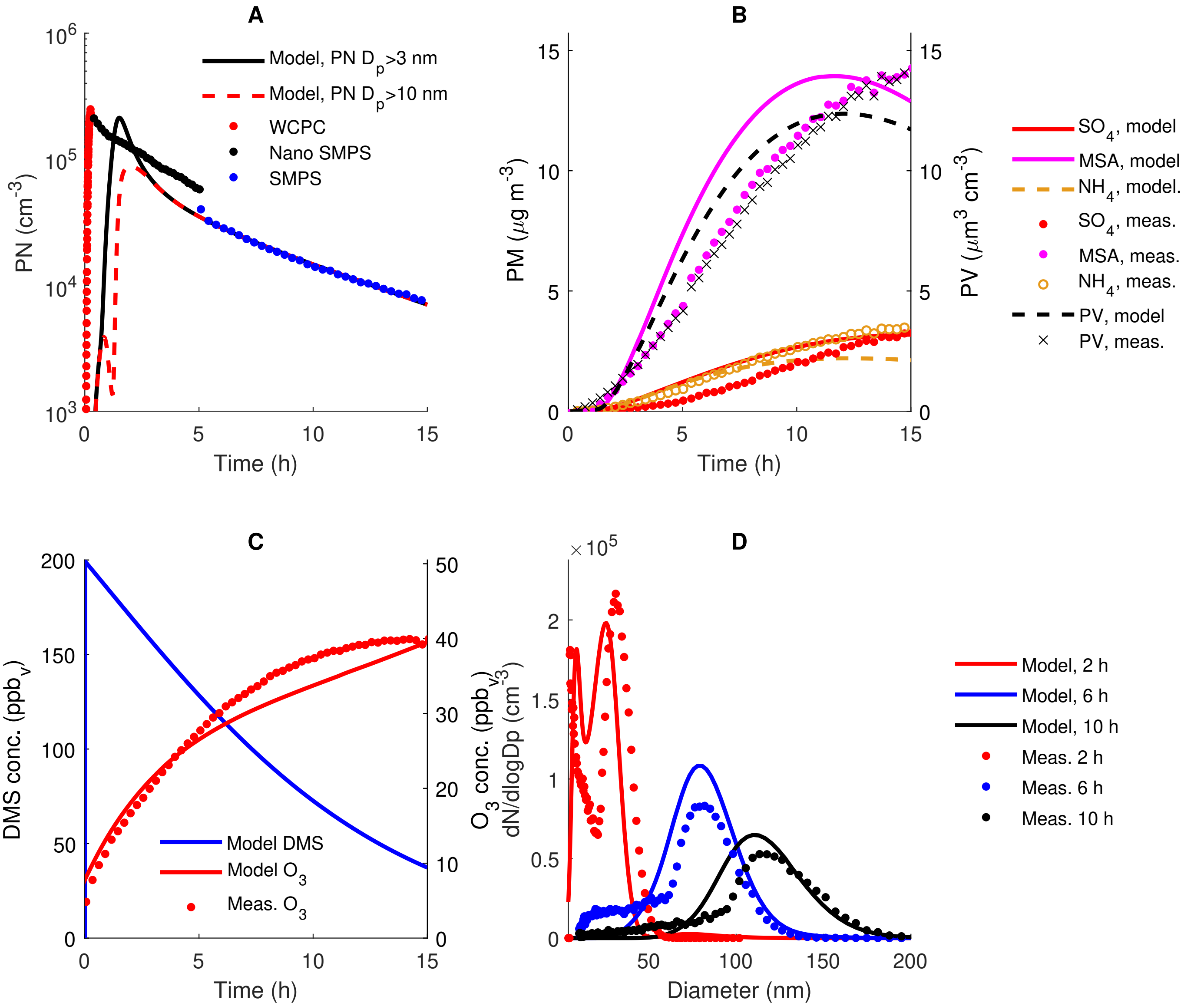

Figure S26. Model and measurement results from the dry DMS experiment DMS1. Panel **A**: measured and modelled particle number concentrations; Panel **B**: measured and modelled particle mass concentrations; Panel **C**: measured and modelled DMS and O_3 concentrations; and Panel **D**: measured and modelled particle number size distributions.

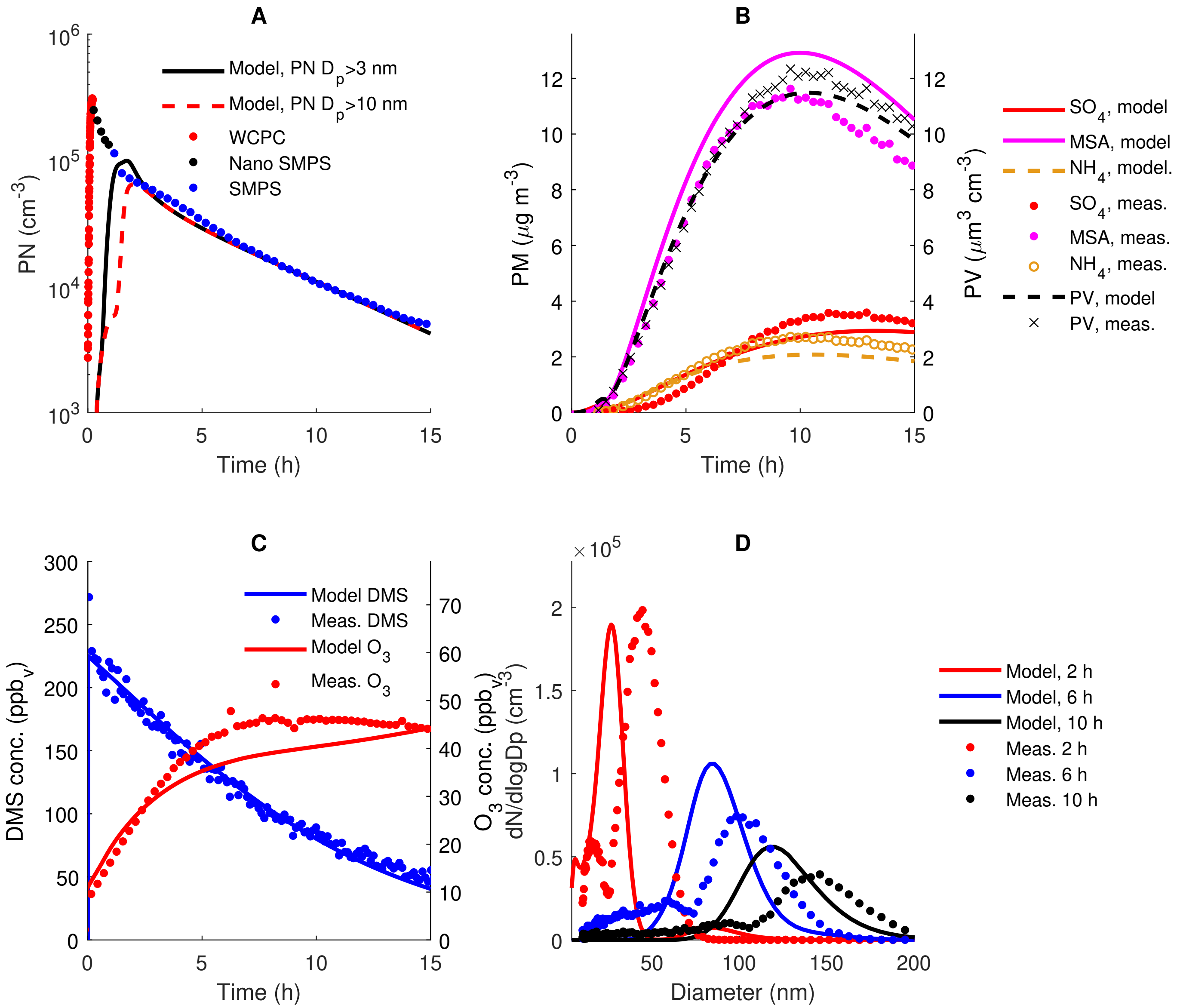

Figure S27. Model and measurement results from the dry DMS experiment DMS2. Panel **A**: measured and modelled particle number concentrations; Panel **B**: measured and modelled particle mass concentrations; Panel **C**: measured and modelled DMS and O_3 concentrations; and Panel **D**: measured and modelled particle number size distributions.

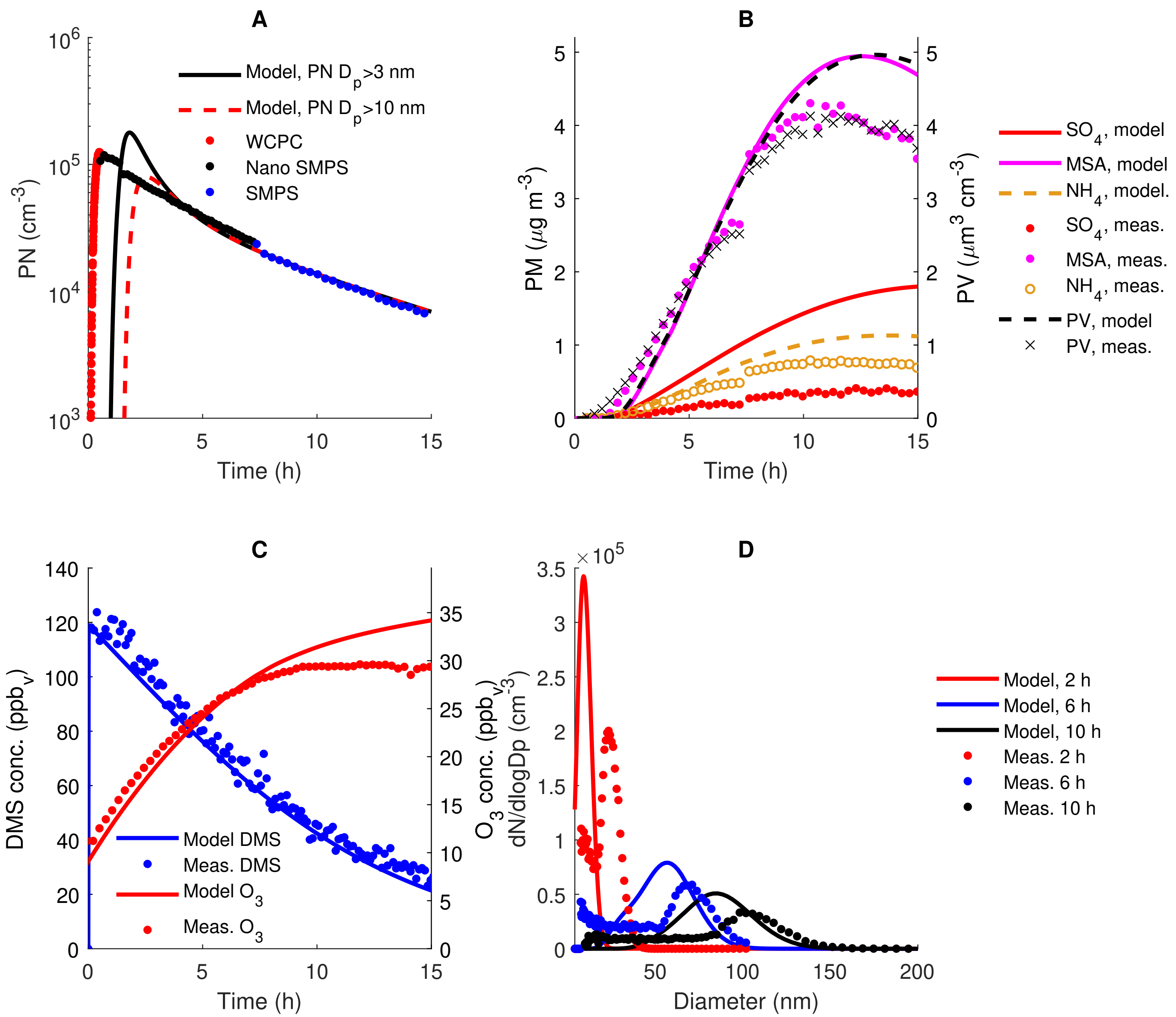

Figure S28. Model and measurement results from the dry DMS experiment DMS3. Panel **A**: measured and modelled particle number concentrations; Panel **B**: measured and modelled particle mass concentrations; Panel **C**: measured and modelled DMS and O_3 concentrations; and Panel **D**: measured and modelled particle number size distributions.

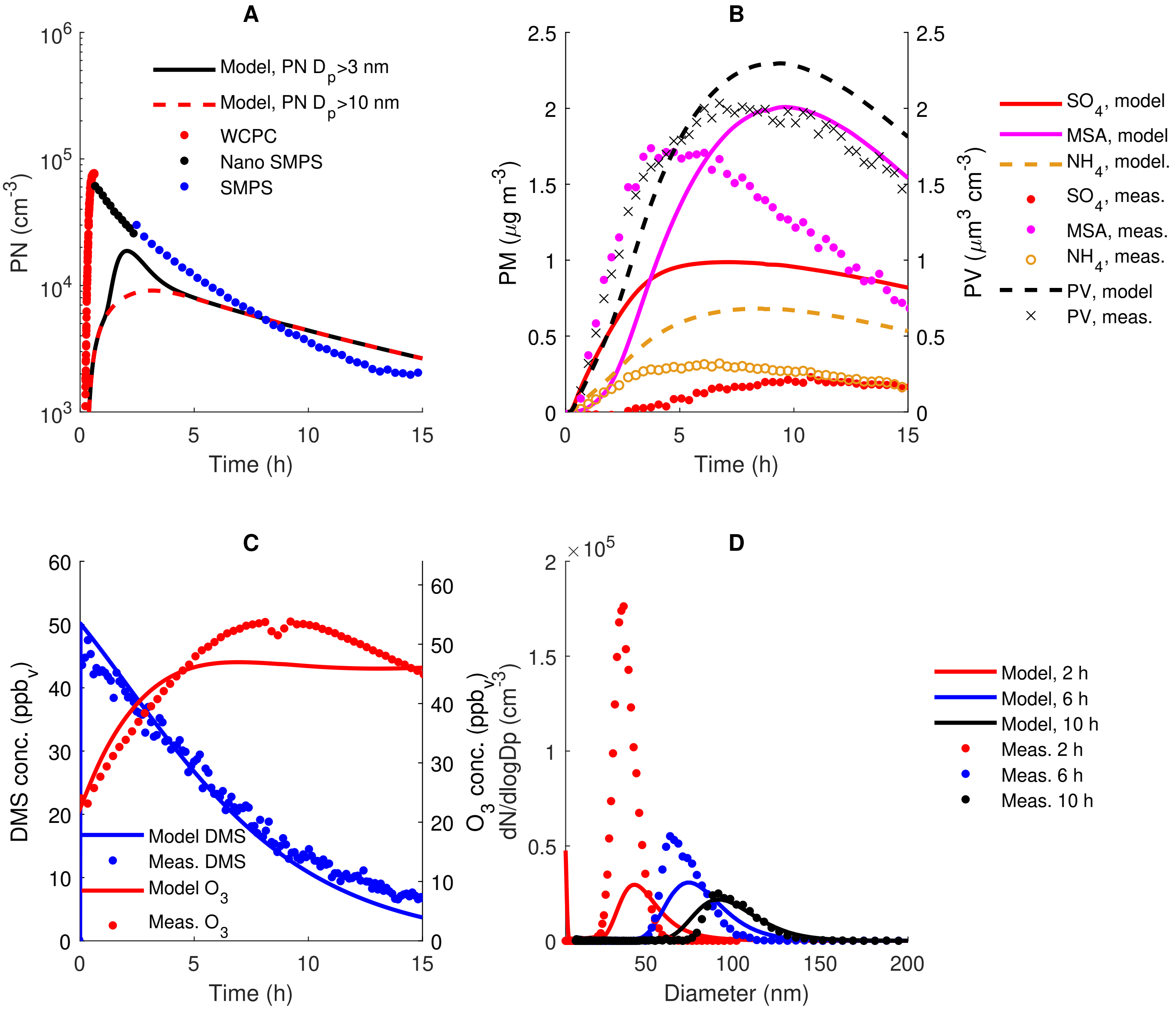

Figure S29. Model and measurement results from the dry DMS experiment DMS4. Panel **A**: measured and modelled particle number concentrations; Panel **B**: measured and modelled particle mass concentrations; Panel **C**: measured and modelled DMS and O_3 concentrations; and Panel **D**: measured and modelled particle number size distributions.

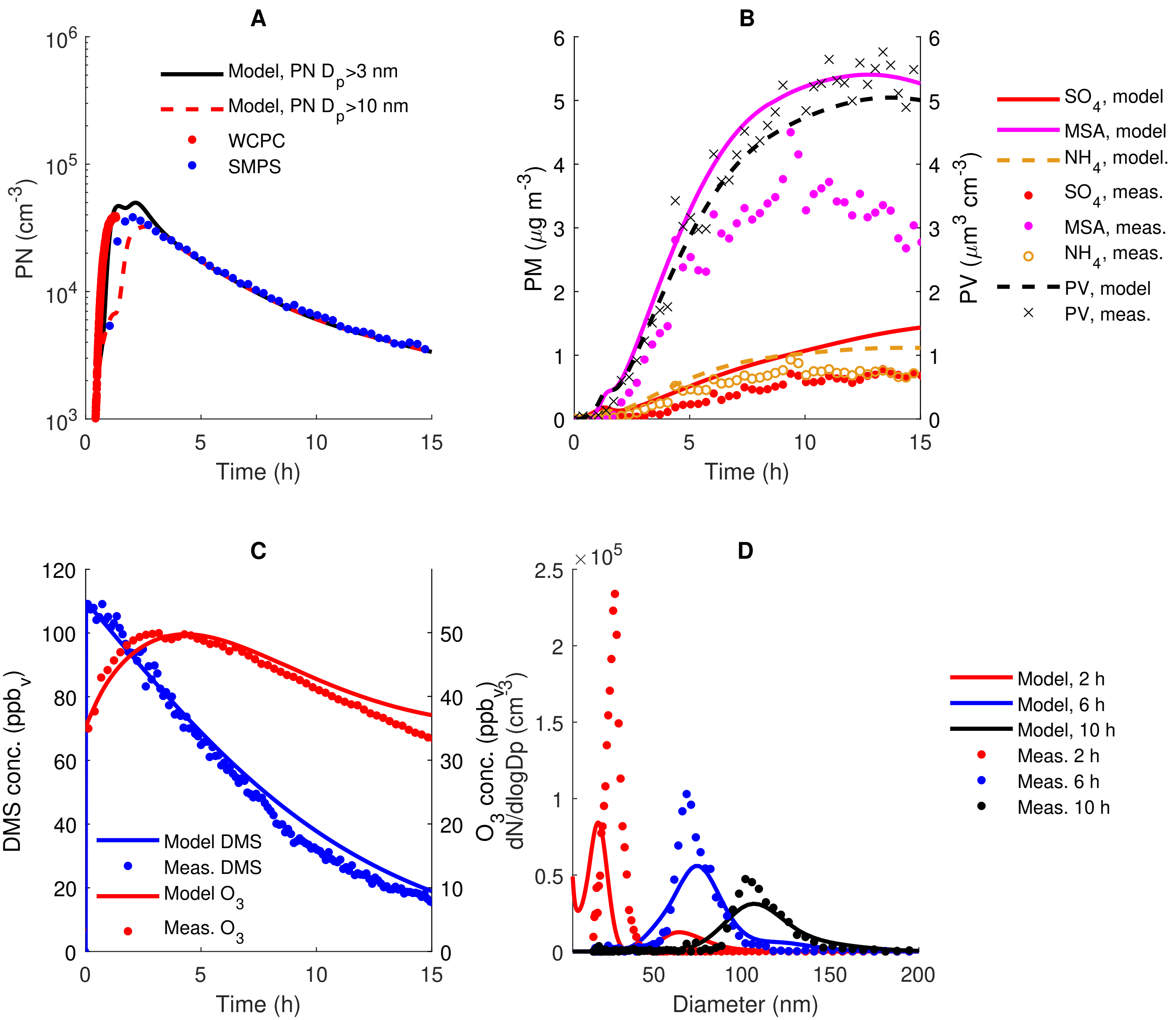

Figure S30. Model and measurement results from the dry DMS experiment DMS5. Panel **A**: measured and modelled particle number concentrations; Panel **B**: measured and modelled particle mass concentrations; Panel **C**: measured and modelled DMS and O_3 concentrations; and Panel **D**: measured and modelled particle number size distributions.

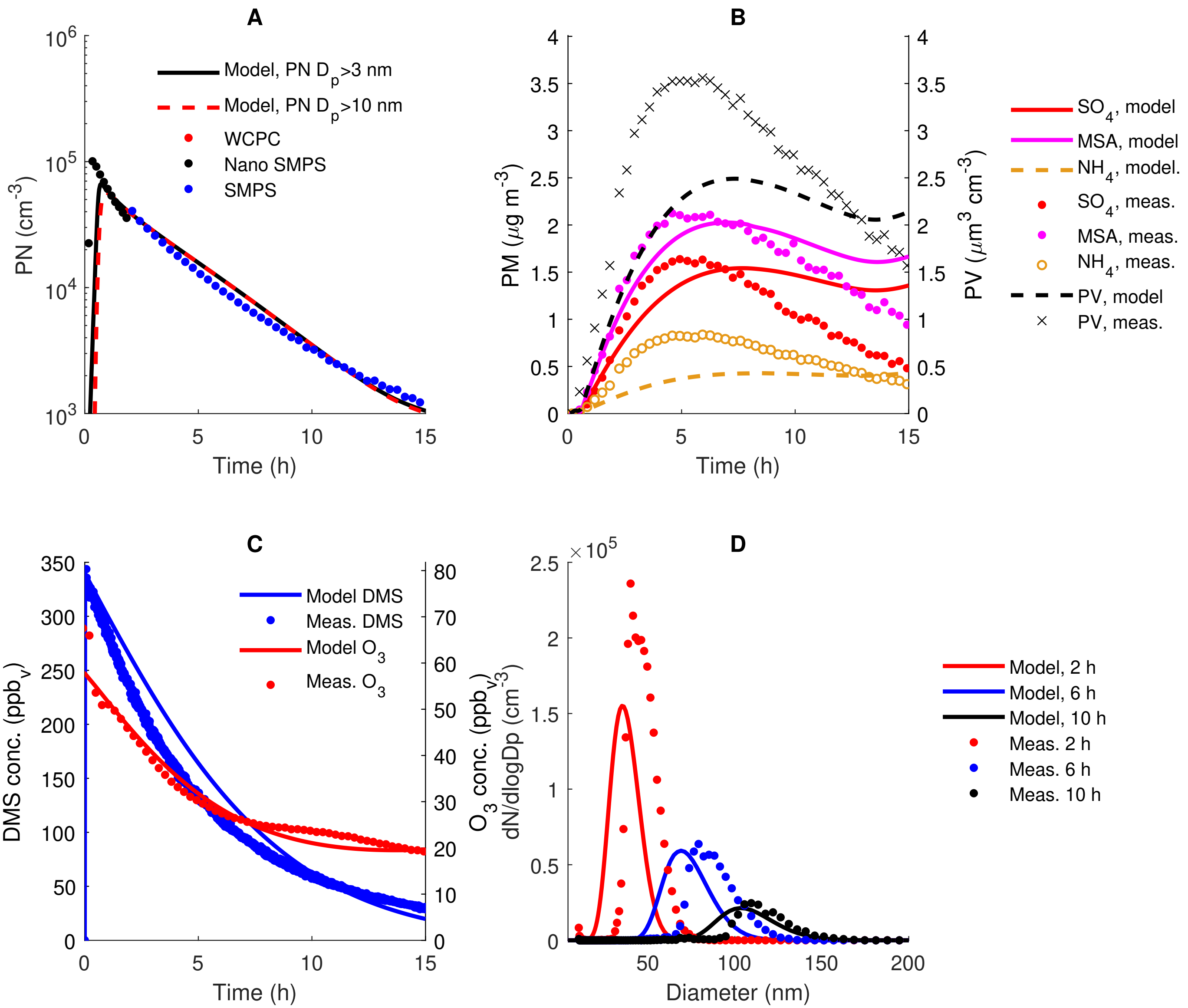

Figure S31. Model and measurement results from the humid DMS experiment DMS6. Panel **A**: measured and modelled particle number concentrations; Panel **B**: measured and modelled particle mass concentrations; Panel **C**: measured and modelled DMS and O_3 concentrations; and Panel **D**: measured and modelled particle number size distributions.

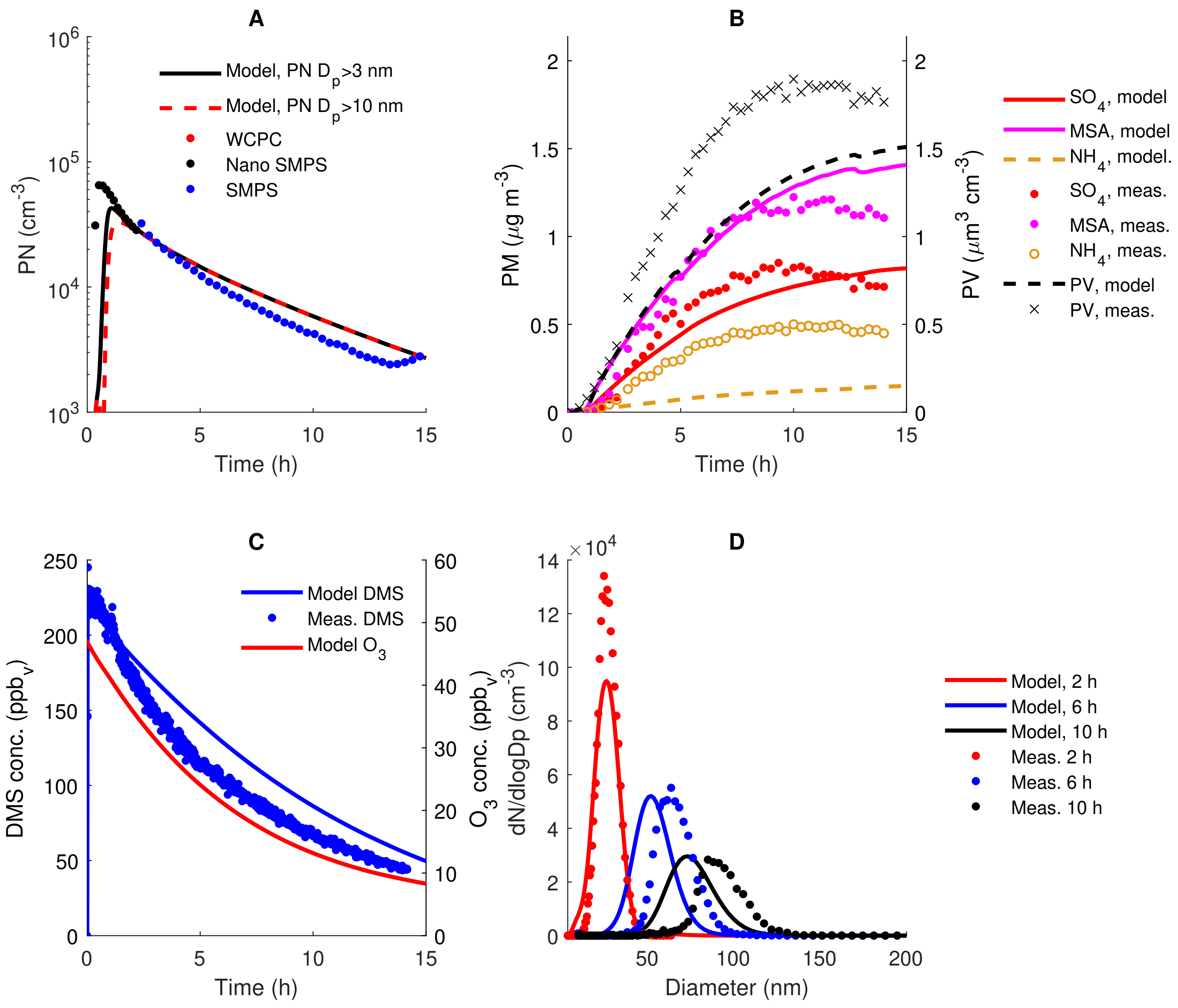

Figure S32. Model and measurement results from the humid and cold DMS experiment DMS7. Panel **A**: measured and modelled particle number concentrations; Panel **B**: measured and modelled particle mass concentrations; Panel **C**: measured and modelled DMS and O_3 concentrations; and Panel **D**: measured and modelled particle number size distributions.

S3.2 HMPTF and MSIA gas-phase chemistry

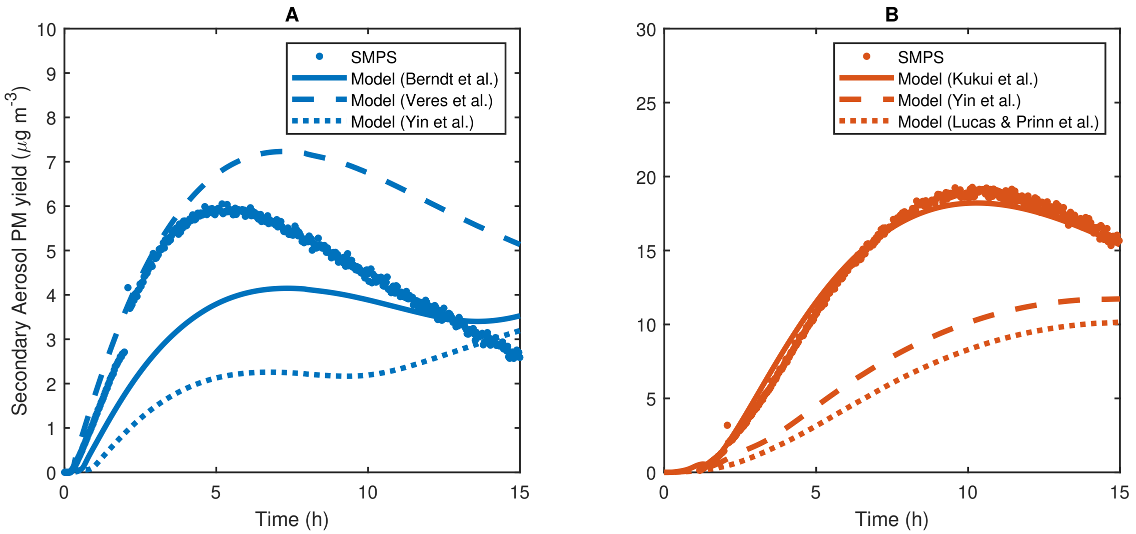

Figure S33. Modelled and measured (SMPS) PM using the CH_3SCH_2OO radical autoxidation rate from Berndt et al. (2019), Veres et al. (2020) or Yin et al. (1990), panel **A**, and the $MSIA + OH$ oxidation rate by Kukui et al. (2003), Yin et al. (1990) or Lucas and Prinn (2002), panel **B**.

S3.3 Atmospheric implication

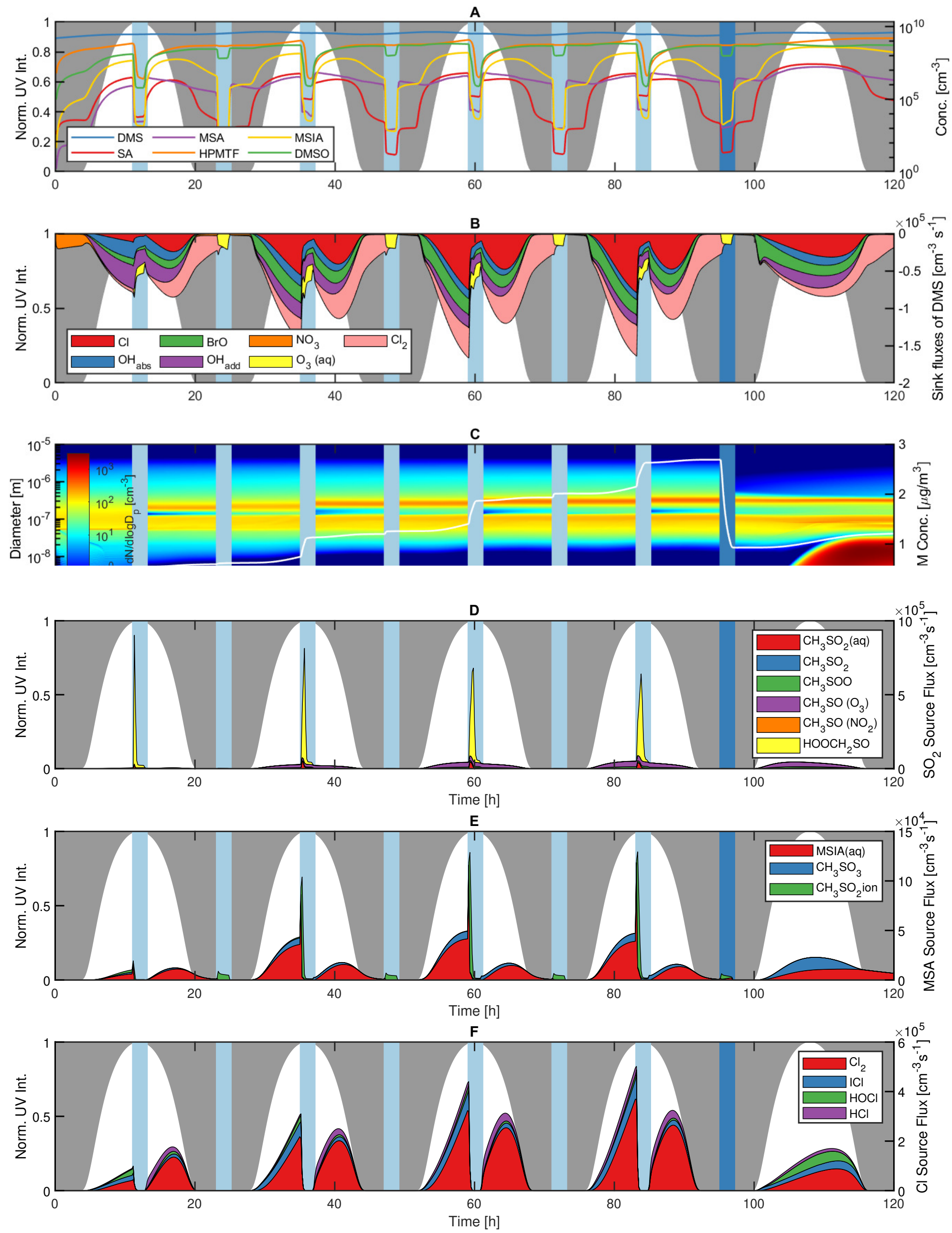

Figure S34. Modelled DMS oxidation and subsequent PM production related to the PolAtm sensitivity run. Panel **A** illustrates the evolution of DMS, SA, MSA, HMPTF, MSIA and DMSO gas-phase concentrations, **B** the sink fluxes of DMS due to Cl, OH, BrO, NO_3 and O_3 and **C** the number size distribution and secondary aerosol PM production. Panel **D**, **E** and **F** denote the source flux of SO_2, MSA and Cl, respectively. Light blue areas denote in-cloud period, in which rain events are represented as dark blue. Night and daytime periods are represented by the normalised UV-intensity and marked by grey and white areas, respectively.

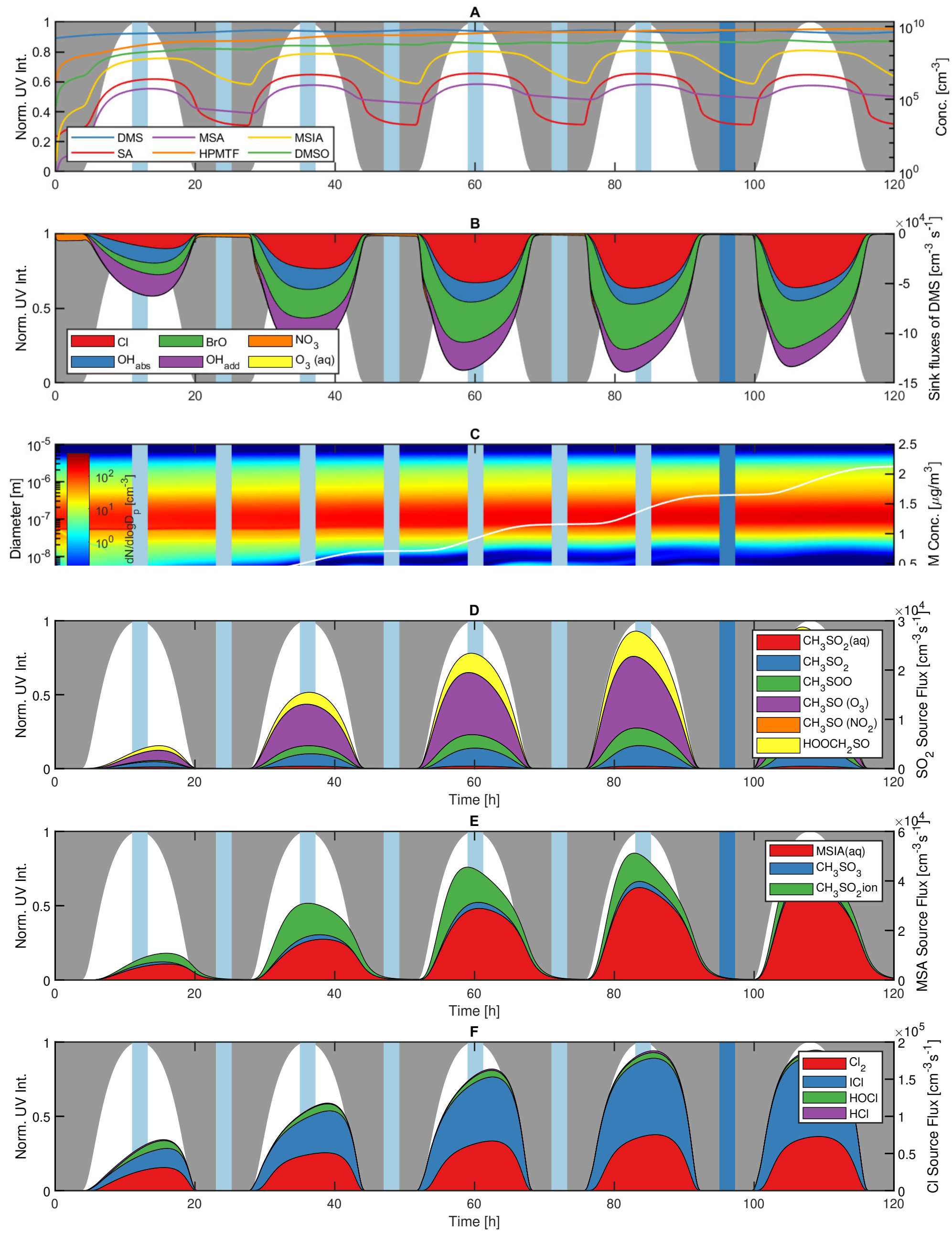

Figure S35. Modelled DMS oxidation and subsequent PM production related to the woCloudAtm sensitivity run. Panel **A** illustrates the evolution of DMS, SA, MSA, HMPTF, MSIA and DMSO gas-phase concentrations, **B** the sink fluxes of DMS due to Cl, OH, BrO, NO_3 and O_3 and **C** the number size distribution and secondary aerosol PM production. Panel **D**, **E** and **F** denote the source flux of SO_2, MSA and Cl, respectively. Light blue areas denote in-cloud period, in which rain events are represented as dark blue. Night and daytime periods are represented by the normalised UV-intensity and marked by grey and white areas, respectively.

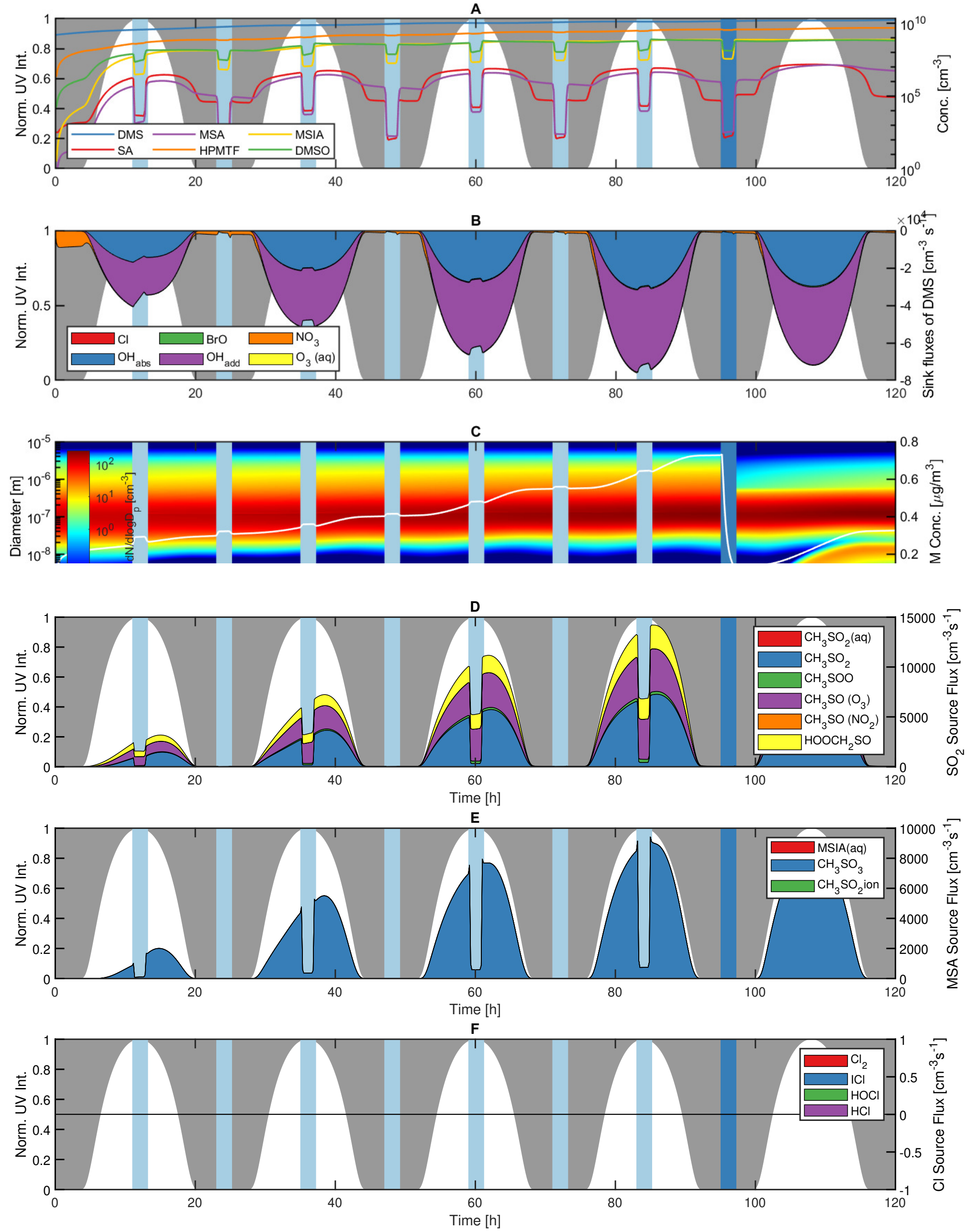

Figure S36. Modelled DMS oxidation and subsequent PM production related to the woAqAtm sensitivity run. Panel **A** illustrates the evolution of DMS, SA, MSA, HMPTF, MSIA and DMSO gas-phase concentrations, **B** the sink fluxes of DMS due to Cl, OH, BrO, NO_3 and O_3 and **C** the number size distribution and secondary aerosol PM production. Panel **D**, **E** and **F** denote the source flux of SO_2, MSA and Cl, respectively. Light blue areas denote in-cloud period, in which rain events are represented as dark blue. Night and daytime periods are represented by the normalised UV-intensity and marked by grey and white areas, respectively.

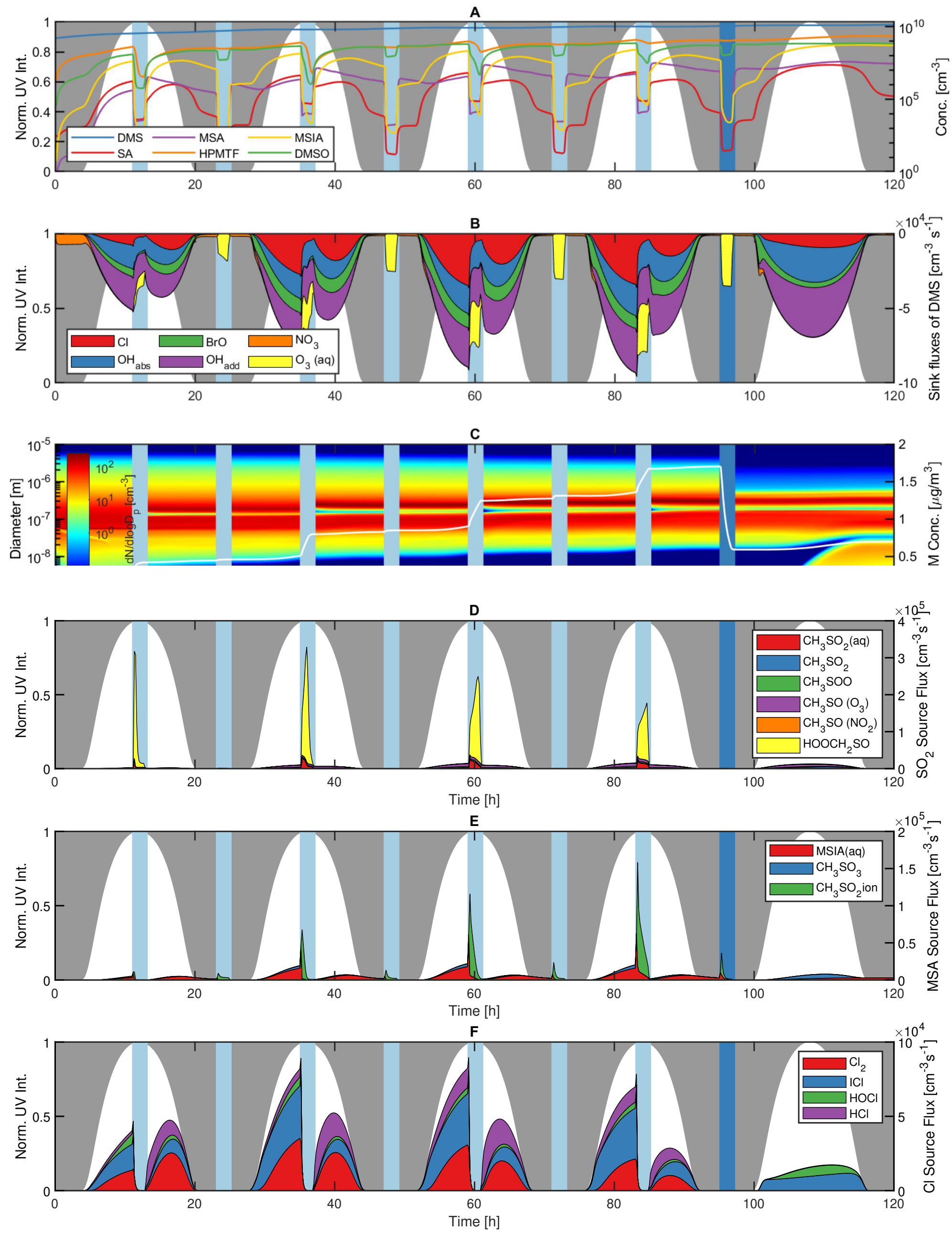

Figure S37. Modelled DMS oxidation and subsequent PM production related to the lowWindAtm sensitivity run. Panel **A** illustrates the evolution of DMS, SA, MSA, HMPTF, MSIA and DMSO gas-phase concentrations, **B** the sink fluxes of DMS due to Cl, OH, BrO, NO_3 and O_3 and **C** the number size distribution and secondary aerosol PM production. Panel **D**, **E** and **F** denote the source flux of SO_2, MSA and Cl, respectively. Light blue areas denote in-cloud period, in which rain events are represented as dark blue. Night and daytime periods are represented by the normalised UV-intensity and marked by grey and white areas, respectively.

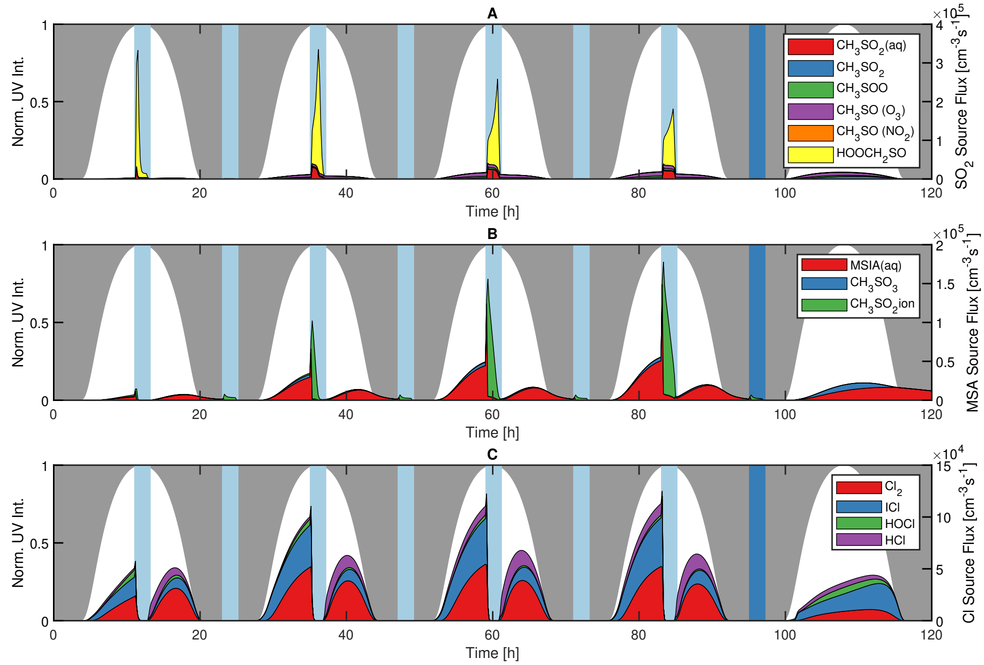

Figure S38. Modelled DMS oxidation realted to the AtmMain base run. Panel **A**, **B** and **C** denote the source flux of SO_2, MSA and Cl, respectively. Light blue areas denote in-cloud period, in which rain events are represented as dark blue. Night and daytime periods are represented by the normalised UV-intensity and marked by grey and white areas, respectively.

References

Atkinson, R., Baulch, D., Cox, R., Crowley, J., Hampson, R., Hynes, R., Jenkin, M., Rossi, M., and Troe, J.: Evaluated kinetic and photochemical data for atmospheric chemistry: Volume III - Gas phase reactions of inorganic halogens, Atmospheric Chemistry and Physics, 7, https://doi.org/10.5194/acp-7-981-2007, 2007.

Atkinson, R., Baulch, D., Cox, R., Crowley, J., Hampson, R., Hynes, R., Jenkin, M., Rossi, M., J, T., and Wallington, T.: Evaluated kinetic and photochemical data for atmospheric chemistry: Volume IV–gas phase reactions of organic halogen species, Atmospheric Chemistry and Physics, 8, https://doi.org/10.5194/acp-8-4141-2008, 2008.

Berndt, T., Scholz, W., Mentler, B., Fischer, L., Hoffmann, E., Tilgner, A., Hyttinen, N., Prisle, N. L., Hansel, A., and Herrmann, H.: Fast Peroxy Radical Isomerization and OH Recycling in the Reaction of OH Radicals with Dimethyl Sulfide, The Journal of Physical Chemistry Letters, 2019, https://doi.org/10.1021/acs.jpclett.9b02567, 2019.

Berndt, T., Chen, J., Møller, K. H., Hyttinen, N., Prisle, N. L., Tilgner, A., Hoffmann, E. H., Herrmann, H., and Kjaergaard, H. G.: SO2 formation and peroxy radical isomerization in the atmospheric reaction of OH radicals with dimethyl disulfide, Chem. Commun., 56, 13 634–13 637, https://doi.org/10.1039/D0CC05783E, http://dx.doi.org/10.1039/D0CC05783E, 2020.

Braeuer, P., Tilgner, A., Wolke, R., and Herrmann, H.: Mechanism development and modelling of tropospheric multiphase halogen chemistry: The CAPRAM Halogen Module 2.0 (HM2), JOURNAL OF ATMOSPHERIC CHEMISTRY, 70, 19–52, https://doi.org/10.1007/s10874-013-9249-6, 2013.

Burkholder, J. B., Sander, S. P., Abbatt, J., Barker, J. R., Huie, R. E., Kolb, C. E., Kurylo, M. J., Orkin, V. L., Wilmouth, D. M., and H., W. P.: Chemical Kinetics and Photochemical Data for Use in Atmospheric Studies, Evaluation No. 18, JPL Publication, 15-10, https://doi.org/http://jpldataeval.jpl.nasa.gov, 2015.

COSMO*conf*: version 4.3, COSMO*logic* GmbH & Co. KG., Leverkusen, Germany, 2013.

Demore, W., Sander, S., Golden, D., Hampson, R., Kurylo, M., Howard, C., Ravishankara, A., Kolb, C., and Molina, M.: Chemical Kinetics and Photochemical Data for Use in Stratospheric Modeling, JPL Publication, 90, 1997.

Hoffmann, E. H., Tilgner, A., Schrödner, R., Bräuer, P., Wolke, R., and Herrmann, H.: An advanced modeling study on the impacts and atmospheric implications of multiphase dimethyl sulfide chemistry, Proceedings of the National Academy of Sciences, 113, 11 776–11 781, https://doi.org/10.1073/pnas.1606320113, https://www.pnas.org/content/113/42/11776, 2016.

Jacobson, M. Z.: Fundamentals of Atmospheric Modelling (2nd edition), Cambridge University Press, Cambridge, United Kingdom and New York, NY, USA, 2005.

Kahan, T., Washenfelder, R., Vaida, V., and Brown, S.: Cavity-Enhanced Measurements of Hydrogen Peroxide Absorption Cross Sections from 353 to 410 nm, The journal of physical chemistry. A, 116, 5941–7, https://doi.org/10.1021/jp2104616, 2012.

Kukui, A., Borissenko, D., Laverdet, G., and Bras, G.: Gas-Phase Reactions of OH Radicals with Dimethyl Sulfoxide and Methane Sulfinic Acid Using Turbulent Flow Reactor and Chemical Ionization Mass Spectrometry, Journal of Physical Chemistry A, 107, https://doi.org/10.1021/jp0276911, 2003.

Kulmala, M. and Laaksonen, A.: Binary nucleation of water–sulfuric acid system: Comparison of classical theories with different H2SO4 saturation vapor pressures, The Journal of Chemical Physics, 93, 696–701, https://doi.org/10.1063/1.459519, https://doi.org/10.1063/1.459519, 1990.

Kurtén, T., Hyttinen, N., D'Ambro, E. L., Thornton, J., and Prisle, N. L.: Estimating the saturation vapor pressures of isoprene oxidation products $C_5H_{12}O_6$ and $C_5H_{10}O_6$ using COSMO-RS, Atmos. Chem. Phys., 18, 17 589–17 600, https://doi.org/10.5194/acp-18-17589-2018, 2018.

Lucas, D. D. and Prinn, R. G.: Mechanistic studies of dimethylsulfide oxidation products using an observationally constrained model, Journal of Geophysical Research: Atmospheres, 107, ACH 12–1–ACH 12–26, https://doi.org/10.1029/2001JD000843, https://agupubs.onlinelibrary.wiley.com/doi/abs/10.1029/2001JD000843, 2002.

McMurry, P. H. and Grosjean, D.: Gas and Aerosol Wall Losses in Teflon Film Smog Chambers, Environ. Sci. Technol., Vol. 19, No. 12,, 19, 1176–1182, 1985.

Quéléver, L. L. J., Kristensen, K., Jensen, L. N., Rosati, B., Teiwes, R., Daellenbach, K. R., Peräkylä, O., Roldin, P., Bossi, R., Pedersen, H. B., Glasius, M., Bilde, M., and Ehn, M.: Effect of temperature on the formation of highly oxygenated organic molecules (HOMs) from alpha-pinene ozonolysis, Atmos. Chem. Phys., 19, 7609—7625, https://doi.org/10.5194/acp-19-7609-2019, 2019.

Rosati, B., Christiansen, S., Wollesen de Jonge, R., Roldin, P., Jensen, M. M., Wang, K., Moosakutty, S. P., Thomsen, D., Salomonsen, C., Hyttinen, N., Elm, J., Feilberg, A., Glasius, M., and Bilde, M.: New Particle Formation and Growth from Dimethyl Sulfide Oxidation by Hydroxyl Radicals, ACS Earth and Space Chemistry, 5, 801–811, https://doi.org/10.1021/acsearthspacechem.0c00333, https://doi.org/10.1021/acsearthspacechem.0c00333, 2021.

Sander, S., Friedl, R., Golden, D., Kurylo, M., Moortgat, G., Wine, P., Ravishankara, A., Kolb, C., Molina, M., Finlayson-Pitts, B., Huie, R., and Orkin, V.: Chemical Kinetics and Photochemical Data for Use in Atmospheric Studies, JPL Publication, 06–2, 2006.

TURBOMOLE: Version 7.11, a development of University of Karlsruhe and Forschungszentrum Karlsruhe GmbH, TURBOMOLE GmbH, 2010.

Veres, P. R., Neuman, J. A., Bertram, T. H., Assaf, E., Wolfe, G. M., Williamson, C. J., Weinzierl, B., Tilmes, S., Thompson, C. R., Thames, A. B., Schroder, J. C., Saiz-Lopez, A., Rollins, A. W., Roberts, J. M., Price, D., Peischl, J., Nault, B. A., Møller, K. H., Miller, D. O., Meinardi, S., Li, Q., Lamarque, J.-F., Kupc, A., Kjaergaard, H. G., Kinnison, D., Jimenez, J. L., Jernigan, C. M., Hornbrook, R. S., Hills, A., Dollner, M., Day, D. A., Cuevas, C. A., Campuzano-Jost, P., Burkholder, J., Bui, T. P., Brune, W. H., Brown, S. S., Brock, C. A., Bourgeois, I., Blake, D. R., Apel, E. C., and Ryerson, T. B.: Global airborne sampling reveals a previously unobserved dimethyl sulfide oxidation mechanism in the marine atmosphere, Proceedings of the National Academy of Sciences, 117, 4505–4510, https://doi.org/10.1073/pnas.1919344117, https://www.pnas.org/content/117/9/4505, 2020.

Wu, R., Wang, S., and Wang, L.: A New Mechanism for The Atmospheric Oxidation of Dimethyl Sulfide. The Importance of Intramolecular Hydrogen Shift in CH3SCH2OO Radical., The journal of physical chemistry. A, 119, https://doi.org/10.1021/jp511616j, 2014.

Yin, F., Grosjean, D., Flagan, R. C., and Seinfeld, J. H.: Photooxidation of dimethyl sulfide and dimethyl disulfide. II: Mechanism evaluation, Journal of Atmospheric Chemistry, 11, 365–399, https://doi.org/10.1007/BF00053781, https://doi.org/10.1007/BF00053781, 1990.